Constanze Ranfeld

Wet etching of printed silver layers using an etch resist structured by flexography

Dissertation

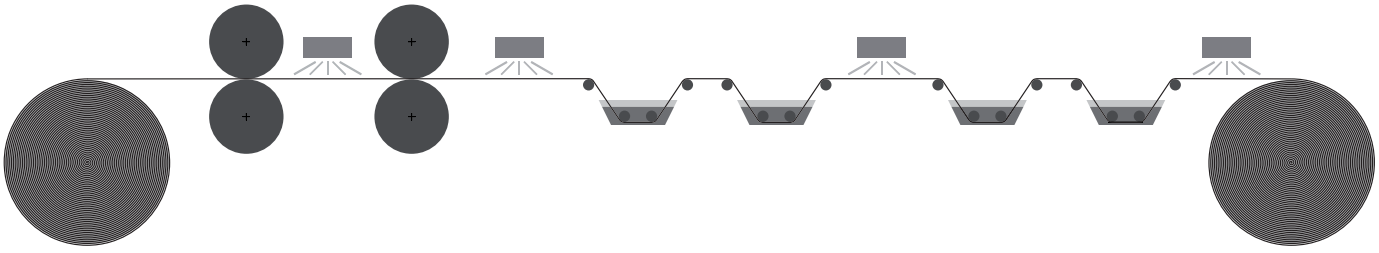

Constanze Ranfeld

Wet etching of printed silver layers using an etch resist structured by flexography

URN: urn:nbn:de:tuda-tuprints-45349
URL: http://tu-prints.ulb.tu-darmstadt.de/id/eprint/45349

Wet etching of printed silver layers using an etch resist structured by flexography

Vom Fachbereich Maschinenbau
an der Technischen Universität Darmstadt
zur
Erlangung des akademischen Grades eines Doktor-Ingenieur (Dr.-Ing.)
genehmigte

D I S S E R T A T I O N

vorgelegt von
Dipl.-Ing. Constanze Ranfeld
aus Schlema

Berichterstatter: Prof. Dr.-Ing. Edgar Dörsam, TU Darmstadt
Mitberichterstatter: Prof. Tim Claypole MBE, Swansea University

Tag der Einreichung: 25.02.2014
Tag der mündlichen Prüfung: 21.05.2014

Darmstadt 2015

D17

Abstract

Flexographic printing is a common technique in the production of printed electronics. Its flexible printing plates offer many advantages, especially regarding printing on rigid and fragile substrates. Nevertheless, one major drawback is the so-called *halo effect* where ink is squeezed at the edges of the raised elements of the printing plate during transfer onto the substrate. The result is a halo-like structure surrounding the desired layout with a zone depleted of ink in-between.

The approach of this study is to utilize the halo effect in flexographic printing for the structuring of a resist layer in wet etching processes of silver layers with the goal of integrating this process into printed electronics production.

For this, three different aspects need to be considered. The first aspect is the influence of post-processing on printed silver layers. I investigated the effect of several parameters of photonic curing on the etching rate and on the sheet resistance of printed silver nanoparticle layers. For the latter, I utilized *design of experiments* (DoE). The second aspect is the impact of printing parameters on the behavior of printed lines regarding the halo effect in flexography. I investigated the halo effect of printed line structures on an IGT F1 printability tester, also utilizing DoE. With this method, I structured a resist layer of poly(methyl methacrylate) (PMMA) for wet etching processes. The third aspect is the transferral of the layout of the printed etch resist to the silver layer using wet etching. For these trials I used nitric acid as etchant.

The results of these investigations are the following: The printed silver layers were homogenous with a roughness of few ten nanometers. As expected, photonic curing does increase the conductivity. The extend of the increase depends on the energy density the sample is exposed to. I found a method to evaluate the isotropy of the electrical properties of printed silver layers using the correction factor in *van der Pauw* measurements.

When printing line shaped elements the halo effect needs to be considered. Nearly all printed samples, regardless the printing parameters, show a more or less pronounced halo effect. Here, the most influential parameter is the pick-up volume: A high pick-up volume results in wide halos around a printed line with a distinct void in-between. The second largest impact has the printing force, whereas the influence of the printing speed is almost negligible.

It was not possible to determine a relation between degree of post-processing, i.e. energy density during photonic curing, and etching rate. The measurements were inconclusive. Therefore, I used a different dilution of the etchant to transfer the layout of the printed resist structures into the silver layer.

Using the halo effect in flexographic printing for structuring the resist layer, we can obtain line widths smaller than those attainable by directly using flexographic printing. To achieve this, anilox rollers with low pick-up volume are needed. Nevertheless, those lines are hardly reproducible. Their line quality needs further improvement regarding edge sharpness, bulging and interruptions.

Kurzfassung

Flexodruck ist ein gängiges Herstellungsverfahren in der gedruckten Elektronik. Gerade die flexiblen Klischees machen es so attraktiv für z. B. starre oder zerbrechliche Substrate. Der Flexodruck hat jedoch einen gravierenden Nachteil, den Halo-Effekt, im grafischen Drucken auch Quetschränder genannt. Dabei wird Fluid an den Kanten der erhabenen Druckformelemente zwischen Klischee und Substrat herausgequetscht. Das Ergebnis sind halo-förmige Strukturen, die das gewünschte Druckbild umranden. Zwischen Druckbild und Halo befindet sich eine fluidarme Zone.

Das Ziel dieser Arbeit ist die Nutzung des Halo-Effektes im Flexodruck zur Strukturierung von Resist-Schichten für Nassätzprozesse gedruckter Silberschichten mit Fokus auf die Integration in die Produktionskette gedruckter Elektronik.

Dafür sind drei verschiedene Aspekte zu berücksichtigen. Der erste Aspekt ist der Einfluss von Nachbehandlungsmethoden auf gedruckte Silberschichten. So wurde die Auswirkung verschiedener Parameter des Photonischen Sinterns (engl. *Photonic Curing*) auf die Ätzrate und den Flächenwiderstand gedruckter Silbernanopartikelschichten untersucht. Für letzteres wurde *Statistische Versuchsplanung* angewendet. Der zweite Aspekt ist der Einfluss von Druckparametern auf die Ausprägung des Halo-Effektes gedruckter Linien. Mit Hilfe *Statistischer Versuchsplanung* wurden Ätzresistschichten aus PMMA (Poly(Methylmethacrylat)) im Flexodruck strukturiert und deren Linienparameter untersucht. Zum Einsatz kam das Bedruckbarkeitsgerät IGT F1. Der dritte Aspekt ist die Übertragung des Layouts der Resiststrukturen auf die Silberschicht mittels Nassätzen mit Salpetersäure.

Folgende Ergebnisse wurden erzielt: Die gedruckten Silberschichten waren homogen mit einer Rauigkeit von wenigen zehn Nanometern. Wie erwartet steigert Photonisches Sintern die Leitfähigkeit der Schichten. Wie stark diese steigt hängt von der Energiedichte während des Sinterns ab. Eine Methode zur Evaluierung der Isotropie elektrischer Eigenschaften gedruckter Silberschichten anhand des Korrekturfaktors der *van der Pauw*-Methode wurde gezeigt.

Beim Flexodruck sollte immer der Halo-Effekt berücksichtigt werden. Dieser trat, mehr oder weniger stark, in allen gedruckten Proben auf. Der Haupteinflussparameter hierbei ist das Schöpfvolumen der Rasterwalze: Ein hohes Schöpfvolumen erzeugt breite Halos um eine gedruckte Linie, sowie eine sehr ausgeprägte Lücke dazwischen. Weiterhin hat die Druckkraft einen hohen Einfluss, während der Einfluss der Druckgeschwindigkeit vernachlässigbar ist.

Ein Zusammenhang zwischen Nachbehandlung (Energiedichte beim Photonischen Sintern) und Ätzrate konnte für 20%ige Salpetersäure nicht festgestellt werden. Die Messergebnisse waren nicht schlüssig. Daher wurden eine höhere Konzentration der Salpetersäure für die Übertragung der Resiststrukturen in die Silberschicht verwendet.

Unter Ausnutzung des Halo-Effektes im Flexodruck zur Strukturierung von Ätzresistschichten und anschließendem Ätzen ist es gelungen, kleinere Linienbreiten zu erzielen, als dies durch direktes Flexodrucken von Silberstrukturen möglich wäre. Um dies zu ermöglichen, werden Rasterwalzen mit geringen Schöpfvolumina benötigt. Jedoch ist die Reproduzierbarkeit solch schmaler Linien gering. Die Linienqualität muss weiter in Hinblick auf Kantenschärfe, Beulenbildung und Durchgängigkeit verbessert werden.

Danksagung

Die vorliegende Arbeit entstand während meiner Tätigkeit als wissenschaftliche Mitarbeiterin am Institut für Druckmaschinen und Druckverfahren der Technischen Universität Darmstadt. Mein ganz besonderer Dank gilt daher Herrn Prof. Dr.-Ing. Edgar Dörsam, der mir diese Zeit ermöglicht hat. Vielen Dank, Herr Dörsam, dass Sie mir die Promotion zutrauten, bevor ich dies selbst getan habe, für die vielen fachlichen und persönlichen Gespräche, und die Aufgaben und Verantwortung, die Sie mir übertragen haben, damit ich daran wachse.

I would also like to kindly thank Prof. Tim Claypole MBE from the Welsh Centre for Printing and Coating at Swansea University for agreeing to be my co-supervisor and his insights in my field of research.

Ich möchte auch meinen Kollegen am Institut für Druckmaschinen und Druckverfahren danken: Thorsten und Steffi für die Unterstützung bei meinen zahlreichen Druckversuchen. Nils, ich hätte keinen besseren finden können, um das Büro zu teilen. Martin, vielen Dank, dass du mich zur Diplomarbeit ans IDD geholt hast und aus dem Betreuer ein Freund geworden ist. Maria, Alex und Simone, ohne euch und Schokolade wäre ich vermutlich an meiner Diss, LaTeXund manchmal auch am Rest der Welt verzweifelt. Maria, danke auch für die Last-Minute-Hilfe beim Plotten in Matlab. Jürgen, danke für die vielen Mittagspausen, die wir mit Diskussionen verbracht haben. Karsten, Felipe, Robert, Ingmar, Evgeny, eure Sprüche haben mich oft zum Lachen und manchmal zur Verzweiflung gebracht, danke. Dem Kochclub danke ich für leckere Alternativen zur Mensa. Liebe (ehemalige) IDD-ler, ich hatte eine tolle Zeit mit euch!

Ebenso danke ich meinen Hiwis und Bacheloranden, die mich bei dieser Arbeit unterstützt haben.

Meiner Familie und insbesondere meinen Eltern danke ich für den Rückhalt, dafür, dass ihr an mich geglaubt und akzeptiert habt, dass ich manchmal keine Zeit für euch hatte.

Ronny, bei dir möchte ich mich ganz besonders bedanken. Du hast mich während dieser ganzen Zeit unterstützt, ertragen und ermutigt, hast an mich geglaubt und mir den Rücken freigehalten. Mahalo!

Contents

Acronyms

a.p.	Latin: aqua purificata, purified water
cf.	confer / compare
et al.	Latin: et alii, and others.
n/a	not applicable
ser. no.	serial number
CAIBE	chemically assisted ion beam etching
CD	cross direction, perpendicular to machine direction
CVD	chemical vapor deposition
DoE	Design of Experiments
DRIE	deep reactive ion etching
EPDM	ethylene propylene diene monomer (M-class) rubber
FIB	focused ion beam
FKM	fluoroelastomer
FPC	flexible printed circuits
FTA	Flexographic Technical Association
FOLAE	flexible, organic and large-area electronics
IBE	ion beam etching
IDD	Institut für Druckmaschinen und Druckverfahren (*English: Institute of Printing Science and Technology*), Technische Universität Darmstadt, Germany
IPA	isopropyl alcohol
IR	infrared
ITO	indium tin oxide
LACVD	laser assisted chemical vapor deposition
LIGA	German: Lithographie, Galvanoformung, Abformung. English: lithography, electroplating, molding
MD	machine direction
MOD	metalorganic decomposition
OFET	organic field effect transistor
OLED	organic light emitting diode
OPV	organic photovoltaics
PCB	printed circuit boards

PC	polycarbonate
PET	polyethylene terephthalate
PEN	polyethylene naphthalate
PMMA	poly(methyl methacrylate)
PVD	physical vapor deposition
RIE	reactive ion etching
RMS	root mean square
UV	ultraviolet

Symbols

Variables related to etching

Symbol	Unit	Description
γ	without unit	degree of anisotropy
l_{Ua}	[nm]; [μm]	anisotropic undercutting
l_{U1}	[nm]; [μm]	isotropic undercutting
r	[nm/s]	etching rate
r_H	[m]	horizontal etching rate
r_{res}	[nm/s]	etching rate of resist layer
r_U	[m/s]	etching rate of undercutting
S_{etch}	without unit	selectivity of etching
t_{etch}	[s]	etching time, duration of exposure

Variables related to printed layers

Symbol	Unit	Description
A	[μm^2]	(cross-sectional) area
a	[μm]	overall line width
b	[μm]	line/peak height
c	[μm]	peak distance
d	[μm]	height of valley
e	[μm]	width of gap
F_{print}	[N]	printing force
h	[nm]; [μm]	thickness of an arbitrary layer
h_{etch}	[nm]; [μm]	thickness of ablated layer, etching depth
$\mathsf{H_{ds}}$	[μm]	width of halo an drive side of printing press
$\mathsf{H_{os}}$	[μm]	width of halo an operating side of printing press
$\mathbf{R}_q$	[μm]	average surface roughness
$V_{pick-up}$	[ml/m^2]; [cm^3/m^2]; [BCM]	pick-up volume of an anilox roller
v_{print}	[m/s]	printing speed / velocity

The units indicated here relate to the dimensions relevant in this study.

Electrical variables

Symbol	Unit	Description
I	[A]	current
i	[A/m^2]	current density
R	[Ω]	electrical resistance
$R_\square$	[Ω/□]	sheet resistance
ρ	[Ωm]	electrical resistivity
σ	[S/m]	electrical conductivity
z	without unit	ion valency

Variables related to photonic curing

Symbol	Unit	Description
l_{pulse}	[μs], [ms]	pulse length
$n_{\mu pulse}$	without unit	number of micropulses
t_{env}	[ms], [μs]	envelop duration
t_{pulse}	[ms], [μs]	pulse length
U_{bank}	[V]	bank voltage
w	[mJ/cm^2]	energy density, energy per area

Variables related to optical measurements

Symbol	Unit	Description
$\Delta\lambda$	[nm]	spectral range
λ	[nm]	wavelength
λ_m	[nm]	mean wavelength
l_C	[nm]	coherence length
NA	without unit	numerical aperture

Material related variables

Symbol	Unit	Description
c_S	[$wt\%$]	solid content of a fluid
ϱ	[kg/m^3]	density
M	[g/mol]	molar mass

Constants

Symbol	Value	Description
F	$9.64853399(24) \cdot 10^4$ C/mol^{-1}	Faraday constant

1. Introduction

1.1. Motivation

Since the discovery of conductive polymers in 1977 and the Nobel prize awarded for this to Heeger, MacDiarmid and Shirikawa, the research on electronics shifted to organic electronics [30]. As many of the polymers are soluble, at least theoretically, it became more and more popular to process them from liquid phase in a non-vacuum environment. Printing and coating techniques are predestined for this purpose as they offer a high efficiency regarding produced area per time and provide the reproduction of small structures (e.g. characters) or large, homogeneous areas.

Nevertheless, volume printing processes commonly known for the production of high quantities in a short time span (screen printing, flexo-, gravure and offset printing) in their current forms are not appropriate for the production of printed electronics since they require special adjustments regarding inking and printing units, printing plates, resolution of reproducible feature sizes and especially printing inks. Li states flexography as one of the major high volume printing processes, but also lists several properties that require optimization: "particle sizes distribution in the inks, solvent evaporation rate, rheological properties, substrate surface energy and printing speed" [88].

Contrary to production processes of printed electronics, microfabrication processes have been well established for a long time. They provide stable, reproducible results in the production of electronic, mechanical, optical and combined devices, even in nanometer scale.

According to their assignment, volume printing processes are limited in their resolution. Generally, the limiting factor is the resolution of the printing plate and its manufacturing. Increasing the resolution would hereby mean altering the manufacturing process of the plates. This implies more costs.

This study gives a contribution to the research field of printed electronics regarding the use of flexography for printing functional layers, post-processing of printed silver layers as well as integrating wet etching into the process chain. The study contains three topics: printing and post-processing of silver layers, printing of etch resist using line-shaped elements and etching said layers.

1.2. Scientific context

1.2.1. Scientific environment and related research

The leading-edge cluster "Forum Organic Electronics", funded by the German ministry of education and research (BMBF), was founded with exactly the goal explained above: To advance the research on organic electronics, especially regarding printable inks and volume printing processes. Some exemplary projects of the cluster are: Polytos (printed organic circuits and memories), Kosadis (complementary circuit technologies for printed displays),

NanoPEP (printing processes and nanostructuring) and PrintOLED (organic light emitting diodes).

This study is part of the research in the cluster, started in the Kosadis-project and migrated into the NanoPEP-project, once Kosadis was completed. Alongside the presented research, also other studies were conducted regarding topics related to advancing printing technologies for FOLAE[1] with emphasis on flexographic and gravure printing. The following paragraphs introduce the topics investigated contemporaneously at research group Functional Printing of the Institute of Printing Science and Technology (IDD) at Technische Universität Darmstadt.

Stahl investigated the influence of printing form and fluid viscosity on the layer thickness of gravure printed layers. He devised a qualitative process modell for gravure printed polymeric layers and their homogeneity and developed a characterization method for those layers using absorption measurements [140]. Bornemann also investigated gravure printed layers, focusing on printing inks based on small-molecules. He contrived a measurement method to determine layer thicknesses over large areas based on reflection and gave a physical understanding of the gravure printing process [21].

Regarding flexography, Theopold investigated the compatibility of different printing plate materials with solvents both from graphical printing and printed electronics. During her research, she derived a method to characterize interaction of plate material with solvents under conditions very similar to the actual printing press and built a unique test station [143]. Griesheimer investigated ink splitting and ink transfer in flexography [51].

Willmann took a broader, more economically driven approach with his research on production theory of printed electronics [159]. He investigated the production process of printed electronics, using OPV (organic photovoltaics) as example device [159].

In the following, I exemplarily introduce some publications relating to the topics of this study. Regarding reducing the feasible feature size using wet etching, Scheinert [129] investigated the generation of precisely defined channel lengths of OFET (organic field effect transistors) in a submicrometer range. She used defined underetching by combining photolithography with a lift-off process [129]. Deganello investigated flexographic printing of thin silver lines forming a conductive grid showing that industrial scale flexography is feasible for the production of conductive networks [36].

1.2.2. Introduction to FOLAE

Many terms are currently used to describe the research field we are looking on: printed electronics, organic electronics, flexible electronics, and many more. Most are more or less accurate as not only organic but also inorganic materials are used, not all processes may be accounted as printing and often, rigid substrates are used. Willmann characterized the research field as "printable electronics" [159] including all feasible kinds of materials and processes. He described printable electronics as the "production of thin films of functional fluids enabling certain functionalities in a layer stack and thus facilitate novel applications" [159].

In this study, I use the term FOLAE -flexible, organic and large area electronics- and printed electronics as a synonym for printable electronics. Although not all materials used are organic, not all substrates flexible and not every printing trial results in an electronic device, this term is appropriate.

[1] FOLAE: Flexible, organic and large area electronics. See Chapter 1.2.2 for further information.

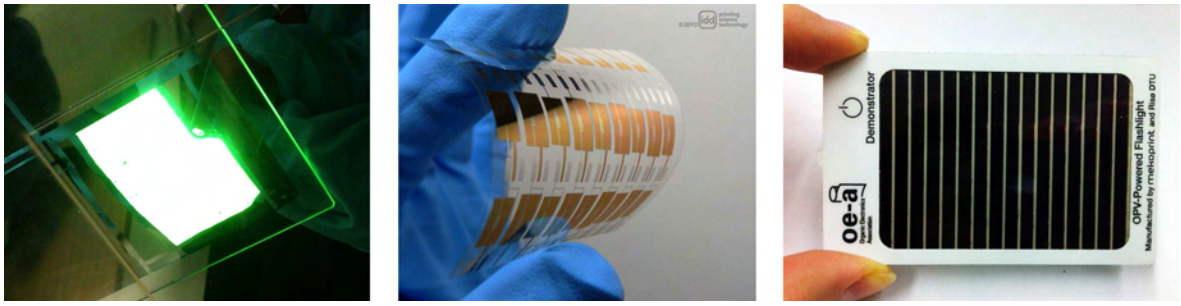

Figure 1.1.: Examples for partially printed, organic electronics. Left: OLED (organic light emitting diode), middle: OFET (organic field effect transistors), right: OPV (organic photovoltaics). Image source for OLED and OFET: IDD.

The research field of printed electronics aims at facilitating the industry to produce devices such as OLED (cf. Figure 1.1, left), OFET (cf. Figure 1.1, middle), OPV (cf. Figure 1.1, right), and other applications such as printed sensors, inorganic electroluminescent devices, printed batteries and combinations of those components. Presently, only few products have reached market maturity. The majority is still in research or on a small, lab and demonstrator scale. One of the focal points of current research are manufacturing methods, especially liquid processing using volume printing techniques [159].

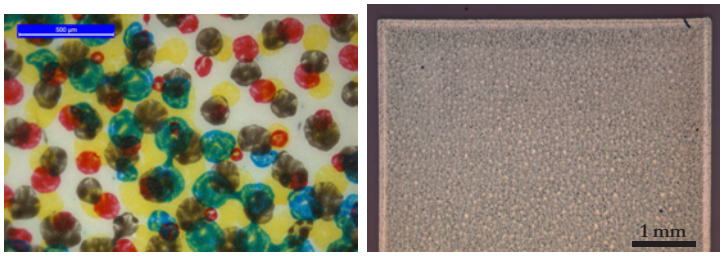

flexography for graphical purposes

flexography for printed electronics

Figure 1.2.: Different intentions and resulting layer properties of graphical (left) and functional (right) printing. Left: screened image consisting of colored dots (scaling bar: 0.5 mm); right: printed silver layer (scaling bar: 1 mm).

Contrary to graphical printing, the purpose of FOLAE processes is not to trick the human eye but to manufacture layers with certain functionalities. Thus, the term *functional printing* also applies. The requirements and process properties known from graphical industry no longer apply. Single layers in graphical printing usually consist of individual dots (cf. Figure 1.2, left) that, viewed from a certain distance, for the human eye merge into a solid area. However, this approach will not work transferred to printed electronics. Here, we require solid layers that either resemble a homogeneous area (cf. Figure 1.2, right) for e.g. semiconductors or plate electrodes. Or we need thin, interruption-free, mostly line-shaped structures e.g. for conductor paths and electrodes for thin film transistors.

1.2.3. Flexography and FOLAE

As it is a very delicate volume printing process also applicable for rigid substrates, flexography is highly wanted in FOLAE production. Literature already gives several applications where flexography was the main or the only production technique and other applications where at least one layer was produced using flexography. The following section gives a short insight into flexography and its use in the production of FOLAE.

The research group of Hübler was one of the first to present electronic devices produced by volume printing processes. First, they used offset lithographic printing [68], later, among others, they proposed flexography [80]. Recently, Hübler showed fully printed loudspeakers on paper, also prominently presented at drupa 2012, in [66]. Another application where flexography replaces screen printing and thus facilitates an easier introduction of printed electronics into packaging, was introduced by Ranfeld [121]: inorganic electroluminescent devices produced mainly by flexography.

A very common application for flexographic printing in FOLAE is the use of conductive traces. Literature states many examples where mainly silver inks are used to print electrodes for thin film transistors [67, 121] and simple conductor paths for various purposes [40, 65]. The research group of Claypole published extensively on the subject of flexographic printing of conductive traces and networks, essentially for the use in transparent electrodes [29, 31, 36, 35].

Exceptional uses for flexography include the patterning of antibodies on polyvinyl alcohol in carbonate-bicarbonate buffer [112] and the printing of seed layers for front-side metalization of silicon solar cells [44]. Huebner showed the printing of electroluminescent layers for OLED [70]. Also, flexography is used as an indirect patterning method for source and drain electrodes for transistors [130]. Other applications include printing of the dielectric layer in thin film transistors [67].

Note that the literature mentioned above is purely exemplary and there is substantially more research going on that is not mentioned here.

2. Method

In this study, I present the concept of integrating parts of the photolithographic process known from microfabrication into the production of FOLAE. Thus, we obtain smaller feature sizes than we would with directly printing the structures. It is not feasible to implement those process steps without alterations. The details concerning those will be described later on in this thesis. This chapter elucidates on the method applied to the present research and the objectives and approach of this work, starting with a short section on the theory of processes and how I use the term in this context. Concluding this chapter, I introduce several guiding questions that arose during the course of my research which will be answered in Chapter 7.

2.1. Process description

The procedure introduced with this research will be briefly explained in the following, starting with a short disambiguation of *process* and related terms. For comparison of single process steps with conventional microfabrication or printing processes, please refer to Chapters 3 and 4.

A process is "a series of actions that produce something or that lead to a particular result" [97]. Thus, it is a chain of action converting, handling or changing input elements into output elements. It may be understood as a black box with elements going in, being handled in some way and going out again. In the context of this study, the input and output elements are physical units (e.g. substrate, printing ink) and the black box is usually a method of application or removal.

To describe processes, we use the following hierarchy as illustrated in Figure 2.1. The top-level is a process chain. It consists of processes which themselves may be divided into several sub-processes. Each sub-process is comprised of process steps. At the bottom level, several "activities" [11] may make up one process step. We always have to regard a process in context with others, because a single process cannot exist solitarily. Its input elements are output elements of other entities of the process chain [11].

The terminology as introduced above is not used consistently throughout literature. Therefore, I will state the usage of the terms throughout this study in the following, illustrated by examples from printable electronics. A process chain combines several processes to convert e.g. raw materials into products. In the context of printable electronics: A *process chain* may be the manufacturing of a printed sensor. The raw materials in this case would be substrates and functional inks, the product said sensor. A *process* may be the printing of an electrode, i.e. a conductive layer. Thus, the input elements are substrates and conductive inks, the output elements substrates with printed conductive layers on top. An example for a *process step* is the ink transfer from the printing form onto the substrate. Note that I skipped the level of *sub-processes* and *activities* as introduced by Becker in [11] as I will disregard both in this study.

The focus of the research lies on the structuring of functional layers by means of wet etching. Structuring in this context implies the ablation of certain areas of a layer to obtain smaller

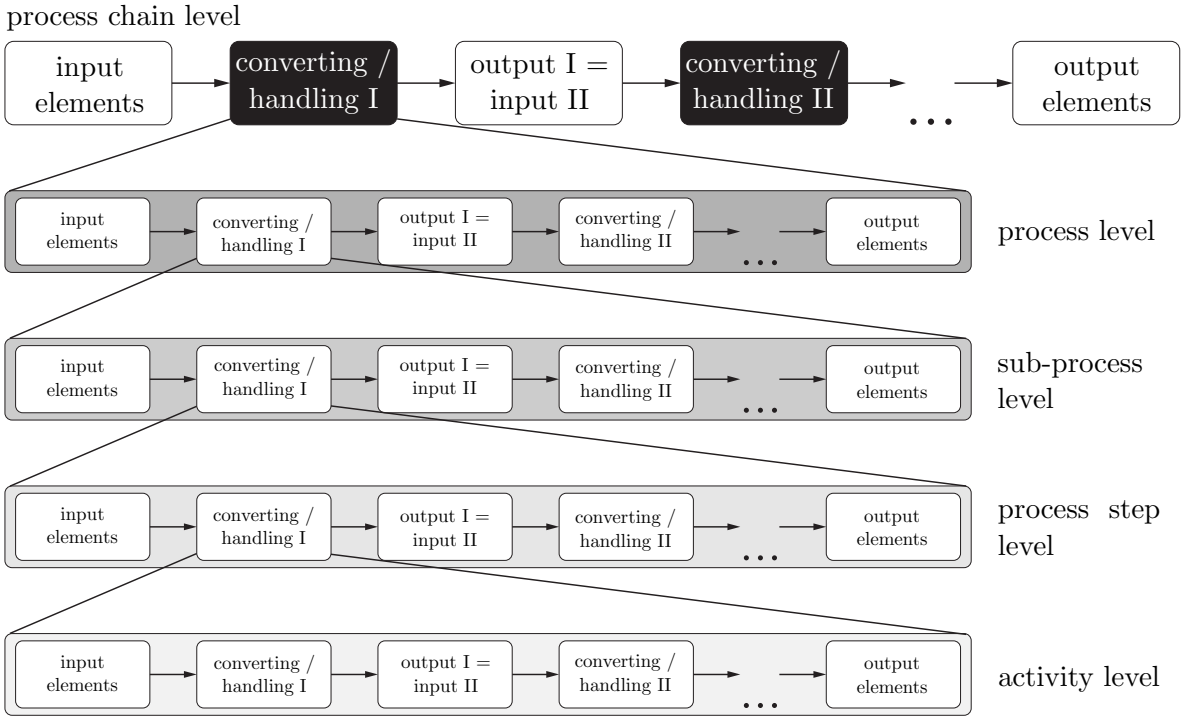

Figure 2.1.: Hierarchy of processes: Top level is a process chain, consisting of several processes as black boxes, their in- and output elements. Processes may be divided into sub-processes, process steps and activities, respectively. Illustration according to conceptions of [11].

feature sizes. The goal may be conductor paths like silver tracks used as an example in the present work.

Therefore, the process starts with an arbitrary solid or coarsely structured functional layer (cf. Figure 2.2, 1). Here, flexography is used as deposition method. Nevertheless, the technique of application of this layer is not relevant for the further process steps.

Onto this layer, an etch resist is deposited by means of flexographic printing utilizing the halo effect as introduced in [121] and explained in detail in Chapter 3.1.3. This results in a three-dimensional profile of the layer features. Figure 2.2 illustrates this phenomenon. An etchant is then applied to the layer stack. Thus, the layout of the resist layer is transferred to the functional layer. The resist is also affected by the etchant, therefore its thickness will decrease during the etching step. Thus, shallow areas of the resist-layout will be removed, leaving the silver layer underneath bare to the etchant. Thereby, the layout of the functional layer will bear roughly the feature size of the halo and thus be smaller than the resist layer. Hence, it is possible to obtain smaller feature sizes utilizing the introduced method than by directly printing them.

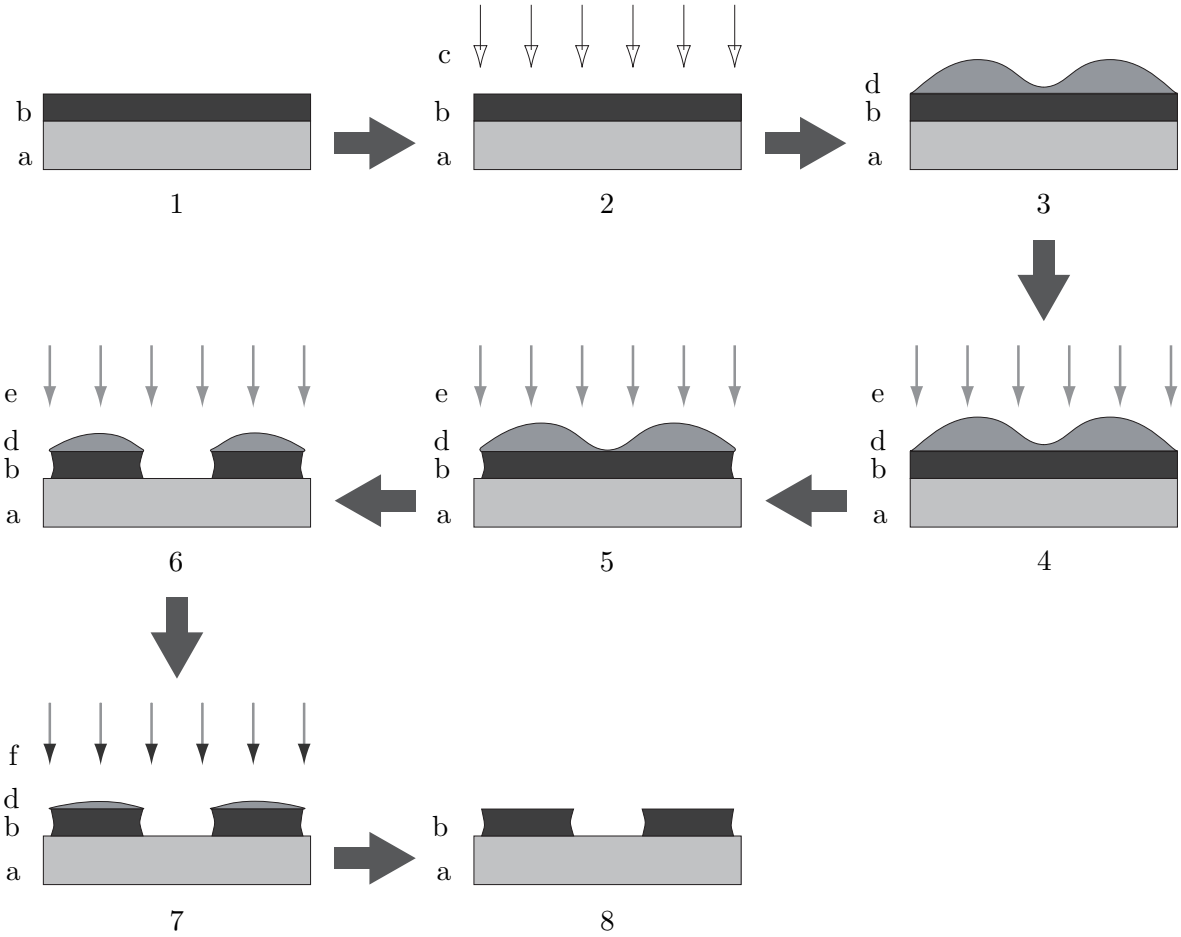

Figure 2.2.: Schematic of the wet etching process using halo-printed resist layer as implemented in this research with a) substrate, b) solid functional layer (silver), c) post-processing agent (electromagnetic radiation, d) resist layer (PMMA), e) etching agent, f) stripping agent. The process starts with a solid functional layer (1), post-processing (2), followed by the application of a resist layer (3). Etching (4 - 6) and stripping (7) steps result in a structured functional layer (8).

Subsequently, the remaining etch resist has to be removed, this process step being called stripping (cf. Figure 2.2, 7). The result is a structured functional layer ready for further processing (cf. Figure 2.2, 8).

The materials I used in this study as functional and resist materials are silver and poly(methyl methacrylate) (PMMA), respectively.

2.2. Objectives and approach

This section describes the objectives of my research and gives a short outline of the general approach.

As mentioned in Chapter 2.1, the individual steps of a lithographic process known from literature cannot be implemented into the production of FOLAE without alterations. Thus, one of the scopes of this research is to adapt them for use in printed electronics.

One part of this is to understand how etchants affect printed functional layers as they show significantly different behavior than bulk layers known from microfabrication. Thus, most data known from literature, e.g. [84], cannot be applied here. Also, printed silver layers have varying attributes according to the processing after the printing process, i.e. drying or sintering. This is not only valid for their electrical parameters but also for their etching behavior. The etching rates for both printed silver and printed PMMA with etchants as used in this study need identification and adjustment according to the requirements of printed electronics production.

Another objective of this investigation is to implement a flexography-based printing process using the halo effect to obtain smaller features than by using conventional flexography. To achieve this goal, the halo effect and its influencing printing parameters need better understanding than possible from hitherto existing literature. Therefore, I will look into the behavior of simple printed lines with different printing parameters (cf. Chapter 4.2.4).

For this, we need to understand three differing topics. The first is the behavior of printed nanoparticle silver inks in relation to their electrical properties. The second is the halo effect in printed lines and the third is the wet etching behavior of printed layers.

Based on those investigations, I establish a process combining flexo-based halo printing and wet etching as known from microfabrication to obtain smaller feature sizes than possible by exclusively using flexography. I applied this process on printed silver layers with different sintering states.

During the course of my research, some topics and interesting questions arose and drove me forward. As these guiding questions also consolidate the approach of this study, I list them here, including a short elaboration for each question. They will run as a thread through this study.

Question 1 Is it possible to obtain smaller line widths of a functional layer by combining the halo effect in flexographic printing for the application of the etch resist and a wet etching process than by flexographic printing alone?

This question is the main motivation for this study. Can we justify the effort and cost of additional process steps for subsequent structuring by a higher resolution than obtainable by structured printing? Is it possible to obtain smaller feature sizes using a structured resist layer for wet etching? And if so, can we utilize the halo effect in flexographic printing for doing so? What process parameters do we need?

Question 2 Can wet etching using a printed etch resist be integrated into continuous production lines (e.g. reel-to-reel printing) for structuring pre-coated solid area layers?

Are the process parameters of the investigated process steps (printing of the resist, wet etching) adequate for integration into printed electronics production? Is the process time sufficient for possible reel-to-reel integration?

Question 3 Do printed silver layers behave significantly different in a wet etching process than layers obtained in vacuum processes (i.e. bulk layers)?

Literature gives plenty of information on silver in electronics production. Nevertheless, this data only applies to bulk silver and thin films obtained from vacuum deposition. Silver inks intended for printing consist of either flakes or nanoscale particles embedded in binders, solvents and other additives. Thus, we expect them to behave differently than bulk layers described in literature. Can we deduce certain properties and generalize them?

Question 4 Do we need new specifications to describe printed lines in flexography, especially regarding the halo effect?

The specifications for printed lines in literature are not sufficient to adequately describe the halo effect in flexographic printing. This is especially true for small feature sizes as required in printed electronics where the halo effect is in the same magnitude as the desired details.

Implicitely, some questions will be picked up in the Chapters *5 Results* and *6 Discussion*, respectively. Chapter 7 *Conclusion* will state how this study contributes answers to these questions.

3. Fundamentals

This chapter addresses the current state of technology and science regarding flexographic printing, wet etching and some relevant details from other microfabrication processes.

Flexographic printing as well as wet etching will both be introduced with a general process description followed by selected details of the respective processes. The halo effect, a characteristic of flexographic printing, will be covered in a separate section to emphasis its importance in this thesis.

The chapter will be concluded by a section comparing printing and microfabrication processes, enhancing their similarities and stating the differences.

3.1. Flexographic printing

Flexographic printing is a relief printing process where the imaging details of the printing layout are elevated. The printing form resembles a flexible stamp, where the elevated details bear a mirrored image of the desired layout and thus transfer ink onto the substrate. A schematic is depicted in Figure 3.1. For further information, I refer the reader to the standard works of the Flexographic Technical Association [42], Kipphan [81], Meyer [99] and Teschner [142].

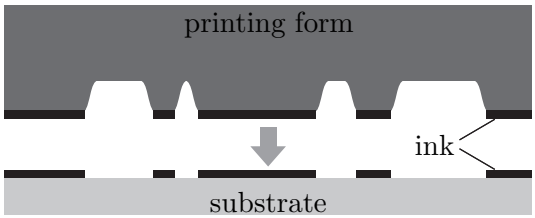

Figure 3.1.: Schematic of the image transfer in relief printing. The imaging details of the printing plate are elevated and covered with ink. Thus, they transfer the image onto the substrate.

3.1.1. General process description

Another approach for describing printing processes was introduced for gravure printing by Bery in 1985 [14]. Based on his publication and that of Fell [41], this approach was used by Dörsam et al.[1] [37] and Bornemann [21] to introduce a generic six-step model applicable for the most common printing process.

[1] Dörsam, Bornemann et al. introduced this model in the lecture notes "Printing Technology for Electronics" within the master course in physics at Heidelberg University in 2011 for gravure printing (adapted from Bery), inkjet, screen and flexo printing [37, Section Flexographic printing]. I principally edited the section regarding flexography.

In general, this model assumes that any printing process may be subdivided into a preset number of fluid related process steps. The following listing enumerates those steps with Figure 3.2 illustrating the description. Note that the markedness of the individual steps may vary regarding the respective printing technique. Not all steps occur in each printing process, some may be joined.

1. Ink acquisition from the reservoir
2. Pre-dosing
3. Dosing of the ink
4. Ink transfer
5. Fluid dynamics on the substrate
6. Solidification

Stahl and Dörsam adapted the model for flexography in [64], combining the steps 2) *pre-dosing* and 3) *dosing of the ink* into "Metering of the Ink" and 5) *fluid dynamics on the substrate* and 6) *solidification* into "Fluid Dynamics on the Substrate and Solidification", respectively. Thus, they abridge the overall process to four steps.

The following paragraphs elucidate the application of the model on flexography as applied in this study with Figure 3.2 illustrating the process steps using an industrial printing unit with a chambered doctor blade as an example. Each step will be described subsequently with further explanation of significant details.

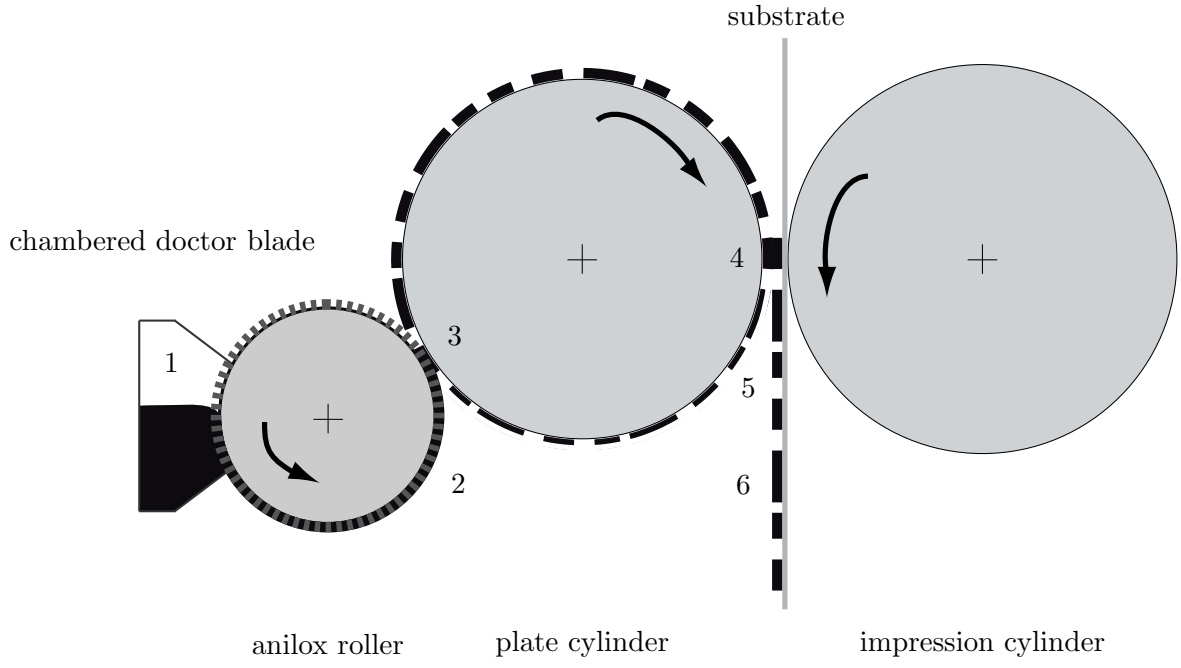

Figure 3.2.: Process steps in flexographic printing process using the example of an industrial printing unit with a chambered doctor blade: 1) Ink acquisition from the reservoir; 2) Pre-dosing; 3) Dosing of the ink; 4) Ink transfer; 5) Fluid dynamics on the substrate; 6) Solidification.

1) Ink acquisition from the reservoir The first process step, *ink acquisition from the reservoir*, marks the boundaries of the process model of Bornemann by incorporating ink into

the environment of a flexographic printing unit. This requires an inking unit. Several design options of inking units are common: A first option, as depicted in Figure 3.2, is the use of a chambered doctor blade. Here, the ink is enclosed on all sides by the reservoir walls, two doctor blades and the anilox roller. Another option is using a (soft) inking roller rotating in an ink filled chamber and transferring the ink onto the anilox roller. Some other, not very common option mostly used in printing proofers or laboratory printing presses is the application of ink directly onto the anilox roller using a pipette.

2) Pre-dosing In flexography, generally an anilox roller is used to pre-dose the fluid before transfer onto the printing plate. The girthed area of the anilox roller is engraved with small, roughly pyramid-shaped cells. The cells pick up the ink from the reservoir either directly (e.g. chambered doctor blade) or indirectly via an inking roller. Thus, the cell volume, ruling and spacing define the volume transferred, in flexography called pick-up volume. It is an important parameter influencing the printing process and its results, respectively. Typically, it is specified in [cm^3/m^2], [ml/m^2] or [BCM][2] and indicates how much fluid will be deposited onto a certain area.

Excess ink, i.e. ink on the land area of the anilox roller, is removed by a doctor blade grazing the surface. Thus, only the cells transfer ink onto the printing plate and a certain volume is ensured. Note that the cells do not empty completely but some residual ink remains in the cells. For further details on anilox rollers and their emptying behavior, I refer the reader to Chapter 3.1.2.

3) Dosing of the ink This process step includes the transfer of ink from the anilox roller onto the printing plate. *Dosing* implies the actual metering of the ink being transferred onto the substrate. In flexographic printing, this amount of ink is defined not only by the cell volume of the anilox roller (cf. 2) *pre-dosing*) but also by the area of the raised elements (ruling and feature size) on the printing plate as they are the actual imaging components. As flexography is a relief printing method, only the imaging areas on the printing plate are elevated and thus carry ink as shown in Figure 3.1.

Both pre-dosing and dosing should not be considered separately from each other. Nevertheless, the area of the elevated plate elements ultimately influences the ink amount transferred onto the substrate. Investigations regarding the wetting of the flexographic printing plate and thus the amount of ink applied there have been conducted by Galton [47] and Hamblyn [55]. Bould stated in [27] that the ink transfer from anilox roller to printing plate also depends on the "ratio between the depth of the cell and the open area": The deeper the cells are, the more ink they can hold but deeper cells also hinder ink release [27].

4) Ink transfer The last process step involving the printing unit is the *ink transfer* from the printing plate onto the substrate. Here, a certain amount of ink from the plate is delivered onto the substrate. This is not necessarily all the volume offered by the printing plate but, depending on the combination of plate and substrate, a certain ratio. Also depending on the parameters of the printing plate (surface tension, surface structuring, feature size etc.), the fluid (rheological properties as viscosity or surface tension) and other parameters (geometry, printing speed), either dot, lamella or film splitting take place. Several printing related parameters also influence the behavior of the ink transfer, e.g. printing speed and impression.

[2] BCM. Billion cubic microns per square inch.

As the ink behavior during transfer is a very wide and complex field of research, I refer the reader to the investigations of Behler [12], Bornemann [21], Hübner [69], Sauer [128], Voss [153] for ink transfer in general, and the very recent studies of Griesheimer [51] regarding flexography.

5) Fluid dynamics on the substrate The first process step not involving the printing unit is *fluid dynamics on the substrate*. After the transfer of the fluid from the printing plate onto the substrate, the fluid will either wet the substrate and form a homogeneous layer or it will show certain dewetting phenomena. The latter may be distinguished into thermal or nucleated and spinodal dewetting [23]. Both start with initially homogeneous films which then will break into smaller features due to thermal fluctations or disturbances (thermal or nuclear dewetting) and long-range molecular forces such as van-der-Wals (spinodal dewetting), respectively. For further information regarding dewetting and other fluid dynamical phenomena and their origins, the research of Bornemann and Sauer shall be recommended (e.g. [21, 22, 23, 128]. Nevertheless, these phenomena are highly undesired in functional printing and FOLAE as mostly homogeneous layers are required.

6) Solidification This last process step is not part of the actual flexographic printing, but rather a fluid related process after the ink transfer and thus after the actual printing is completed. Depending on the class of fluid used, it may either be a polymerization (for UV curing inks), drying (evaporation of solvent) or curing and sintering process (e.g. for metallic inks), respectively. The time a film needs to solidify can significantly influence its homogeneity as Bornemann showed in [21].

3.1.2. Selected details of the flexographic process

Flexographic printing plates

The printing plates in flexographic printing are eponymic: Flexible, rubber-like plates made of either photopolymers or elastomers. The imaging details of the plate are raised above a supporting base of bulk material (cf. Figure 3.3). The most common thicknesses of photopolymeric flexo plates are 1.7 mm or 1.14 mm in total, including 0.8 mm and 0.75 mm of relief depth, respectively [99]. Figure 3.3 illustrates a cross section of a photopolymeric printing plate.

There are two classes of flexographic printing plates: photopolymeric and rubber plates. The former are easier to manufacture whereas the latter show a higher resistance to solvents [144]. Rubber plates are commonly used in sleeve form whereas photopolymeric plates are mainly produces as sheets.

For imaging of a photopolymeric printing plate, the back of a blank plate or thin film of liquid is exposed to UV light. This starts a polymerization process providing a solid base of the plate. The duration of the UV exposure regulates the relief depth (cf. Figure 3.3, 5) as it defines the base of the plate (cf. Figure 3.3, 4). Next, the front of the plate is exposed to UV light through a negative mask to generate the layout of the printing image (cf. Figure 3.3, 2). To remove the unexposed, hence uncured, areas of the plate, a wash out step is required. Another exposure to UV light "cure[s] floor and character shoulders" [42, Vol.4]. To finalize platemaking, the plates need to be dried to remove residual solvents or water from wash out [42, Vol.4].

Figure 3.3.: Cross section of a photopolymeric printing plate with 1) shoulder, 2) plateau, resp. raised element (i.e. printing element), 3) backing, 4) base, 5) relief and 6) caliper (i.e. overall height). Following [42].

Rubber plates nowadays are usually imaged directly by an engraving process. A laser beam writes the layout of the printing image into the blank sleeve by vaporizing and thus evaporating the non-printing areas creating the raised printing areas [42, Vol.4].

Anilox roller

As stated in Chapter 3.1.1, pre-dosing of the ink in flexography is achieved by using an anilox roller. The anilox roller resembles a cylinder with its girthed area engraved with small cells to meter and transport the ink from the reservoir onto the printing plate. To describe the amount of ink the roller is able to transport, we use the term pick-up volume. It specifies the volume the cells in a certain area are able to hold and is typically given either in [cm^3/m^2], [ml/m^2] or [BCM]. The main factors influencing the pick-up volume are the cell geometry and the amount of cells in an area, i.e. cell ruling. Figure 3.4 shows a schematic of an anilox roller with an enhancement of several cells to illustrate cell geometry and cell ruling, following [81].

Note that Figure 3.4 shows a hexagonal cell shape as this is the one used in this study. Also other geometries are possible, such as hachures, cells composed of small spherical segments or S-shaped channels (e.g. Apex GTT).

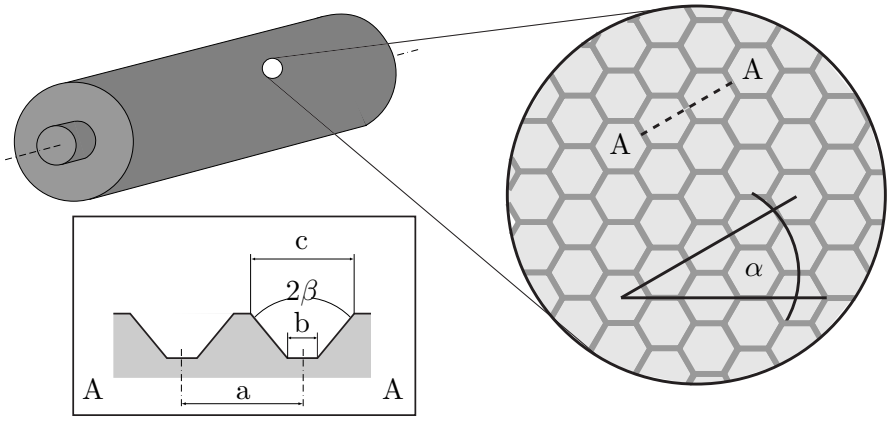

Figure 3.4.: Schematic of an anilox roller and its engraving with enhancement of cell structure to illustrate screen ruling and screen angle α. 2β is the angle of the cell walls, a is the distance of two cells (i.e. the reciprocal of the screen ruling), b the width of the cell ground and c the width of cell opening. Cross section following [81].

Commonly, there are two kinds of anilox rollers: Chromium and ceramic rollers. Chromium rollers are actually blank rollers, covered with a thin layer of copper. This layer is either engraved using mechanical equipment or by means of wet etching using a mask. The engraved copper is then chromium-plated to ensure a higher mechanical stability. Chromium rollers are cheaper to manufacture but the variety of their cell geometry is limited due to the manufacturing process [81].

In ceramic rollers, the engraving layer is a plasma-coated ceramic layer. After polishing the surface, the cells are engraved by evaporation with a laser beam. With this manufacturing method, higher cell rulings, different pick-up volumes at constant screen ruling and different cell geometries are possible. Ceramic rollers are more expensive than chromium ones, but they also show higher resistance to wear [81].

Several attributes characterize the engraving of an anilox roller: cell geometry (angle of cell walls, cell depth, footprint), screen angle and ruling, the latter being the number of cells per unit of length (i.e. cell count).

In graphical flexographic printing, as a rule of thumb, the cell count of the anilox roller should be at least three times higher than the resolution of the printing plate [102]. This is due to the avoidance of so-called dot dipping, where the smallest structures on the printing plate (i.e. single screen dots) dip into the cell and thus wet not only on the plateau but also on the shoulders. As the resolution of printing plates increased in recent years, the anilox roller had to keep up. Kipphan stated in the year 2000 the cell ruling for chrome rollers with up to 200 L/cm [3] and for ceramics rollers up to 600 L/cm, respectively [81]. For laboratory use, IGT testing systems offers ceramic anilox rollers with cell rulings of up to 710 L/cm [71]. For high resolution printing plates, screen count of about 600 L/cm are suggested for light areas by anilox roller manufacturers [6].

The screen angle was fixed at 45° for a long time [142] but recently, also other angles are common. For laboratory use, IGT testing systems also offers a screen angle of 53° for chromium rollers and exclusively 60° for ceramic rollers [71]. The emphasis on IGT specifics is due to their use in the experimental section of this study.

As Bornemann showed in [20, 24] for gravure cylinders as used in e.g. rotogravure printing, the pick-up volume indicated by the manufacturer is merely a theoretical one. Less than 50% of the indicated pick-up volume is actually transferred from the cells onto the substrate [20, 23, 24] with the ink system of small molecules in solvent he used. This can be assigned to flexographic printing as the fluid transfer from the anilox roller (corresponding to gravure cylinder) onto the printing plate (corresponding to the substrate). Thus, the actual ink volume transferred onto the plate is significantly lower than the pick-up volume indicated by the manufacturer. Bornemann conluded for chrome coated gravure cylinders that "approximately 44% [...] was actually transferred" [23]. This knowledge should be taken into account when choosing an anilox roller because it mainly influences the thickness of the printed layer. If a certain thickness is required, e.g. as a dielectric in printed electronics, the qualifying anilox rollers should be tested first according to the trials of Bornemann to ensure the actual pick-up volume matches the required one.

The main explanation for this phenomenon given by Bornemann is the partial filling of the cells after the doctor blading process. A fraction of the cell volume, the difference between the meniscus and the theoretical conceived cover of the cell, is already lost. The "cell fill

[3] The unit of the cell ruling, [L/cm], is the same as the unit for resolution and will be explained later in the section *Resolution*.

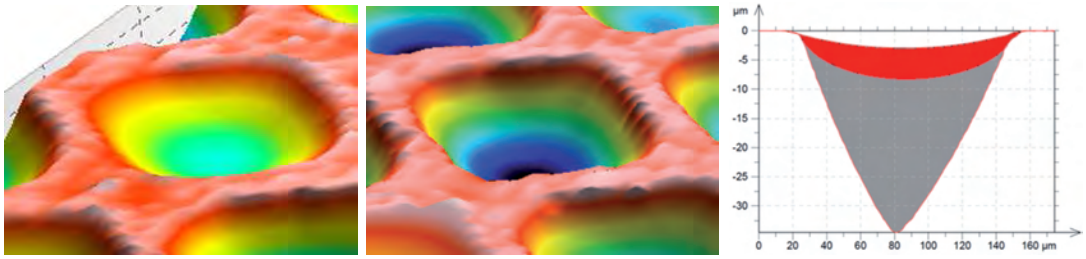

after doctor blading | after printing | cross section of both, overlayed

Figure 3.5.: Magnified single cells of a gravure cylinder, diameter of the opening about 120 μm. Left: filled with ink after doctor blading. Middle: Partially emptied after printing and thus ink transfer to the substrate. Right: Cross section of both states with grey indicating residual ink after the printing process and red as amount of ink actually transferred [20]. Reproduction with consent of the originator.

ratio after doctor blading" (i.e. the ratio of the cell volume by the volume actually filled with ink) depends on the ink viscosity and printing speed for "classical transfer ratio" and is independent of both parameters for the "real transfer ratio" as defined by Bornemann [24]. Also, experiments showed that a significant amount of ink remains in the cells after the actual printing process. Figure 3.5 illustrates some of those results with the left image showing a three-dimensional microscopic image of a filled cell after doctor blading. The middle image is a shot of a similar cell after printing. Note the residual ink in the cell and also the difference of ink volume before (left) and after (middle) printing, highlighted by the cross section in the right graph of Figure 3.5 [20, 21].

A third reason for differences between theoretical and actual pick-up volume is the entrapment of air bubbles in the cells. Those bubbles are introduced into the ink chamber either by empty cells entering the chamber and not filling up completely or by entrapment between substrate and printing form on first contact [21].

If the actual transfer volume of the ink is essential to printing trials, then the respective ratios as introduced by Bornemann in [21] should be measured and calculated beforehand. Nevertheless, the pick-up volume of the anilox roller should be chosen according to the requirements of the respective layers or devices intended to obtain.

As shown by Deganello, the pick-up volume influences the geometry of printed lines: A higher pick-up volume results in slighter higher line width with a higher thickness resulting in "a substantially higher cross-section area" [35].

Substrate

The choice of substrate usually depends on the intended use of the product to be printed. The most common substrates used in flexographic printing for graphical applications are paper and cardboard, corrugated board, laminates and plastic films [42]. Mostly, their intended usage is packaging or labelling applications. The choice of substrate also influences the selection of ink. Non-absorbing substrates require other ink properties than absorbing ones [81].

In FOLAE, the majority of substrates used is non-absorbing. This is a consequence of the requirements of the printed layers. With few exceptions, they have to be highly homogeneous, of a certain thickness and very even. As absorbing substrates usually consist of fibers, are

porous or both, most of the requirements cannot be met. Hence, the most common substrates in printed electronics are polymer films and glass because they provide quite even surfaces.

Plastic films are flexible and thus fit for roll-to-roll processing. Their thickness varies from 12 μm to 350 μm [115], depending on the requirements of the device to be produced. Still, most foils such as PET withstand processing temperatures below 130 °C, as they start degradation at 160 °C [29]. Unfortunately, some materials, e.g. silver ink, often need higher temperatures for drying and sintering, respectively.

Flexograhpy on rigid substrates is also feasible though hardly used in graphical printing. It became common in functional printing, although rather for sheet based, not for reel-to-reel manufacturing. Blayo suggests rigid polymers, metals and glass [16] while printing seed layers for front side metallization of solar cells on silicon wavers was shown by Frey [44], Lorenz [90] and Thibert [145]. Flexible glass substrates are also an option for flexographic printing. Glass can be produced with thicknesses as low as 30 μm. Because it is so brittle, it is coated with a polymeric layer as reinforcement to improve its handling. Thus, the barrier properties of glass can be combined with flexibility [33].

Engagement

In flexographic printing, the engagement defines the distance between the cylinder axis of the plate cylinder in kiss print[4] and during actual printing. Bould defines engagement as "the positive displacement of the printing plate on to the substrate" [27]. Figure 3.6 (left) illustrates this with (a) being said distance. Typically, the engagement is stated in [μm]. This equals the distance with which the (theoretical) circumferences of both plate and impression cylinders are overlapping. As the printing plate in flexography is soft, the circular circumference of the plate on the plate cylinder is actually indented as also depicted in Figure 3.6 (left) [31].

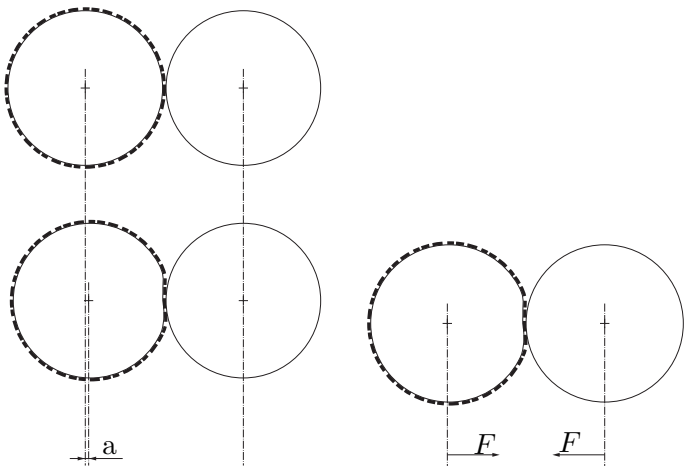

Figure 3.6.: Engagement (left) vs. impression (right). In the left schematic, a illustrates the engagement as used in distance controlled printing presses. The right schematic illustrates the printing force F in a force controlled printing press, e.g. IGT F1. Engagement modeled after [27] and [31].

[4]Kiss print, also kiss impression: "The lightest possible impression which will transfer a film of ink [...] from the entire print surface of the printing plate to the material being printed" [42, Vol. 1].

Printing press operators in industry commonly adjust the engagement according to their operational/practical knowledge. They correct the engagement as to produce a "good" result. Commonly, press operators start with kiss print[4] where the printing plate barely touches the substrate, i.e. the engagement is roughly 0 μm. From there, they adjust the engagement according to what they think appropriate as printed image. It is difficult to give exact numbers for the engagement primarily used for certain subjects as it also depends on the diameter of the cylinders of the press. Johnson investigated the pressure and the length of impression in [78]. She used 100 μm, 200 μm and 300 μm as default values for engagement with an impression cylinder diameter of 0.9 m. Whereas Bould investigated the deformation of printing plates at engagements of 0 μm, 25.4 μm, 50.8 μm and 76.2 μm [25] with a diameter of about 190 mm.

In industrial flexographic printing presses, the engagement is regulated by distance control. Nevertheless, some laboratory presses are force controlled. One example is the *F1 printability tester* from IGT testing systems as used in the presented research (cf. Chapter 4.2). Here, the printing force may be varied from 10 N to 500 N [72] resulting in different, not clearly defined engagements.

Most affected by varying engagement is the printing result: Is it sharp or blurry, how marked are dot gain and the halo effect? With higher impression also the impact on the three-dimensional shape of more delicate substrates and surfaces may be affected, e.g. the compression of flutes of a corrugated board sheet [63] or indentations in the surface of soft plastic films.

As Yusof showed in [163] for numerical simulations and actual impression results, the engagement directly influences the line width: The higher the engagement is, the wider the width of a line will be.

Resolution

In the context of the flexographic industry, resolution is generally determined as the screen ruling. Thus, its unit is specified in number of lines or dots per unit of length. The most common units are [lpi], i.e. lines per inch or [L/cm], i.e. lines per centimeter. Both units may be converted into one another: 100 L/cm = 254 lpi.

The Flexographic Technical Association (FTA) [42] classifies screen rulings into coarse and fine, given in the following:

- coarse screen ruling: $<$ 100 lpi
- fine screen ruling: $>$ 150 lpi

with the range between 100 lpi and 150 lpi being the most common [42].

Depending on the application, the screen ruling in industry varies from 45 lpi to 175 lpi, but it can also be as high as about 300 lpi [42, 114]. Post-printing of corrugated board generally requires lower resolution whereas package printing on films and foils necessitates higher resolutions [156]. For flexography in printed electronics, Blayo sets the minimum resolution at 152 lpi [16].

Regarding printed electronics, the term resolution also indicates the smallest achievable feature size, e.g. line width. Thus, some publications state a *minimal achieved resolution* in a unit of length, typically [μm]. Loydd et al. reported printed line widths of $<$ 60 μm for precursors of ZnO nanowires with line widths on the printing plate of 50 μm [89]. Willmann

defines in [159] minimal line width as the line width being barely printable without disrupting the actual line. This is essential for conductor paths to ensure their operativeness [159]. In this thesis, I use both terms *minimally achievable resolution* and *line width* interchangeably, using units of length.

The limit of minimally accomplishable resolution is influenced by the printing parameters such as printing plate, substrate, ink properties and anilox configuration. The principal limiting factor for (photopolymeric) printing plates is the aspect ratio of line or dot width and the height of a raised, printing element. The aspect ratio should not be observed, as small screen dots may buckle resulting in uneven prints. Another limiting factor is the minimal resolution of the laser used for imaging of the plate. The smaller the focus size of the laser and the more precise its positioning, the higher the resulting resolution [144].

3.1.3. Fundamentals of the halo effect

Since the term "halo effect" relates to very different things in various topics non-related to flexographic printing, I will first give a short explanation of the most prominent one from psychology[5]:

- While statistically analyzing the ratings of several groups of test persons of American authors in 1907, Wells observed a cognitive bias, where one positive attribute of a person is projected onto other, unknown attributes [157]. Thorndike picked up this effect in his research on the evaluation of military officers by their cadets in 1920 and named it the "halo" [148]. The term *halo effect* is still used in contemporary psychology to refer to the phenomenon discovered by Wells [91, 113].
- Several books were published in the last decade, all referring to the effect discovered by Wells. The most prominent example is "The halo effect and the eight other business delusions that deceive managers" published by Rosenzweig in 2007, where he criticizes that seemingly scientific studies explaining business success of some companies are almost all biased by the halo effect [126].

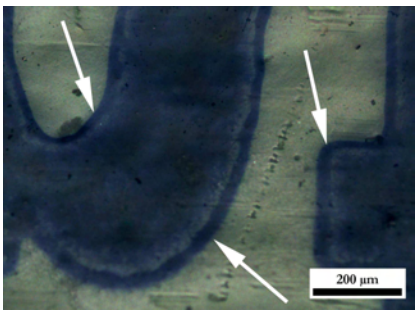

Figure 3.7.: Halo effect in flexography, surrounding printed letter.

In flexographic printing, an accumulation of ink surrounding the desired print layout is common. An example is depicted in Figure 3.7, indicated by the white arrows. Thus, the term *halo* as defined by Merriam Webster [96] as "a differentiated zone surrounding a

[5]When typing the term "halo effect" into online search engines (e.g. google.com or bing.com), the first hits refer to the halo effect in psychology or its application in marketing or management.

central zone or object" is highly appropriate. In German, the expression *Quetschrand*, which literally means *squeezed edge* is consistently used both in science and industry. Nevertheless, there is no undisputed notation for this effect in the English language that is used throughout the scientific or industrial community. Terms as "squeezed edge effect" [92], "dot fringe" [103], "crushed edges" [151] or "ink squash" [124] may cause confusion. *Donut* is used synonymously for the same effect but rather for single screen dots than for shaped solid areas [42, Vol. 2].

I introduce the following definition of the halo effect which I educed from the one given by Merriam Webster [96] and the literature stated below. I will use it throughout this study when referring to the effect:

In flexography, the halo effect refers to a phenomenon where the desired print layout is surrounded by an area depleted or void of ink again surrounded by a fringe of access ink. For small feature sizes, the desired image may not be visible leaving a stripe (for lines) or plain (for circles or squares) depleted of ink surrounded by mentioned fringe of access ink.

In graphical as in functional printing, this effect is usually undesired as it may blur the image and decrease its sharpness [16, 42, 87]. There is no unanimous opinion as to what the cause of the halo effect is. Mostly, it is attributed to a too high or non-uniform printing pressure [135]. Thus, the relief of the printing plate is deformed and ink is squeezed out at the edges of the raise elements [16, 94, 99]. Another cause is either too hard a printing form or mounting tape [94] or wrong coupling of both where the plate is too soft and the tape is too hard [99] and the general elasticity of the printing form [87]. Causes attributed to printing parameters are speed differences between plate and imaging cylinder, too much engagement between anilox roller and plate cylinder, low pressure in the chambered doctor blade or an anilox volume that was chosen too high [135]. Mathes mentions three effects that are ink-related: First, a too high ink volume transferred, second, too low viscosity and third, too much ink draw [94].

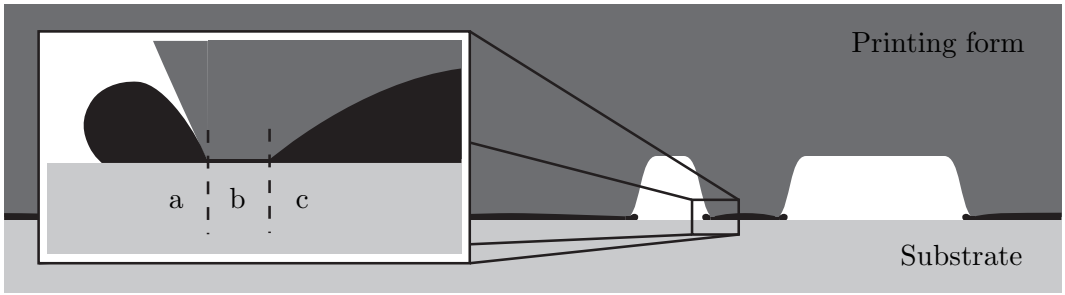

Figure 3.8.: Schematic of squeezed ink at the edges of a raised printing plate detail: a) halo, b) zone depleted of ink, c) inner layout.

A schematic of the halo effect is shown in Figure 3.8: The excess ink on top of the raised elements of the printing plate is squashed out at the edges and forms the halo. Between the inner layout and the halo, the edges of the raised elements on the printing plate form a zone depleted of ink.

The result of this phenomenon is a fringe of excess ink resulting in a "peripheral outline of the printed image" [42]. A by-product of the halo effect is usually dot gain[6], as both phenomena result from similar origin [142] and often occur together.

3.2. Printed silver layers

This chapter elucidates on specifics of printed silver layers. A short overview of different kinds of silver inks for flexography is followed by an overview over the most common drying and sintering methods used for printed conductive layers.

3.2.1. Silver inks for flexography

The origin of silver inks, or rather silver pastes, lies in the production of printed circuit boards. Here, conductive traces were applied using screen printing of silver pastes with high viscosities and high solid contents. Since then, both ink composition and printing techniques have evolved and expanded their application.

There are three different kinds of silver inks: nanoparticle inks, organometallic inks and inks containing silver flakes. The following sections introduce the inks and their respective characteristics.

Nanoparticle inks

Nanoparticle inks contain more or less spherically shaped silver particles in a base of water or solvent. Additives such as dispersants, defoamer or wetting agents [111] are also part of the ink. Silver nanoparticle inks have a solid contents of $40\,wt\% \ldots 60\,wt\%$ of silver [73, 108]. The particle sizes range between 10 nm and 40 nm [29, 109].

Nanoparticle inks are usually the ink of choice for flexograhpy as their particle size allows for easy dosing by the cells of an anilox roller. They usually form even layers with low surface roughness.

Organometallic inks

Organometallic inks, also called MOD (metal organic decompositions) [88], consist of chemical compounds where silver is bonded to organic molecules. In order for the thusly printed layers to be conductive, the organic residuals have to be removed. Generally, "dry organometallic compounds [...] are dissolved in an organic solvent", e.g. toluene or ethanol [88]. The resulting inks usually "do not require colloidal stabilisers" [111]. After deposition of the ink onto a heated substrate, the solvent evaporates [88], forming a dry film. In order to establish a conductive layer, we need a decomposition of the precursor which takes place at "elevated temperature[s]" of about 300 °C [88] for periods longer than 30 min [111], resulting in "contamination-free metal films" [88].

As organometallic inks have a low solid content, their main application methods are printing techniques handling very low ink viscosities, e.g. gravure [34] or inkjet [111]. There are hardly

[6] The term *dot gain* implies the mechanical and optical enlargement of a printed dot from layout / printing plate to substrate. The area on the substrate actually covered by ink usually is, and often appears even more so, larger than the dot on the printing plate. This results in darker images. For further information, I refer the reader to the investigations of Happel [56].

any scientific publications regarding organometallic inks for flexography, although patents have been filed [77].

Flake-based inks

Flake-based silver inks are eponymic: The silver particles are shaped as flakes with aspect ratios of more than 5:1 [127]. They have a solid content of up to 75 $wt\%$ [104]. Their composition also contains wetting agents, resins, defoamer and a base which is either water or solvent [127]. Flake-based inks are easier to produce and therefore cheaper. Some flake-inks are binder-based, e.g. thermoplastic resins [2].

Because of the flake size and shape, their processing using flexography requires anilox rollers with high cell volume and cell opening for the flakes to be dosed and transferred. If the particle size is too large, few particles will be transferred onto the plate because they cannot fill the anilox cells and are thus held back by the doctor blade. Experiences with other large particles (Bariumtitanate for inorganic electroluminescent displays) [122] reinforce this assumption. Particle sizes in flake-based flexo inks range from diameters of 0.4 μm to 2 μm [104].

General considerations

As the market for printed electronic product is still an emerging one, few products are actually sold [159]. This also affects the ink manufacturers and sometimes leads to short product life cycles. During the course of my research, I have seen and sometimes tested inks that either were on the market for a very short time or did not reach market stage.

Experiences show that some inks vary strongly in their properties between batches. Early printing trials with the ink used in this study (InkTec TEC-PR030) from a different batch resulted in different sheet resistance using the same printing parameters.

3.2.2. Post-processing

To better understand printed silver layers and their behavior, it is essential to also understand the concepts of their conductivity. As explained above, silver inks consist not only of silver particles but also organics, solvents or other additives. Therefore, printed silver layers are usually not or hardly conductive after printing. To convert printed silver layers into conductive silver layers, they require post-processing to bring the individual silver particles into contact and allow for a current to flow.

This section gives a short introduction to post-processing of printed silver layers. At the beginning, I explain the difference between curing and sintering. Then, I give a short overview over several post-processing methods in order to achieve a certain conductivity of printed silver layers.

The difference between curing and sintering

The terminology regarding the post-processing of printed conductive layers is not consistent. Drying, curing, sintering, annealing and others are often used synonymously. The subsequent explanations follow the concepts of Perelaer who stated the difference between curing and sintering in [111]. In this study, I keep to Perelaer's concepts.

Transforming silver ink into a conductive layer requires several stages of post-processing, explained in the following using nanoparticle ink as example, with Figure 3.9 as illustration. Directly after printing, we still have residual solvent in the printed layer (cf. Figure 3.9, 1) that is removed by drying. For some inks, this happens under ambient conditions, for others we need an external heat source like a hot plate or oven. The nanoparticles are still covered with organic coating (cf. Figure 3.9, 2), the layer also most likely still contains other ink residues, e.g. binders. Note that Perelaer includes this stage in the curing.

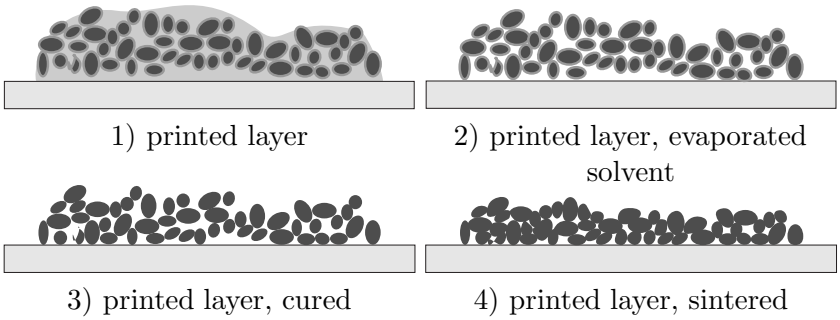

Figure 3.9.: Schematic of printed silver layers at different stages of post processing, following the concepts of [111].

The next step is to remove the coating of the nanoparticles in order to bring them into contact (cf. Figure 3.9, 3). This includes removal of binders and other additives and is usually achieved by a period of heating. After this process, we will already see a certain conductivity [111]. However, the resistivity is still very high as the particles only touch with their surfaces [111] resulting in few, long and narrow paths for current to flow.

The last stage, sintering, involves the actual melting of the particles so they are enabled to form necks between them (cf. Figure 3.9, 4) [111]. This will strongly increase conductivity as the porosity of the layer decreases [111]. As the scaling effect applies to the particle size in nanoparticle inks, the temperature needed for sintering is significantly lower than the melting temperature of bulk silver [132].

The term *sintering* has its origin in powder metallurgy, where metallic powders are condensed and cemented together using heat and/or pressure [38]. Although in printed layers, the materials are dispersed rather than powders, the term is appropriate. Here, small particles are baked together as well, using different energy source as explained in the next sections.

Curing and sintering with heat

The oldest and most common method to cure and sinter printed metallic layers is heating them. Possible equipment for heat treatment of printed layers are hot plates, belt dryers or different kinds of ovens (box, ventilated, vacuum etc.).

With this kind of treatment, not only the printed layer but also possible layer stacks underneath and the substrate will be heated to the specified temperature. Therefore, the respective maximal temperatures should be taken into consideration. Foil substrates usually only withstand temperatures below 150 °C, with more expensive foils (e.g. polyimide) as exceptions.

Photonic curing

Photonic curing [131], also called photonic sintering [158] or flash sintering [162], is a sintering method using a high energy, short length light pulse, commony produced by a Xenon flash lamp.

The basic principle of photonic sintering is the absorption of electromagnetic radiation in the range of visible, near-IR and also UV spectrum by a printed layer, commonly of nanoparticle ink. As the layer absorps the radiation energy, its nanoparticles are heated by the photothermal effect. Due to their size and the scaling effect, they start to melt at temperatures significantly lower than the melting temperature of the respective bulk material.

As this process happens in the millisecond-range, the substrate is hardly affected by the temperatures in the printed layer caused by high energy input. Thus, photonic sintering qualifies for both delicate, heat sensitive substrates and fast processes with high throughput.

Some photonic sintering devices, e.g. those of NovaCentrix, allow for shaping of the light pulses regarding length, height, and even splitting the pulse into micropulses [4]. However, the understanding of the exact mechanisms of how those micropulses affect the samples, especially regarding differences to single pulses is mainly empirical to this date.

Other sintering methods

As a consequence of the fast moving market of printed electronics and the need for post-processing methods for metallic layers on polymer foil, other sintering methods have evolved. Here, I mention three of the more common ones.

Reinhold presented the sintering of printed silver tracks on polymer substrates using low pressure Argon plasma [123]. His results showed resistivities "less than one order of magnitude higher than the bulk value" [123]. Perelaer showed another method of sintering utilizing the selectivity of absorption of microwave radiation [110]. Polymer foils are nearly transparent to microwave radiation while metals readily absorp it and thus heat up [110]. Using this method, silver layers can be sintered within a period of less than one minute [110].

Sintering using a laser was described by Li. The basic principle of laser sintering is the same as with photonic sintering. Due to the energy absorption, the particles heat, melt and form necks. As laser sintering is selective, i.e. the "laser follows the conductive tracks", it does not affect the substrate [88].

3.3. Wet etching

This chapter focuses on wet etching starting with a general introduction to microfabrication, its processes and why wet etching is such an integral part of the process chain. Thereafter, a general description of the wet etching process is given. The chapter concludes with a section elaborating on selected details of some process parameters and materials involved.

3.3.1. Microfabrication techniques

The term *microfabrication* in general refers to the production of electronic, mechanical and electro-mechanical systems in the micrometer- and lately also in the nanometer-scale. This includes all processes and materials necessary to built such devices. Usually, those production processes are implemented in a clean room environment. For historical reasons, the

explanations and details given on those processes refer to wafer shaped samples. A wafer in microfabrication is a thin slice (some ten or hundred micrometer), commonly of silicon.

It is feasible to classify microfabrication processes into how they affect the sample: They can be either additive, thus applying an additional layer or subtractive, meaning the removal of a layer. Also, we distinguish whether a process affects the whole layer (i.e. unstructured) or just parts of it (i.e. patterning, direct writing). Generally, the term for the layer affected by those processes is *functional layer*, which I will also use throughout this thesis.

The following section contains the most common additive and subtractive processes used in microfabrication followed by Table 3.1, compiling and classifying the mentioned processes. The following paragraphs give a general explanation on the most important *additive processes* in microfabrication mentioned in Table 3.1. Details, especially regarding special types, may be obtained from literature such as [45, 49, 61, 98, 152].

CVD In chemical vapor deposition (CVD), an inert carrier gas supports a reactive, thermally instable gaseous precursor into a vacuum chamber, where the non-volatile compounds will condensate onto the substrate, dissociate and form a thin, even layer. A precondition for such processes are gases containing the functional material as a component. Either high temperatures of at least $500 \ldots 1,200\,^{\circ}\mathrm{C}$ on the wafer or in the zone above will induce a process where the reaction takes place directly above the wafer surface. Or two gases will react in the recipient (i.e. the vessel containing the wafer) to a solid phase condensing on the wafer surface and a gas phase. Reaction products not included in the layer formation (i.e. the aforementioned gas phase) are drained from the vacuum chamber. CVD processes provide the deposition of very dense and pure layers. As most chemical processes implemented in CVD are either endothermic or need a certain activation energy this provides a tool to control the deposition by adjusting the applied thermal, plasma or radiation (laser) energy. There are several processes based on CVD but varying on one or the other of the process features. As their names are eponymic, I list them below without further explanation:

- Athmospheric Pressure CVD (APCVD)
- Reduced Pressure CVD (RPCVD)
- Low Pressure CVD (LPCVD)
- Metal Organic CVD (MOCVD)
- Vapour Phase Epitaxy (VPE)
- Plasma Enhanced CVD (PECVD)
- Microwave CVD (MWCVD)
- Laser Assisted CVD (LACVD)

For further details, I refer the reader to the following literature [61, 62, 98, 152].

PVD Physical vapor deposition (PVD) describes a class of processes where the functional material is transferred onto a substrate in a vacuum without additional chemical reactions. The transition of the functional material from solid into gas phase takes place by means of physical processes. The most common methods are evaporation and sputtering. In evaporation, the active material to be deposited is heated until it evaporates. It then precipitates on the surface of the substrate because of the temperature gradient (condensation and adsorption, respectively). This method will not achieve a uniform layer

on very rough substrates due to the direction of the molecule path being perpendicular to the wafer surface. Contrary to evaporation, sputtering uses firing of chemically inert, ionized particles (e.g. Argon) onto a target of active materials to generate a vapor which will then condense on the substrate surface. Physical vapor deposition summarizes several processes which will be given in the following without further explanation [61, 98, 152]:

- Evaporation (including Reactive Evaporation and Ion Assisted Evaporation)
- Sputtering (including DC-/HF-Sputtering, Ion Beam Sputtering and others)
- Molecular Beam Epitaxy (MBE)

Spin Coating Spin Coating is an additive technique depositing from a liquid phase, commonly under ambient conditions in a clean room environment. The substrate is placed on a platform (chuck) with the fluid being dispensed by a syringe or other. The substrate is then put into rotation. The angular acceleration distributes the fluid evenly, creating a uniform layer. The following factors influence the thickness of the dried layer. The rotational speed defines the wet layer thickness: the higher the turning rate u, the lower the thickness. The chuck may be heated to alter the drying rate during the application and thus also adjust the layer thickness. Whereas the solid content c_S and hence the viscosity of the fluid influences the thickness h of the dried layer (cf. Equation 3.1, [152]).

$$h \propto {c_S}^2 \cdot u^{-1/2} \tag{3.1}$$

The most common materials applied by spin coating are varnishes, polyimids, liquid glasses or other diluted solid state materials [61, 152].

Subtractive processes may be subdivided into dry and wet etching technologies. Both ablate whole or partial layers by means of either liquid-phase (i.e. wet etching) or plasma-phase (i.e. dry etching) methods. As wet etching is a central topic of this research, it will be explained in detail in Section 3.3.2. The following paragraphs give a general overview over dry ablation processes. For more detailed information see the pertinent literature of [45, 49, 61, 98, 152].

Plasma Etching In plasma etching, a radio frequency electric field lights a chemically reactive gas into a plasma which than dry etches the wafer surface. Plasma etching requires a vacuum in order for the gas to ignite. A very common application is the dry removal of photoresist after lithography [3].

Ion Beam Etching Ion beam etching (IBE) rates among the physical etching techniques. The ions of a beam of Argon or Xenon directed perpendicular to the wafer surface knock out particles when they reach the functional material. As the loose functional molecules or atoms cannot bind to the inert process gas, they tend to redeposit at the walls or other vertical edges inside the vacuum chamber. To inhibit this behavior, the technique was refined into chemically assisted ion beam etching (CAIBE). It benefits from an additional reactive gas that is able to bind the knocked out particles and helps drain them from the chamber thus resulting in a cleaner process [61].

RIE/DRIE Reactive ion etching (RIE) is a dry etching technique combining physical and chemical processes. High velocity ions are fired onto the functional material thereby activating its surface by weakening or destroying its bonds. Thus, a reactive gaseous

Table 3.1.: Classification of microfabrication processes by way of affection and structuring.

<table>
<tr><th></th><th>unstructured</th><th>patterning via mask</th><th>direct writing</th></tr>
<tr><td rowspan="2">additive</td><td>thermal oxidation
spin coating</td><td>local oxidation of Si</td><td rowspan="2">(screen) printing</td></tr>
<tr><td colspan="2">PVD
CVD
epitaxy
electroplating</td></tr>
<tr><td>subtractive</td><td colspan="2">wet etching
sputter etching
RIE / DRIE
IBE / CAIBE</td><td>FIB
Laser ablation</td></tr>
</table>

agent can access the functional atoms more easily and remove them from the surface. The reaction products are then drained from the vacuum chamber. Due to its easy to control process features such as etching rate, homogeneity and others RIE is the most prevalent dry etching technique. RIE is feasible for both isotropic and anisotropic etch profiles as well as small feature sizes in the range of 100 nm. The Bosch process, generally referred to as deep reactive ion etching (DRIE), is a further level of RIE with cyclically repeating the steps of passivation, commonly oxidation, and RIE of the emerging crevice. It enables high aspect ratios[7] > 200 [15, 61, 76].

FIB Focused ion beam (FIB) etching uses a highly focused ion beam of high mass, commonly from a liquid metal ion source for the structuring of a surface. An optical system of several lenses allows not only focusing of the ion beam but also its shadowing thus further reducing its diameter. The mechanism of action is the same as in RIE, but with smaller attainable feature sizes [49].

Laser ablation Laser ablation describes processes where material is removed from a surface, commonly using a pulsed laser beam. Depending on the energy density brought into the layer, the material is ablated by evaporation, sublimation or, at very high energies, turned into a plasma [10]. Laser ablastion is, like FIB, a direct writing technique. Thus, no mask is needed.

Table 3.1 compiles and summarizes the above mentioned processes in microfabrication and classifies them according to the way they affect the sample and whether or how they pattern the layer, respectively.

As most processes described above affect the whole area of the wafer, we need masks for structuring said layers. The masks used in microfabrication processes can be distinguished between shadow masks and adhesive masks. Shadow masks are "aperture[s with a defined layout] at a defined distance from the substrate surface" [85], usually structuring a functional

[7] The aspect ratio of a shape in this context is its height divided by its width. A high aspect ratio therefore describes a high but lean object.

layer during additive and dry etching processes. Adhesive masks are commonly used for subtractive processes as wet etching and resemble structured, sacrificial layers, applied directly onto the functional layer. The most common material used is photoresist (cf. Section 3.3.3). Adhesive masks allow for very small feature sizes ($< 100\,\mu$m) with high edge definition. They require an inert behavior in order to not affect the active layer underneath [45, 85]. A schematic illustrating both kinds of masks is depicted in Figure 3.10.

Figure 3.10.: Schematic illustrating the difference between a shadow mask (left) and an adhesive maks (right). Adhesive masks are commonly used for wet etching.

Combining some of the above mentioned processes, we obtain one of the core processes in microfabrication: photolithography or lithography, which is actually not a single process but rather a section of a process chain. Its goal is the structuring of a functional layer using an adhesive mask. Photolithography is split into the following process steps (cf. [5, 61]) with Figure 3.11 illustrating them schematically. Note that optional steps are not included in the figure.

1. Application of a solid layer of functional material (e.g. by CVD or PVD).
2. Application of a solid layer of resist, commonly an organic photoresist, being an "emulsion of an organic monomer in a suitably volatile carrier liquid" [5] (e.g. by spin coating).
3. Optional: Soft bake step to cure the resist layer.
4. Patterning of the resist layer by exposure to an electromagnetic radiation source with wavelength lower than $\lambda = 400\,$nm, usually UV radiation, an electron- or X-ray-beam.
5. Developing of the resist to remove unwanted areas of the layer.
6. Optional: Hard bake step to further anneal the resist structures.
7. Etching to transfer the layout of the resist into the functional layer.
8. Removal of residual resist, also called stripping.

I include etching and stripping (steps 7 and 8, cf. Figure 3.11, 7a, 7b, 8) into lithography although some authors see them as separate steps, e.g. Jackson [76, 125].

3.3.2. General process description of wet etching

Etching is a subtractive process where chemical or physical reactions remove material from a functional layer. The essence of etching processes is the interaction of particles from a mobile phase (i.e. etchant or etching agent) with particles on the surface of a solid (i.e. functional layer) such that the latter will leave the solid. It is necessary to distinguish between two types of etchants: liquid-phase (also called wet etching) and plasma-phase (also called dry etching) [84].

Two different tasks can be assigned to an etching process in microfabrication: First, the ablation of an entire top layer (e.g. for cleansing) and second, the removal of unwanted areas thus creating either small, individual structures or cavities. An illustration of the assignments of etch processes is depicted in Figure 3.12: 1) illustrates the ablation of a certain thickness of the whole layer, 2a) exemplifies the forming of small structures by removing the material in-between and 2b) depicts the creation of individual cavities.

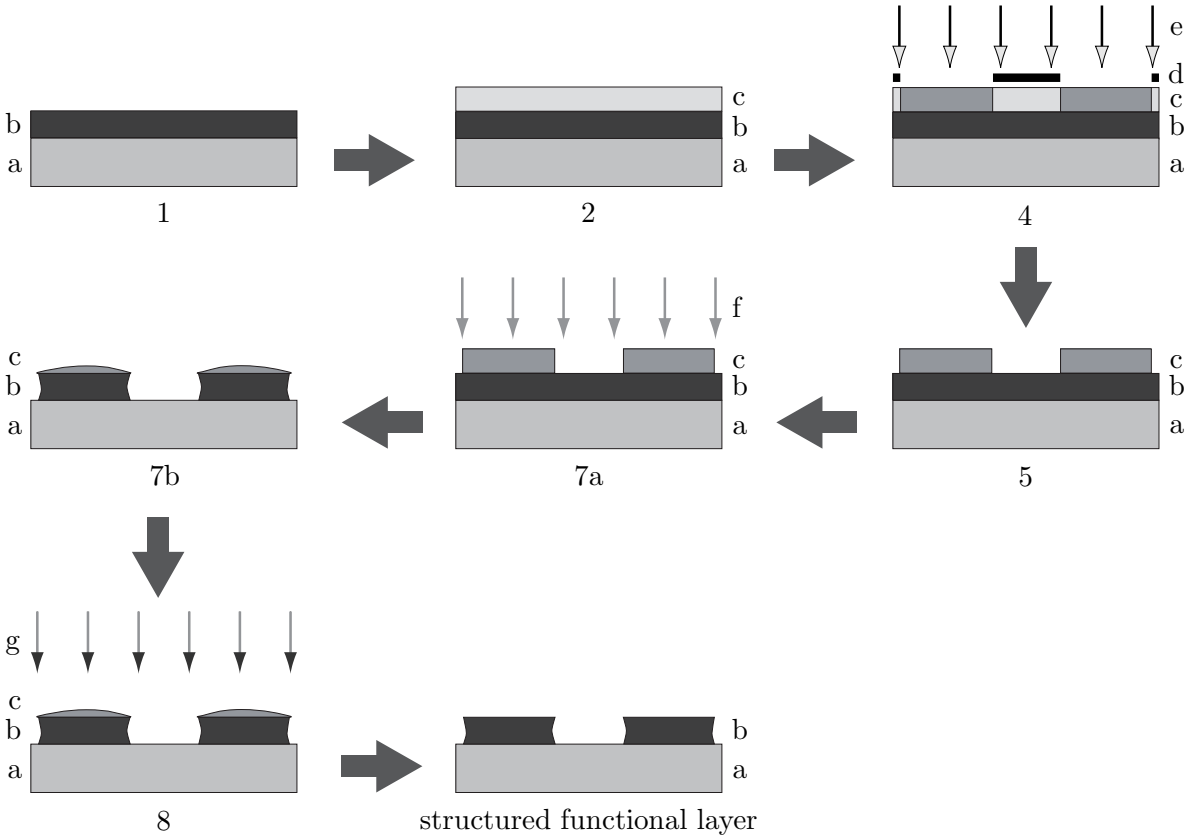

Figure 3.11.: Schematic of a photolithographic process in inorganic semiconductor device production with a) substrate, b) functional layer, c) resist, d) shadow mask, e) electromagnetic radiation, f) etchant, and g) stripping agent. The numbers indicate the process steps as described above.

Wet etching consists of two interacting mechanisms: chemical interactions between the etchant and the functional or resist layer, respectively and transportation mechanisms moving the particles in the etchant and at the surface of the solid. Transportation processes consist of three steps. First, the active particles in the etchant move to the surface of the wafer where they start the etching. In a second step, they enter the solid phase of the sample. And last, the detached functional particles are moved away from the solid surface [84].

The difference in concentration in the etchant generates a mass transport and thus the movement of particles: If the particle distribution is not uniform, their thermal energy drives them to thoroughly mix the substances thus reducing the gradient of concentration [84].

Near the surface, the interacting particles form an imaginary layer of high diffusion. The thickness of said layer depends on the viscosity of the etchant and convection being present. The layer properties, especially its thickness, strongly influence the etching rate: The higher the concentration gradient, the higher is the velocity of diffusion and thus the etching rate. Hence, a thin diffusion layer will shorten the distance functional particles will have to cross to leave the diffusion layer. Several options may also speed up the etching rate: Convection accelerates the transportation process and moving the sample in the etchant increases the concentration gradient [84].

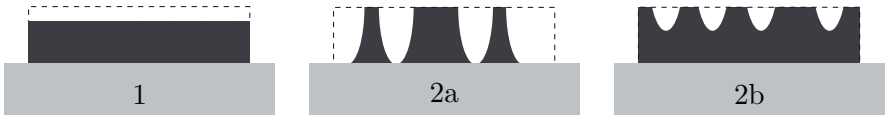

Figure 3.12.: Assignments of etch processes: 1) ablation of top layer, 2a) creation of small structures, 2b) creation of cavities.

Wet etching processes in non-monocrystalline materials are almost always isotropic, i.e. the etching rate is constant in all spatial directions. Thus, material is evenly removed in all directions as well. As a consequence, underetching is inevitable. The term *underetching* describes the lateral ablation of the functional layer underneath the adhesive mask.

Anisotropic etching implies the ablation of material only in a certain direction, e.g. perpendicular to the solid surface. Hence, the layout of the mask layer is precisely transferred to the functional layer [61]. This occurs mostly in dry etching processes.

When etching materials made of crystal lattices, anisotropic etching also results in structures parallel to certain crystal directions. A good example is monocrystalline silicon, where trapezoidal shaped trenches with side walls angled 54.7° are common, due to the orientation of the {111}-plane [45].

Vossen describes several etching techniques for wet etching in [154]. Although this book dates back to 1978, the basic principles remain the same and these etching techniques are still widespread today. Thus, I give a short introduction into the some techniques, according to Vossen in the following.

Immersion etching Here, the sample is completely submerged in the etchant. Note that the volume of the etchant should be sufficiently high to avoid "reactant depletion" [154]. Moving the sample in the etchant ensures an even etching rate [154].

Spray etching In spray etching, the etchant is applied to the sample using a spray thus ensuring "good process control and uniformity" [154] as the etchant constantly renews and removes reaction products in the process [154]. Spray etching usually is the basis of continuous etching systems in industry, prevalent for printed circuit board production.

Electrolytic etching A significantly more complicated but better controllable etching technique is electrolytic etching. Here, an electromagnetic field is applied to the sample (anode) thus allowing metal ions to leave its surface and move to the cathode. By adjusting the electric field, we can control the etching process [154].

3.3.3. Selected details of the wet etching process

The following section gives a more detailed view on the process of wet etching, starting with an overview of the most common and important parameters characterizing the process. Following, the interaction between etchant and functional layer comes into focus. The section will be concluded by a circumstantial look on the etch resist and its properties.

Parameters characterizing the etching process

To characterize the etching process, we require several physical quantities and figures of merit. Subsequently, the most important definitions are given.

The etching rate r of a solid matter (e.g. functional layer) defines the layer thickness being ablated in a certain amount of time (cf. Equation 3.2, [84]). In wet etching, its value mainly depends on the combination of functional layer and etchant and the concentration of the etchant. The etching rate of the resist is given the index *res*, thus it is r_{res}. Generally, the unit of the etching rate is specified in unit of length per unit of time, depending on the specific process and its velocity, either in [μm/s] or [nm/s].

$$r = \frac{h_{etch}}{t_{etch}} \tag{3.2}$$

As the etching rate r in isotropic etching is uniform in all directions, the etching rate underneath the edge of the mask in horizontal direction r_H equals the etching rate perpendicular to it, thus the rate of layer ablation (cf. Equation 3.3, [84]). The horizontal etching rate r_H is specified in the same unit as the etching rate r. Note that in wet etching, the undercutting may be significantly higher than the thickness of the ablated layer because the lateral etching rate often accelerates at the end of an etching process [84].

$$r_H = r \qquad \text{(for isotropic etching)} \tag{3.3}$$

Undercutting describes the etched length parallel to and directly underneath the resist layer. It is a concomitant phenomenon of isotropic etching as the etching rate here is uniform in all directions. Concluding from Equation 3.2 and Equation 3.3, the length of the undercutting l_{Ui} equals the etched depth of the layer (cf. Equation 3.4, [84]). Depending on the relevant structure sizes, the undercutting length generally is given in [μm] or [nm].

$$l_{Ui} = h_{etch} \qquad \text{(for isotropic etching)} \tag{3.4}$$

The degree of anisotropy γ rates the direction dependent tendencies of material properties. If the ratio of the etching rate perpendicular to r_H and in etching direction r are equal, the degree of anisotropy will equal zero (cf. Equation 3.5, [84]). The lower the horizontal etching rate is, the higher γ will be. The degree of anisotropy is without unit.

$$\gamma = 1 - \frac{r_H}{r} \tag{3.5}$$

In practice, most processes are neither exclusively isotropic nor exclusively anisotropic but rather a combination of both. For those cases, the length of undercutting l_{Ua} can be calculated using the degree of anisotropy γ described above (cf. Equation 3.6, [84]). As with isotropic undercutting l_{Ui}, the anisotropic length of undercutting l_{Ua} generally is given in [μm] or [nm].

$$l_{Ua} = (1 - \gamma) \cdot h_{etch} \qquad \text{(for } (0 < \gamma < 1)\text{)} \tag{3.6}$$

A figure of merit of etching processes is the selectivity of the etching agent S_{etch}. It describes the relation of the etching rate of the functional material (r) and the resist material r_{res} (cf. Equation 3.7, [84]).

$$S_{etch} = \frac{r}{r_{res}} \tag{3.7}$$

Generally, a high selectivity is desired to ensure the necessary removal of the functional layer without removing too much of the resist layer. As the selectivity describes a ratio of two etching rates, it is without unit.

Etchant and functional layer

As mentioned above, the etching rate predominantly depends on the etchant and how it affects the functional layer. Common etchants for silver used in microfabrication are shown in Table 3.2. Note that the etching rates literature gives for this agents only apply to bulk silver[8]. They will be significantly different (i.e. higher) for printed silver layers as explained in the following section.

Table 3.2.: Etchants for silver as used in microfabrication with their respective etching rates.

etchant	contents	etching rate (bulk silver)	references
thiourea-iron nitrate-ammonium fluoride solution	$Fe(NO_3)_3$ NH_4F $CS(NH_2)_2$	5 nm/s	[84]
	10 g $Fe(NO_3)_3$, 9 ml H_2O; 44 . . . 49 °C	20 μm/min	[154]
nitric acid	HNO_3	very fast, not suitable for small structures	[84]
iodine-potassium iodide solution	KI, I_2	300 . . . 1,000 nm/s	[84, 154]
ammoniacal-methanole hydrogen peroxide solution	NH_3, H_2O_2, CH_3OH, H_2O	5 nm/s	[84]
	$4CH_3OH$, $1NH_4OH$, $1H_2O_2$	6 nm/s	[154]
	$1H_2O_2$ (35%) NH_4OH (25% NH_3) CH_3OH H_2O	3 nm/s	[152, 154]
phosphoric acid, mixed with nitric acid diluted in a.p.	H_3PO_4, HNO_3, H_2O	unknown	[141]

Commonly, we etch metals in electroless etching processes. Still, they consist of an intrinsic anodic and a cathodic partial process. The following paragraphs elucidate on the processes of etching an arbitrary metal. In the anodic partial process (oxidation), the metal (M) builds the

[8] Globisch refers to bulk silver as basic material [49]. In this context, bulk silver refers to dense silver layers obtained by e.g. CVD or melting as opposed to printed silver layers that are still porous, possibly with residual additives.

ionic form with M^{z+} as the metal ions, z a control variable and e^- an electron (cf. Equation 3.8, [84]) whereas the number of released electrons equals the charge of the metall ion [84, 154].

$$\mathsf{M} \rightarrow \mathsf{M}^{z+} + z \cdot e^- \tag{3.8}$$

To maintain the reaction, we need an oxidant (OX) to bind the released electrons. This is the cathodic partial process (reduction, cf. Equation 3.9, [84]). Note the control variable y.

$$\mathsf{OM} + y \cdot e^- \rightarrow \mathsf{OX}^{y-} \tag{3.9}$$

Thus, we obtain the overall reaction equation as presented in Equation 3.10 [84].

$$y \cdot \mathsf{M} + z \cdot \mathsf{OX} \rightarrow y \cdot \mathsf{M}^{z+} + z\mathsf{OX}^{y-} \tag{3.10}$$

The etching rate of metals in an electroless etching process, i.e. without external power feed, may be calculated according to the following equations (following [84]). As the etching rate r of metals is defined by the intensity of the anodic partial process, it is proportional the anodic partial current I_+ being interchanged over the surface of the functional layer A_+, which equals the partial current density i_+ (cf. Equation 3.11) [84].

$$i_+ = \frac{I_+}{A_+} \tag{3.11}$$

To balance the charges in the reaction, we use Faraday's Law in Equation 3.12 with n being the number of ions present, z their valency and F the Faraday constant[9].

$$I_+ \cdot t = n \cdot z_+ \cdot \mathsf{F} \tag{3.12}$$

With Equation 3.12 and Equation 3.13 which calculates the number of ions from mass m, molar mass M or density ρ, Volume V, molar mass M, respectively, we obtain Equation 3.14 [84].

$$n = \frac{m}{M} = \rho \cdot \frac{V}{M} \tag{3.13}$$

$$i_+ \cdot A_+ \cdot t = \rho \cdot \frac{V}{M} \cdot z_+ \cdot \mathsf{F} \tag{3.14}$$

Transposing Equation 3.14, we obtain the etching rate for metals in currentless etching processes depending on the partial current density, the Faraday constant, the molar mass, the ions' valency and the density of the metal (cf. Equation 3.15, [84]).

$$r = \frac{i_+}{\mathsf{F}} \cdot \frac{M}{z_+ \cdot \rho} \tag{3.15}$$

Unfortunately, we will not be able to calculate the exact etching rate of printed silver layers as silver fluids intended for printing commonly contain not only silver but also solvents, binders, dispersing agents and other additives such as surfactants. The wet layer applied onto the substrate consists only of about $40\,wt.\%$ of silver [73]. Therefore, the etching rate calculated for silver is not valid for the whole layer as the additives from the ink have different etching rates. The overall etching rate is a combination of those.

[9] $\mathsf{F} = 9.64853399(24) \cdot 10^4\,\mathrm{C/mol}^{-1}$ [84]

In the past, curing processes in printed electronics were mainly drying-based, meaning the evaporation of the solvent. Binders and other additives remain in the dried layer. The silver particles in the layer, due to their shape, only touch at small spots on their surface, thus resulting in a low conductivity and a high sheet resistance.

Lately, sintering techniques with low thermal effect on the substrate emerged using short light flashes (i.e. flash sintering or photonic curing). They use a microsecond broad band light pulse with a high energy density. The silver layer will absorb the light whereas the absorption range of the substrate (usually PET film) hardly overlaps with the spectrum of the lamp. Thus, the substrate stays relatively cool whereas the silver layer will be heated to high temperatures. Because of the high amount of energy brought into the silver layer and scaling effects[10] of the silver particles they will actually melt and combine to a coherent layer [132].

Still, this layer is not comparable to bulk silver regarding its density due to its sponge-like texture created by voids binders and additives left after their thermal removal. The free surface is substantially higher than a layer of bulk silver with the same area. Therefore, we expect a higher etching rate as the etchant can affect the silver at a higher amount of surface.

Etch resist

Structured etching commonly requires an adhesive mask typically provided by a structured etch resist. Generally, two types of resists can be discerned: Positive and negative ones. They differ by their behavior during patterning. Figure 3.13 shows a schematic of the patterning process of both types of resists, using UV radiation.

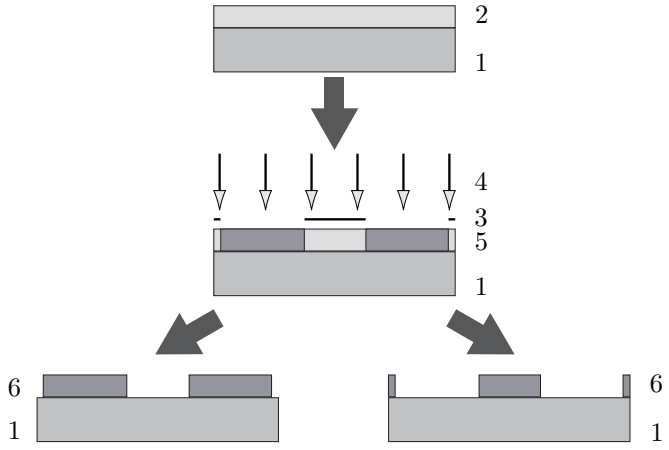

Figure 3.13.: Schematic of structuring negative (left) and positive (right) etch resist materials with 1) substrate, 2) resist (not crosslinked), 3) shadow mask, 4) UV radiation, 5) resist layer (partially crosslinked), 6) resist layer (structured, fully crosslinked).

Positive resists display a positive image of the mask. I.e., the open areas of the mask result in empty areas in the resist layer (cf. Figure 3.13, right). Negative resists behave vice versa: When the UV radiation passes through the open areas of the mask, it starts a polymerization

[10] As the size of a particle decreases down to nanometer-scale, their surface becomes more important because the ratio of surface to volume increases significantly. Thus, the properties of the bulk material become less important with surface related properties increasing.

resulting in solidified areas in the resist layer (cf. Figure 3.13, left). PMMA, the resist material used in this study, behaves as a positive resist when used in a lithographic process (cf. Figure 3.13, right).

Subsequent to exposure, the non-polymerized parts of the resist layer have to be removed. This process step is called development. Commonly, organic solvents serve as developer agents to dissolve the non-solidified parts of the resist layer. For the removal of residual unwanted resist, an additional processing step with oxygen plasma is an option [3].

As they provide higher resolutions resulting in smaller feature sizes, "thinner resist layers are preferred for nanostructures" [85]. Resists acting as adhesive masks require several properties, where the most important one is a certain resistance to the etchant used [85]. This resistance reflects in the etching rate of the resist r_{res} which should be significantly higher than the etching rate of the functional layer r to provide a sufficient selectivity as explained above in Equation 3.7.

Another necessary property of the resist layer is a sufficient adhesion to the substrate, in this case the functional layer. This interface needs to be highly stable [85] to provide sufficient protection of the functional layer and inhibit the etchant to affect the protected areas of the functional layer.

3.4. Microfabrication and printing

Essentially, flexographic printing is a production method which applies structured layers commonly with thicknesses of about $0.75 \ldots 2\,\mu$m [147] successively with a register accuracy of about $+/-0.5\,$mm in industrial flexographic printing presses [18]. The lowest reproducible feature size in lateral dimension has to be larger than $10\,\mu$m in flexography [143].

Table 3.3.: Printing and microfabrication - overview of advantages and drawbacks.

	printing	microfabrication
advantages	ambient conditions fast processing low cost	smaller feature sizes higher layer quality (purer materials)
drawbacks	low accuracy material limitations elaborate materials needed (fluids where solvents and additives need removal)	long processing time complex processes mostly vacuum environment needed

Microfabrication originated from the production of integrated electronic components and printed circuit boards (microelectronics production). Integral part of this field is the application, structuring and removal of layers in a micrometer and sub-micrometer range in all spatial directions. Here, register accuracies lower than $0.5\,\mu$m [49] and feature sizes in the submicrometer range are common. As the feature sizes decreased in the last years, the term *nanofabrication* became fashionable.

When comparing the description of both printing and microfabrication, it becomes apparent that the origin of both lies in the patterning of planar layers. Nevertheless, both serve different goals: microfabrication intends to provide certain, mostly electrical functionalities of the layers whereas printed layers in the graphical industry relay certain visual information. Still, both areas do have many common elements. Printing is even an integral part of electronics fabrication since the first printed cicuit board was introduced by Eisler in the early 20th century [83]. Basically, the additive application of a material in microfabrication is printing, according to the definition of the Institute of Printing Science and Technology: Printing is the "reproduction of structures by transferring matter [...] onto a surface by means of mechanical contact [...], hydrodynamics or electromagnetic fields" [146].

Table 3.3 summarizes the advantages and drawbacks of printing and microfabrication. Where printing represents fast processing under ambient conditions, microfabrication represents complex processes, usually involving vacuum and/or a clean room environment. On the other hand are accuracy, feature size and layer quality better in microfabrication than in printing. Both fields of research have their specific applications and particular features. This is one of the reasons, combinations of both topics are a focal point of today's research.

4. Measurement techniques and experiments

This chapter elucidates on the experimental part of this study. Starting with a short introduction to the most important parameters of the printing and etching trials as well as their characterization, it segues into the techniques of their measurement. The second part of this chapter describes the actual experiments, the equipment I used and how I conducted the printing and etching trials.

4.1. Properties of printed layers and the corresponding measurement techniques

This section gives an overview over the parameters most important for this study and the techniques necessary for their measurement. Predominantly, those are properties of printed layers and the respective materials. I start with geometric parameters, then introduce some electrical parameters important for conductive layers and end the section with miscellaneous properties.

4.1.1. Geometric parameters

When characterizing the impression after a printing trial, we discern whether the layout is a large area or fine structures, e.g. lines. Both have their respective applications and thus, different requirements. Some parameters describing the impression of both large, solid areas and small structures are the same and some are specific for each of them. This section explains the most important parameters characterizing printed solid areas and printed line structures.

Properties of solid areas

The most important properties of printed solid areas in FOLAE are homogeneity, surface roughness and thickness. Their lateral geometric parameters and the sharpness of their edges are usually less important, because of their usage as dielectric or semi-conducting layers or as plate electrodes where layer integrity across the area is essential while edges may often be neglected as they are outside the electrical active area.

The homogeneity of a functional layer defines its electrical properties as Hernandez-Sosa et al. illustrated in [60]. Several units of merit describe the homogeneity of a layer [60]. Stahl defines the homogeneity of a layer in [140] as its waviness and thus the deviation of the layer thickness from a mean value. Note that he disregards a waviness less than a few micrometers [140]. Bornemann links the homogeneity of a layer to its roughness [21].

There are several parameters describing the roughness of a surface. Equation 4.1 gives on of the most common ones, the average surface roughness $\mathbf{R}_q$, also RMS (root mean square). The height information is represented by h, the lateral coordinates by x_m and y_n with M and N as control variables, following [38]. It represents the arithmetic mean of absolute deviations within a reference length.

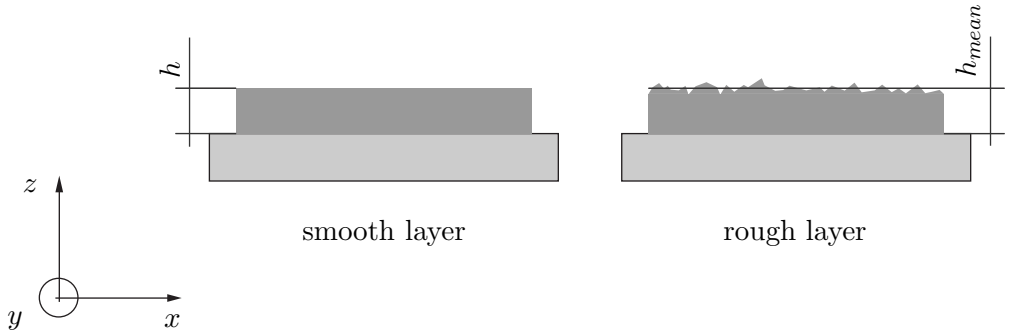

Figure 4.1.: Schematic cross section of layer roughness in solid areas. Left: smooth surface and right: rough surface.

$$\mathbf{R}_q = \sqrt{\frac{1}{MN}\sum_{m=1}^{M}\sum_{n=1}^{N}\left(z(x_m, y_n) - \langle z\rangle\right)^2} \tag{4.1}$$

We assume that the reference plane for calculation of $\mathbf{R}_q$ is parallel to the xy-plane. The unit of the average surface roughness $\mathbf{R}_q$ is a unit of length, depending on the roughness given either in [μm] or [nm]. Figure 4.1 illustrates schematically a smooth (left) and a rough (right) layer. Note that $\mathbf{R}_q$ does not distinguish between peaks and troughs.

The layer thickness h, typically given in [μm] or [nm], indicates the distance between top and bottom of a specific layer. As printed layers tend to be not very homogeneous, the thickness is usually an average value over a certain area (cf. Figure 4.1, right: h_{mean}). Depending on the roughness of the layer surface, the mean thickness is more or less accurate.

ISO 13660 gives several attributes of printed solid layers. The standard is intended for printed monochromatic text and images. Table 4.1 lists and assesses the respective attributes for printed electronics. The darkness of a large area has no effect in printed electronics. Extraneous marks in the background may affect the functionality of printed devices. This is especially applicable if the marks occur in a layer stack which is very sensible to thickness variations and misplaced materials. The best example is an organic field effect transistor (OFET): If a speck of conductive material from one of the electrodes is in the channel, in the semiconducting or even the dielectric layer, we will most likely get a short circuit thus rendering the OFET faulty. The layer attributes graininess, mottle and especially voids from ISO 13660 can be translated into homogeneity parameters in printed electronics.

Table 4.1.: Attributes of large, printed areas according to ISO 13660 [1] and their applicability for printed electronics.

ISO 13660	applicability for printed electronics
darkness, large area	not applicable
graininess	homogeneity, small scale undulations
mottle	homogeneity, larger scale undulations
extraneous marks, background	limited applicable
void	homogeneity

Properties of printed line structures

Contrary to solid areas, printed line structures require several parameters defining their lateral and, if applicable, their vertical geometry. Roughness is usually less important than edge sharpness. In FOLAE, printed lines are commonly used as electrode structures or conductive paths.

We can describe printed lines by means of lateral and vertical properties. The most important lateral ones are length and width, the most common vertical one is height. By nature, printed lines do not resemble ideal geometrical lines: they are not necessarily straight, their cross section is usually not a rectangle as expected and their ends are often differently shaped than the middle section. Thus, the properties length, width and height are not sufficient to describe printed lines, especially in printed electronics.

Figure 4.2.: Schematic of printed line, divided into three sections: one middle section (M) and two similar end sections (E).

To characterize printed lines, we need more properties than the ones described above. Illustrated by Figure 4.2, we can divide arbritratry straight printed lines into a middle section (cf. Figure 4.2, M) with similiar "ends" on both sides (cf. Figure 4.2, E). When talking about printed lines and their cross section, we generally consider the middle section and disregard the ends.

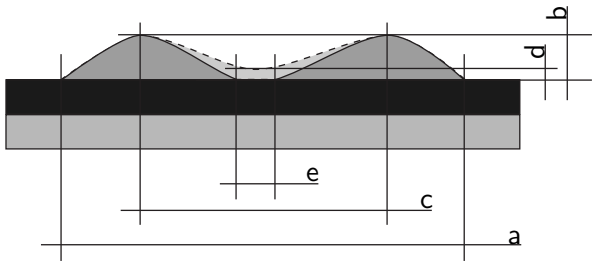

Figure 4.3.: Cross section of a printed line labeling the parameters as used in Figure 4.14: a) width overall; b) peak height; c) peak distance; d) height of valley; e) width of gap.

Duineveld describes a similar approach for inkjet printed lines composed of single drops: "The lines are clearly somewhat more widened at the start, probably because in this phase the pattern changes from one with a truncated spherical symmetry (drop) to a truncated cylinder symmetry (line)" [39]. However, this approach is not sufficient for characterizing lines printed by flexography. Disregarding their ends, their cross section does not resemble a truncated cylinder. This is due to the nature of the ink transfer in flexography. The ink sits on top of the raised line shaped element of the plate. While transferring the ink from the plate onto the substrate, the thin raised line of the plate dips into the ink layer on the substrate, thus the cross section in this moment resembles two peaks with a valley in-between (cf. Figure

4.3). Depending on the ink and the actual geometry of the element, the surface tension of the ink may level the two peaks into a cross section resembling more of the shape of half an ellipse or even circle.

Figure 4.3 illustrates some geometric parameters of printed lines in flexographic printing by means of a cross section. As already described in Chapter 3.1.3, flexographic printed elements show a halo around the edges. When printing a very narrow line, the actual line may not be visible any more. The impression will only show the halo with a more or less pronounced void in-between. Thus, the cross section of such a line will show two peaks with a valley between them.

We can obtain attributes of printed lines from ISO 13660. Some attributes are applicable for printed electronics, others do not apply for this topic. Table 4.2 lists some of the attributes of printed lines [1] and assesses their applicability for printed electronics.

Table 4.2.: Attributes of printed lines according to ISO 13660 [1] and their applicability for printed electronics.

ISO 13660	applicability for printed electronics
blurriness	limited applicable
raggedness	very important, cf. viscous fingering and formation of dendrites
line width	very important
darkness	limited applicable
contrast	not applicable
fill	homogeneity
extraneous marks	limited applicable
background haze	limited applicable

ISO 13660 defines line width as "the width of the line measured normal to the line from edge threshold to edge threshold" and blurriness as "hazy or indistinct in outline; a noticeable transition of blackness from background to character" [1]. The line width from ISO 13660 corresponds to the width overall a (cf. Figure 4.3) in this study. Blurriness has no corresponding parameter in this study but may be applied to edge sharpness of e.g. conductive traces in printed electronics. This also applies to raggedness. Darkness, contrast, extraneous marks and background haze have limited applicability in printed electronics and can therefore be neglected here.

Determining the homogeneity of printed layers

Haas presents in [53] a method to determine the homogeneity of transparent printed films using direct shadowgraphy. As shadowgraphy highlights thickness variations and curvature of layers, these properties show as "derivatives of the intensity" of captured images converted to gray scale [53]. The higher the derivative of the intensity is in a spot, the higher is the deviation of the layer thickness in this spot from the neighboring one. A high count of spots with high derivatives in a measured area indicate a low homogeneity. Haas defines the homogeneity rate as the ratio of "number of points of recorded digital image where absolute value of intensity gradient is below noise threshold" by area of this spot [53].

In [140], Stahl develops a technique to measure the homogeneity of printed, transparent layers using absorption. He defines the homogeneity of a printed layer as the coefficent of variation of a matrix of the surface. Low coefficents of variations indicate high homogeneity [140].

As the silver layer used in this study is opaque, we can apply none of the above described methods. We can, however, assess the printed layers using microscopy or interferometry as explained below and utilizing the layer roughness as indicator for the homogeneity as proposed by Bornemann [21].

Confocal microsocopy

For a three-dimensional characterization of the printed test strips, I used a confocal microscope Sensofar Plu neox. This microscope offers an objective with an enlargement of 50 times and a high numerical abberation of 0.95. This allows the user to obtain a good and valid three-dimensional measurement of very sharp edges with steep flanks.

Confocal microscopy "relies on the optical sectioning effect of pinholes for illumination and imaging" [28]. A pointed light source and a pinhole exclude light that is not in the focal plane. Hence, only the areas of the sample that are in the same focal plane provide light for the image [28].

With a provision for moving the objective in vertical direction, one for providing the respective height information and an appropriate image processing software, three-dimensional topographies of a surface can be obtained [28].

As confocal microscopy uses light, which is non-destructive to the surface, it does not damage the sample. Compared to mechanical profilometry (i.e. using a stylus), it is also much faster [28].

Whitelight Interferometry

For some layers, it is more expedient to use interferometry instead of confocal microscopy to measure their surface structure or obtain three-dimensional images of the sample.

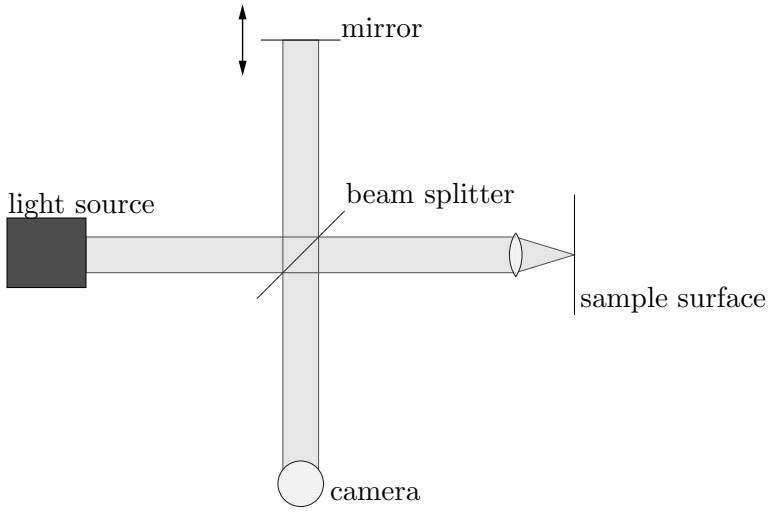

Figure 4.4.: Functional principle of a whitelight interferometer, following [59].

The working principle of an interferometer as used in this study is the superimposition of beams of coherent light. A beam of light, here: white light of narrow band width, is sent onto the sample surface. On its way back, it is superimposed on a reference image (created by the mirror, cf. Figure 4.4) [59]. In areas with the same optical path length, constructive interference occurs. When capturing this interference on a screen or detector, we obtain a pattern of lighter and darker shades. By moving the mirror, every height of the sample surface can be compared to the reference image. With knowledge of the respective height information of the mirror and appropriate image processing software, a complete profile of the surface topography may be obtained [48].

$$l_C = \frac{{\lambda_m}^2}{\Delta\lambda} \tag{4.2}$$

Equation 4.2 shows the calculation of the coherence length l_C from the mean wavelength λ_m and the spectral range $\Delta\lambda$ [48].

$$\delta = \frac{0.61\lambda_m}{NA} \tag{4.3}$$

Using the mean wavelength λ_m and the numerical aperture NA of the imaging optics used, we can also calculate the lateral resolution δ being possible with this system (cf. Equation 4.3) [59]. The white light interferometer used in this study is a Sensofar Plu neox with a lateral resolution δ of 0.31 μm in the highest magnification of 50× [133].

Optical microscope

I conducted two-dimensional optical measurements using an optical microscope Leica DM4000. With this microscope and the appropriate software[1], it is possible to measure lateral distances in images taken with a magnification factor of up to 100.

Optical images with a lower enlargement may be obtained to get an overview of the sample. Then, specific details of the sample may be investigated with an objective allowing for higher enlargements.

Note that optical microscopy as introduced here only allows for two-dimensional images without any information about layer thickness. It is feasible to investigate the homogeneity of a layer using transmitted light mode where the sample is placed between illumination source and camera. Thus, holes and areas with low layer thicknesses may be observed as lighter and darker shades in the obtained image.

Using incident lighting, the sample surface may be observed as variations in the lightness of the imaged layer. Here, also the coloring of the surface should be taken into account.

4.1.2. Electrical properties

Each layer in printed electronics has a certain function, typically an electrical one. Therefore, we need physical values to characterize the properties of a layer. The following section introduces the most important values in this thesis for measuring the electrical properties of a layer.

[1] Leica Application Suite, Version 3.7.0.

Resistivity

Resistivity ρ is an intrinsic material property describing the current flow through the material (at a given temperature), cf. Equation 4.4 [75]. The higher the resistivity the more difficult is the flow of electrons. Resistivity typically is specified in [Ωm].

$$\rho = R \cdot \frac{A}{l} \tag{4.4}$$

Conductivity

Conductivity σ is the inverse of resistivity (cf. Equation 4.5 [75]). Thus, it quantifies the current flow through a material as well. A high conductivity implies an easy flow of electrons. The unit for conductivity is specified in Siemens per meter [S/m].

$$\sigma = \frac{1}{\rho} \tag{4.5}$$

As both conductivity and resistivity are "intrinsic physical propert[ies, they are] independent of the particular size or shape of [a] sample" [155].

Sheet resistance

"The sheet resistance is numerically equal to the measured resistance of a square piece of the material" [155]. It does not depend on the size of the square measured but implies a thin layer of the material.

$$R_{\square} = \frac{\rho}{h} \tag{4.6}$$

The sheet resistance can also be calculated from the resistivity ρ of a material and its known layer thickness h (cf. Equation 4.6). The physically correct unit for sheet resistance is [Ω], but [Ω/□] (Ohm per square) is widely used to differentiate from resistance R [155].

Determining electrical parameters using van der Pauw-theory

The measurements of the specific resistivity were conducted by using a measuring station consisting of a probe station (Intertek) with 4 needle holders (Carl Suss) and two source-meter units (Keithley 2400). I determined the specific resistivity using the *van der Pauw*-theory.

Van der Pauw showed in [150] that it is possible to measure the specific resistivity of a sample by placing four contacts (A, B, C, D) along the circumference and measuring the resistance $R_{AB,CD}$, $R_{BC,DA}$ and the thickness of the layer. This method is applicable, if the sample is flat, has an even layer thickness to be measured and the contacts are "sufficiently small" [150]. The shape of the area may be arbitrary as long as it is continuous, thus without holes [150].

In this thesis, the areas measured are rectangular, with the contacts placed at the corners of the area (cf. Figure 4.5). Van der Pauw defines the resistance $R_{AB,CD}$ "as the potential difference $V_D - V_C$ between the contacts D and C per unit current through the contacts A and B" [150]. The resistance $R_{BC,DA}$ is defined analogically.

$$e^{-\pi R_{AB,CD} h/\rho} + e^{-\pi R_{BC,DA} h/\rho} = 1 \tag{4.7}$$

Figure 4.5.: Measurement electrodes A, B, C, D placed on the circumference of a rectangular sample.

Equation 4.7 shows the relation of $R_{AB,CD}$ and $R_{BC,DA}$ and can be transposed as a solution of ρ

$$\rho = \frac{\pi h}{\ln 2} \frac{(R_{AB,CD} + R_{BC,DA})}{2} f\left(\frac{R_{AB,CD}}{R_{BC,DA}}\right) \tag{4.8}$$

with f being the correction factor, a function of the ratio $R_{AB,CD}/R_{BC,DA}$ and h being the layer thickness. The derivation of f (Equation 4.8) can be obtained from [150]. Basically, it gives an indication of the isotropy of the sample material. The lower f is, the lower is the isotropy.

As the thicknesses of the measured samples for this thesis can be assumed as equal, I use the sheet resistance $R_\square$, rather than the specific resistivity. The sheet resistance can also be obtained using the *van der Pauw* method if the layer thickness h is not included (cf. Equation 4.6).

4.1.3. Other properties

This section explains two parameters that are relevant for this study, but may not be assigned to the topics above. The first elucidates on the surface tension of liquids and solids and the second on the etching rate.

Surface tension

Solids and fluids are held together by intermolecular forces. These forces attempt to minimize a surface by reducing the number of molecules present at the surface as this is their energetic optimum [7]. The surface tension is a measure for these forces: It indicates the amount of energy needed to create a surface by adding molecules to the surface [7].

We can determine the surface energy of a liquid by analyzing the shape of a drop hanging from a capillary or the shape of a sessile drop on a surface with known properties. The theory of Owens, Wendth, Rabel and Kaelble states that the surface energy may be divided into a disperse and a polar fraction. Using several known liquids and measuring their contact angle on the solid surface, determination fo the surface energy of the solid is possible [107].

To illustrate those measurements, diagrams with the polar fraction plotted against the disperse fraction of the surface energy are common. The plotted data is the solution of the Owens-Wendth-theory for a contact angle of 90 °C. The area between both axes, the abszissa for the disperse and the ordinate for the polar fraction of the surface energy, form the so called wetting envelope (cf. Figure 4.6). From this plot, it is possible to predict whether a liquid will wet this surface: If the surface tension of the liquid lies within the wetting envelope, its contact angle is less than 90 °C and thus it will wet the surface. If the surface tension of

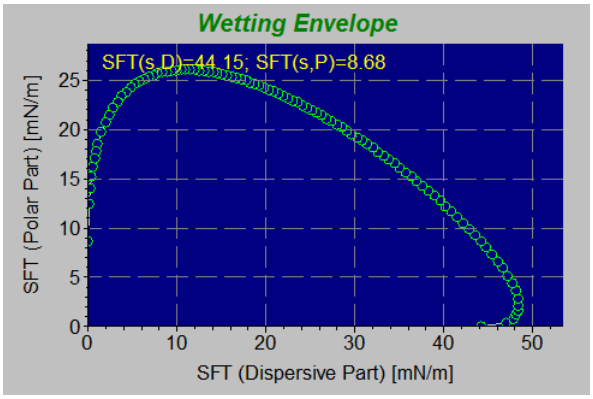

Figure 4.6.: Wetting envelope of PET-foil (Hostaphan GN4600), created by generated by the disperse (abszissa) and polar (ordinate) fraction of the PET's surface tension, data measured with Krüss DSA 100.

the liquid lies outside the wetting envelope, its contact angle is higher than 90 °C and thus it will not wet the surface.

Figure 4.6 exemplarily illustrates such measurements. It depicts the wetting envelope of PET-foil, one of the substrates used in this study. The disperse and polar fractions of the PET's surface tension are plotted against each other. Thus, it is possible to determine whether a liquid with a known surface tension (both disperse and polar fractions have to be known), will wet the PET surface or not.

Etching rate

One of the most important parameters in this study is the etching rate. As introduced in Chapter 3.3.3, the etching rate is the ratio of ablated layer thickness and ablation time. It is difficult to directly measure the actual etching rate during an etching process. The most accurate measurement of the etching rate is possible by in-situ monitoring of the layer thickness during the etching process. Appropriate tools are ellipsometry or interference spectroscopy. Thus, the progression of the etching rate may be obtained [84]. Those methods are commonly applied in dry etching techniques [13].

Another, less accurate method is the determination of a mean etching rate r after the actual etching process. Here, we use the ratio of a layer thickness h_{etch} ablated in a certain amount of time t_{etch} (as adapted from Equation 3.2 in Equation 4.9 [84]) to calculate the mean etching rate r.

$$r = \frac{h_{etch}}{t_{etch}} = \frac{h_{before} - h_{after}}{t_{etch}} \tag{4.9}$$

In this thesis, I make use of the latter method, accepting lesser accuracy by gaining easier laboratory processes.

4.2. Printing tests

This section elucidates on the printing trials conducted for this study. I start with an introduction of the experimental setup and then give specific details of printing the silver and resist

layer, respectively, and post-processing of the silver layer. Also included in this section is a short introduction into design of experiments (DoE) as I used it to evaluate the influencing parameters of printing the resist layer and post-processing parameters of the silver layer.

4.2.1. Experimental setup

This section includes details of the machine and the substrate I used for printing. Specifics regarding printing inks are not included in this section, they are explained in Sections 4.2.2 and 4.2.4.

Flexographic printability tester IGT F1

All printing tests in this study were conducted on an IGT F1, a printability tester for flexography. Figure 4.7 shows an image of the actual machine and Figure 4.8 depicts a schematic of the printing unit. The IGT F1 emulates the flexographic printing process (cf. Figure 4.8): It consists of a very simple inking unit (anilox roller (a) and doctor blade (b)), a plate cylinder (c), a flat substrate carrier (d) and an impression cylinder (e).

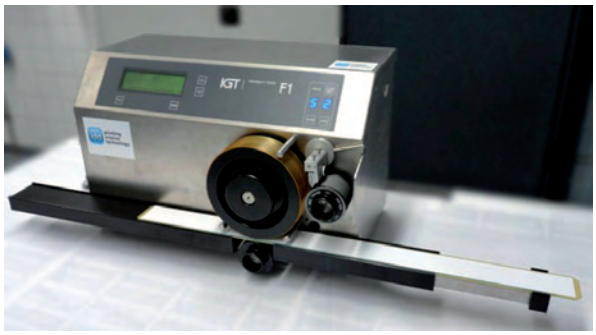

Figure 4.7.: IGT F1 printability tester.

The inking unit consists of an interchangeble anilox roller (a) and a doctor blade (b), where the fluid is applied manually with a pipette (f). From the anilox roller, the fluid is transferred to the printing plate and from there onto the substrate. The substrate is transported through the nip on a carrier, the motion of which is provided by the plate cylinder.

The IGT F1 printing proofer is a useful device when conducting printing tests on a small scale, e.g. when only small amounts of liquid or small areas of substrate are available. However, it does not reflect the actual flexographic printing process as is in an industrial printing press. First of all, there is no continuous ink flow as e.g. in a chambered doctor blade. The machine parts covered with ink have to be cleaned after each print run to ensure reproducibility. If we use inks with fast evaporating solvents, sometimes the ink already dries on the anilox roller or printing plate before it reaches the substrate.

Another characteristic of the IGT F1 printability tester is the single-sided bearing of the rollers and cylinders. This leads to a non-uniform distribution of the printing force across the nip as shown by Langner[2] [86]. As all cylinders are put on the printing proofer manually,

[2] Langner conducted his Bachelor-Thesis under my supervision. He designed a test rig to investigate the printing nip from perspective of the impression cylinder using a high-speed camera. One of his main results is the documentation of the non-uniformity of the IGT F1 printing nip.

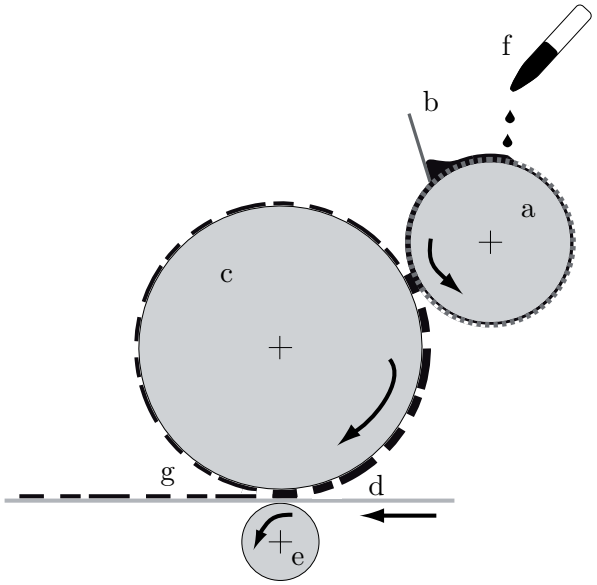

Figure 4.8.: Schematic of an IGT F1 flexographic printing proofer with a) anilox roller, b) doctor blade, c) plate cylinder with printing plate, d) substrate support, e) impression cylinder and f) fluid dispensing using a pipette.

this problem might be emphasized by putting a momentum on the shaft during setup, thus bending it.

In industrial printing presses, the engagement is adjusted using distance control. The IGT F1 only provides the configuration of a printing force. Thus, the engagement and the printing varies with the substrate, the printing plate and its layout. As I compare printing results using the same combination of substrate, plate and layout, the printing force is a reasonable instrument.

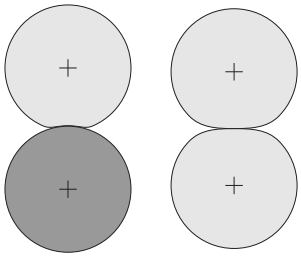

Figure 4.9.: Stiffness pairing of roller materials (hard-soft; soft-soft).

For transportation of the substrate through the printing proofer, IGT provides a substrate carrier made of fiber reinforced composite, with a layer of foam and a hard polyester as cover [72]. The substrate carrier travels through the nip on a guiding appliance. The latter supports the carrier to offer a plane motion and keep it in position relative to the plate cylinder. When using the ex-factory equipment and printing on foil or paper, the pairing of roller materials is not in accordance with standard industry practice. In industrial printing machines the pairing is usually hard-soft (cf. Figure 4.9, left). With the foam-covered substrate carrier, the

pairing of the IGT F1 is soft-soft (cf. Figure 4.9, right). Thus, the nip geometry is a different one.

For printing on PET-foil, I therefore used a custom made aluminum substrate carrier. To accommodate printing on glass slides, I used another custom made substrate carrier. This carrier consists of a base of fiber reinforced composite with bearer lines at the edges to ensure a) a continuous engagement without jumping of the plate cylinder on the substrate because of height differences and b) a reproducible mounting of the glass slide in the middle of the carrier and thus the plate.

Substrate

I used two kinds of substrates for the printing trials: PET-foil[3] and glass slides[4]. The former, I used for preliminary trials to establish a sensible parameter space and also for the post-processing trials with DoE as glass slides allow for easier handling.

As the foil-substrates show a certain waviness, I discarded them for the main trials. Glass slides have a more even surface with less waviness, thus thickness measurements may neglect the waviness and facilitate large-area, stitched measurements.

Preliminary tests showed an insufficient bonding of the silver layer on the glass substrate. Therefore, I used a thin, spin-coated PMMA-layer as bonding agent. Thus, I improved the bonding significantly, as so-called Tesa-tests showed. The Tesa-test is a common test in printing industry, evaluating the bonding of a printed layer to the substrate. A strip of adhesive tape is attached to the printed layer and then ripped of. If the printed layer adheres to the strip of adhesive tape, the bonding between printed layer and substrate is insufficient. Figure 4.10 illustrate the bonding of the silver layer without (left) and with (right) the PMMA-layer.

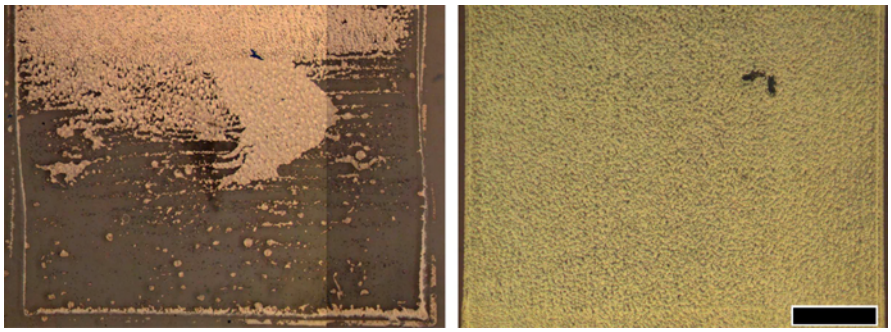

Figure 4.10.: Results of Tesa-test of printed silver layer (microscopic images, the scaling bar indicates 500 μm). Left: silver printed directly on a glass slide with significant areas of the layer ripped off by adhesive tape. Right: silver printed on PMMA-layer as bonding agent, the adhesive tape has almost no effect on the silver layer. Clearly, the PMMA-layer provides better bonding on the glass substrate.

To ensure wetting of the inks used in this study on the substrates, I measured their surface energy. All were in the wetting envelope (cf. Chapter 4.1.3).

[3] Hostaphan GN 4600 of Mitsubishi Polyester Films with a thickness of 175 μm, coated on one side [100].
[4] Glass slides, 50 mm × 50 mm, 1 mm, Glaswarenfabrik Karl Hecht AG.

4.2.2. Specifics of printing silver layers

The silver dispersion used in these printing trials is a commercial silver nanoparticle ink for flexography: InkTec TEC-PR030. The diameter of the silver particles is about 40 nm, dispersed in an "organic matrix containing solvents, polymeric compounds and dispersants" [29]. The ink has a solid content of about 40 $wt\%$ of silver [73]. As explained in Chapter 3.2.1, some inks show strong variations of their properties between batches. Therefore, I conducted all printing trials using the same batch of ink.

The layout of the silver layer is an array of rectangles with a width of 5 mm and a length of 10 mm. Figure 4.11 shows their arrangement on the printing plate with solid lines at the edges of the plate in printing direction as bearer lines. The plate material is a photopolymer. For further information on the printing plate and the complete layout of the plate, I refer the reader to Appendix A.2 on page 119.

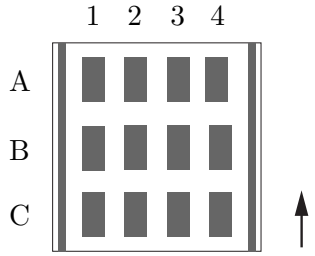

Figure 4.11.: Nomenclature of the printed silver layers as arrays of rectangles: Lines are named using letters, columns using numbers. The arrow indicates the printing direction, with row A being printed first.

As the substrate is a 50 mm × 50 mm glass slide, with proper alignment, four by three rectangles are printed onto one slide. For easier processing of the samples, the individual rectangles on the slide are tagged as indicated in Figure 4.11. If a row of rectangles is printed incompletely at the start or end of the glass slide, it will be discarded. Thus, some samples do not have three rows.

I printed the silver layer onto the glass slides using the IGT F1 printability tester as introduced above. To adjust to the rigid glass substrate, I used a custom made substrate carrier. This substrate carrier ensures a certain rigidness to avoid bending of the glass and thus prevent breaking it. Also, the sample is held in the middle of the holder by bearer lines thus ensuring an even distribution of forces in cross direction.

Table 4.3.: Printing parameters for printing of the silver layer.

printing parameter	value
printing speed	0.5 m/s
printing force	35 N
pick-up volume	4.5 ml/m^2

I determined the right printing parameters for this layer in extensive preliminary trials. I state them in Table 4.3 without further elaboration.

4.2.3. Specifics of post-processing printed silver layers

After printing silver layers we need to process them further in order to ensure a sufficient conductivity, as Chapter 3.2.2 showed. This section elucidates on the post-processing of printed silver layers as used in this study. First, I give a short overview of the technique used for post-processing. The trials were conducted using design of experiments. Therefore, I give a short introduction into this method and explain the parameters varied during the trials.

As I have no facility to determine whether the silver layers in this study are cured or sintered, I keep to the term *post-processing* when refering to the process in general and *photonic curing* when talking about specific post-processing using NovaCentrix PulseForge 1200.

Post-processing using photonic curing

Manufacturer's information on the silver nanoparticle ink I used in this study suggest a "firing temperature" of 120 °C for up to 5 min using IR or a "circulating heat oven" to achieve sufficient conductivity [73]. However, preliminary test showed that these drying conditions are insufficient to achieve an adequate conductivity. Therefore, I used another method for post-processing of the silver layer thus increasing their conductivity: Photonic curing (cf. Chapter 3.2.2). Here, a short, broad-band light pulse heats the silver layer to very high temperatures with very low thermal affection of the substrate. This is possible because a) the light pulse or the series of pulses is very short in a range of microseconds to few milliseconds and b) the spectrum of the light bulb matches the absorption spectrum of the silver layer while having only small overlap with the absorption spectrum of the substrate. As equipment for sintering of the silver layers, I used a NovaCentrix PulseForge 1200[5], cf. Figure 4.12.

Figure 4.12.: NovaCentrix PulseForge 1200.

Following Schroder [131], I introduce the process of photonic curing in the following. We print a thin layer of silver with a thickness of h_{Ag} on a PET-substrate with a thickness h_{PET}. During sintering, the silver layer absorps the high energy light pulse whilst the substrate does not. Thereby, the silver layer will reach very high temperatures "far beyond maximum working temperature of the substrate" [131]. As the silver layer is very thin (about 0.3 μm) compared to the PET-foil (175 μm), it is heated thoroughly for a short time and then the

[5]The photonic curing tool PulseForge 1200 from NovaCentrix is intended for laboratory use. It offers the creation of custom pulse shapes and a uniformity of exposure of ± 2% [105].

heat drains into the PET-foil. The shortness of the light pulse ensures that the properties of the PET-foil will not change significantly during the time of high temperature [131].

Using the PulseForge 1200, it is possible to shape the pulse of the light bulb. In its most simple form this includes the pulse length and its height, i.e. the voltage with which the bulb is driven and therefore the energy density on the sample surface. Using a more complex mode, the pulse can be split into several smaller ones. Thus, we expand the parameter space by the number of pulses, their individual lengths, spacing and heights. To investigate the post-processing behavior of printed silver layers with such a large parameter space, I utilized design of experiments.

The factors varied are the following:

Bank voltage The bank voltage U_{bank} indicates the energy per area the light bulb exhibits. The unit of U_{bank} is [V]. The "amount of energy in an individual pulse increases with the square of the voltage" [106].

Envelope duration of the pulses When splitting a long pulse into micropulses, the time spanning the pulses and the waiting time in-between is called envelope. Its length is the envelope duration t_{env}.

Number of micropulses The number of micropulses $n_{\mu pulse}$ is eponymic, it indicates the number of individual pulses contained in an envelope. It is without unit.

Pre-drying Pre-drying P indicates whether the sample experiences a series of very short pulses at the beginning of the curing process. As P is a binary factor, its values are either *yes* or *no* without unit.

There are several other parameters we can vary using photonic curing, among them the distance between flash bulb and sample surface and whether or not to use an inert gas during firing. As I kept them constant, they are not further considered.

Short introduction into design of experiments (DoE)

When planning experiments in laboratory or industry environments, we have several options to design those to obtain information. The first option is to vary each parameter and combine it with each variation of every other parameter. This approach is called full factorial [134]. Thus, we cover every potential parameter combination and obtain the most information possible. As Equation 4.10 demonstrates, the cost of this information is a vast number of individual printing trials n_{trials} with equally high effort of evaluating the (measurement) data afterwards. Typically, full factorial approaches are used when little is known about the interdependence of factors [8].

$$n_{trials} = n_{variations}^{n_{factors}} \tag{4.10}$$

To reduce the number of individual printing trials and increase the information gain, design of experiments (DoE) was created. The aim of DoE is to minimize the required number of trials while minimizing the information loss [82]. Viewing the investigated process as a black box, we have explanatory variables as well as disturbance variables going in and effect variables coming out. Figure 4.15 illustrates this model for the present investigation, following [134]. The explanatory variables are the ones we can vary and adjust in our process, also called factors or input variables. Here, those are parameters of the PulseForge 1200 we can adjust as introduced above. We usually cannot influence the disturbance variables, hence their name. Here, they are climate conditions, human factors and aging of the flash bulb. The

effect variables are the results obtained from our process. In this study, we focus on the sheet resistance.

With the help of a software[6], an experimental design is created, combining different variations of the factors. Apart from establishing an experimental design, the DoE-software also provides an analysis of the results using regression analysis.

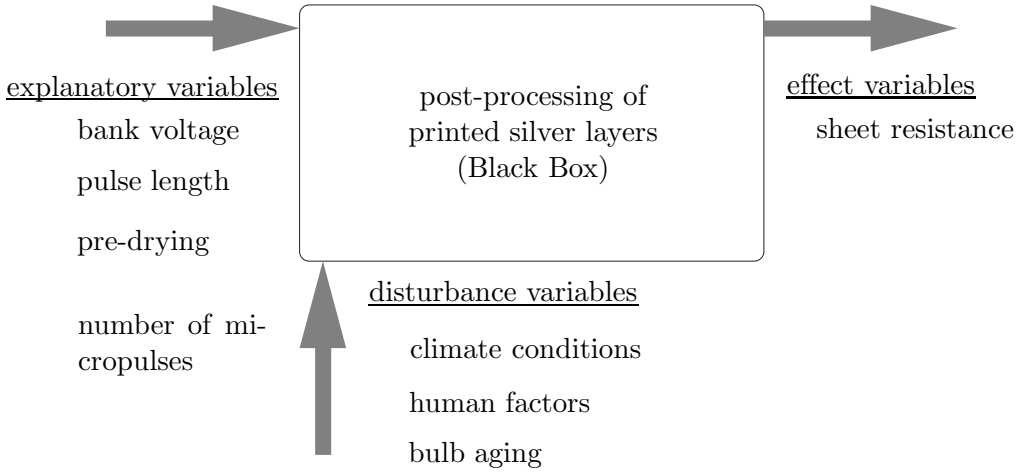

Figure 4.13.: Qualitative process model of post-processing printed silver layers, adapted from [134].

After conducting the trials and evaluating the results, the measured data is fed into the software which will then calculate the interrelation of the factors, also taking into account the disturbance variables. The result is an assessment of how the input parameters influence the output parameters. Thus, it is possible to evaluate a large parameter space in a relatively short amount of time. Furthermore, interactions between factors may become apparent that would not be visible with a more conventional approach [134]. In this study, I used the software Cornerstone[7] to build an experimental design plan.

Depending on the desired complexity, linear (Equation 4.11 and 4.12), quadratic (Equation 4.13) or cubic models are used. Equations 4.11 to 4.13 give respective examples for regression analyses with three variables $x_1 \dots x_3$.

$$y = a_0 + a_1x_1 + a_2x_2 + a_3x_3 \tag{4.11}$$

$$y = a_0 + a_1x_1 + a_2x_2 + a_3x_3 + a_4x_1x_2 + a_5x_1x_3 + a_6x_2x_3 \tag{4.12}$$

$$y = a_0 + a_1x_1 + a_2x_1^2 + a_3x_2 + a_4x_2^2 + a_5x_3 + a_6x_3^2 + a_7x_1x_2 + a_8x_1x_3 + a_9x_2x_3 \tag{4.13}$$

In the equations above, x_i are factors and a_i are parameters fitting the model to the data to minimize deviations. For minimizing the deviations of a_i, commonly least mean squares is used [134].

[6]Examples for software are Design Expert, Cornerstone, GlobalOptimize or JMP.
[7]Cornerstone is a data analysis software from the company camLine. I used Release 5.1.

Design of experiments is a very powerful tool to plan, conduct and evaluate laboratory trials. As I use it in its most basic characteristic, I will not go into further details regarding its possibilities to plan trials and interpret measurement data beyond what I actually use for this study. Extensive information on DoE and the use of the software Cornerstone may be obtained from Haas [54].

Quotient space

First, I chose a linear approach to assess the influence of pulse length and height and thus energy density applied onto the surface of the functional layer on the sheet resistance of said layers. Splitting the pulse into smaller ones, I then used a quadratic approach. Table 4.4 lists the factors for the latter. The bank voltage U_{bank} indicates the charge of the capacitors driving the bulb, and thus the energy per area during post-processing. The higher the bank voltage is, the higher is the energy per area. The pulse length t_{pulse} is the period of time the sample is exposed to a light pulse. As stated above, we can split the pulse into micropulses with $n_{\mu pulse}$ indicating their number. The time spanning individual pulses and the waiting time in-between is the envelope duration t_{env}. I chose a ratio of 0.5 between pulses and waiting time. The following example illustrates the interrelation between said parameters: In an envelope of $t_{env} = 1$ ms, $n_{\mu pulse} = 5$ and a ratio of 0.5, the individual pulse length calculates to $t_{pulse} = 0.1\,\text{ms}$.

Pre-drying P indicates the usage of three short ($100\,\mu$s) pulses with a spacing of $300\,\mu$s before the actual pulse envelope starts. The aim of pre-drying is to gradually increase the heating of the functional layer.

Table 4.4.: Factors, i.e. input parameters of post-processing printed silver layers using PulseForge 1200.

factor	symbol	variation
bank voltage	U_{bank}	260/270/280 V
envelope duration	t_{env}	400/450/500 μs
number of micro pulses	$n_{\mu pulse}$	4/5/6
pre-drying	P	yes / no

As Schroder explained in [131], there are boundaries limitting the amount of energy in the process. Examples are warping of the substrate or ablation of large areas of the film [131]. As I stayed within these boundaries, I will not go into detail here.

4.2.4. Specifics of printing etch resist in the form of line shaped elements

This section combines two challenges: printing etch resist and understanding printed lines. Thus, I begin with a hypothesis on the behavior of cross sections of printed lines when increasing the printing force. Then, I introduce a process model for the design of experiments for printing line shaped elements. I elaborate on the quotient space and conclude the section with details of the actual printing trials, such as ink or printing plate.

Hypothesis on the behavior of cross sectional parameters of a printed line in relation to printing force

One of the main influencing factors on the formation of printed lines in flexography is the engagement and thus the printing pressure. This section explains a hypothesis on the behavior of printed lines when increasing the engagement. I use the cross section of a line for the contemplations. I derived this hypothesis from preliminary printing trials and experiences with different material systems.

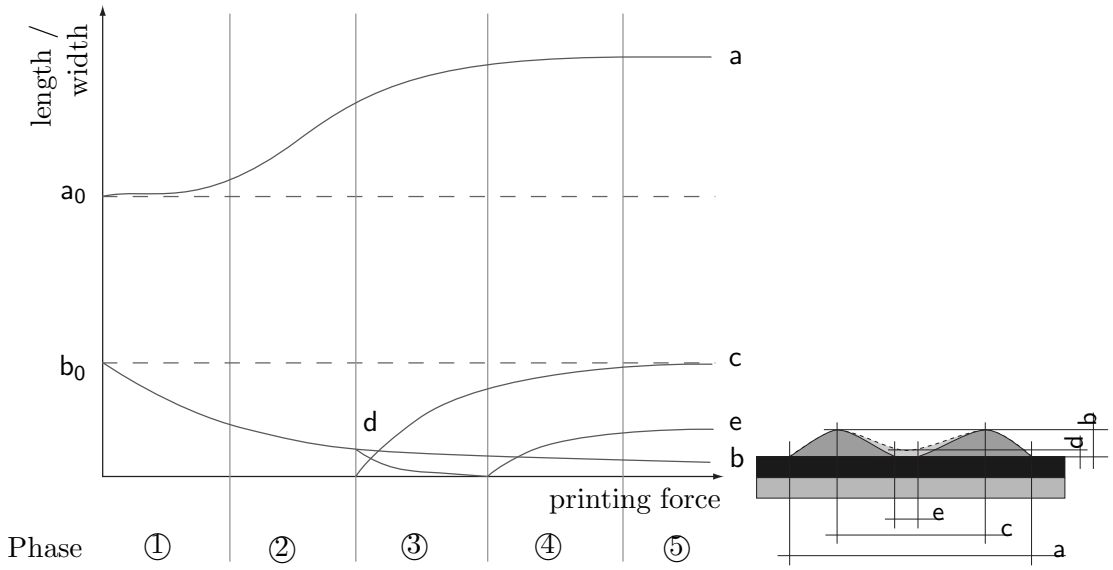

Figure 4.14.: Hypothesis of the expected behavior of several geometric parameters describing the cross section of a printed line in relation to the printing force, phase diagram.

Figure 4.14 shows five different phases of line formation, depicted as different geometric parameters of the cross section of a line. Note: The schematic of the cross section is a reprint from Figure 4.3 on page 41. As I conducted all printing trials in this study on an IGT F1 printability tester which only allows for adjustment of printing force, I use the printing force as influencing parameter in this hypothesis.

Phase 1 With a very low printing force, i.e. kiss print being used, the line width a is almost constant. We start with an initial line width a_0 and height b_0. In this phase, the cross section of the line roughly resembles a section of an ellipse. The ends of the line E (cf. Figure 4.2, page 41) are shaped as truncated half spheres. Note that phase 1 is very short.

Phase 2 With increasing printing force, line width a will also increase. The length of phase two depends on the amount of ink offered on the elevated elements of the printing plate.

Phase 3 When the printing force increases to a certain level, the cross section will morph from a section of an ellipse to a shape resembling two hills with a valley in-between (cf. Figure 4.14, right). Thus, more parameters are needed to describe the geometrical form of the cross section: Apart from the overall line width a and the peak height b, we also use the distance of the peaks c and the height of the valley in-between d to describe the

cross section. As the printing force increases, so will the distance between the peaks while the height of the valley will decrease.

Phase 4 With furthing increasing engagement, the height of the valley `d` will ultimately decrease to zero, thus forming a gap between the two hills and introducing a new parameter `e`: the width of the gap. With increasing printing force, `e` will also become wider.

Phase 5 At some point, all parameters will reach a saturation. A further increase of engagement will not affect them anymore.

I derived this hypothesis from preliminary printing trials and experiences with different material systems. Note that this hypthesis is not based on statistical evidence.

Process model of printing line shaped elements

To utilize certain features of flexographic printing as e.g. the halo effect for structuring of resist layers, we first need a better understanding of printing basic geometries. Above, I explained the expected behavior of printed lines. Now, we validate the hypothesis by using design of experiment for printing the resist layer shaped as lines.

Figure 4.15 illustrates the implementation of a generic process model on printing of line shaped resist layers. Factors, i.e. explanatory variables here are parameters of the IGT F1 printability tester: printing force F_{print}, printing speed v_{print}, and pick-up volume $V_{pick-up}$ of the anilox roller. The effect variables are properties of printed lines: line width, width of the halos and width of the void. Climate conditions and human factors are disturbance variables.

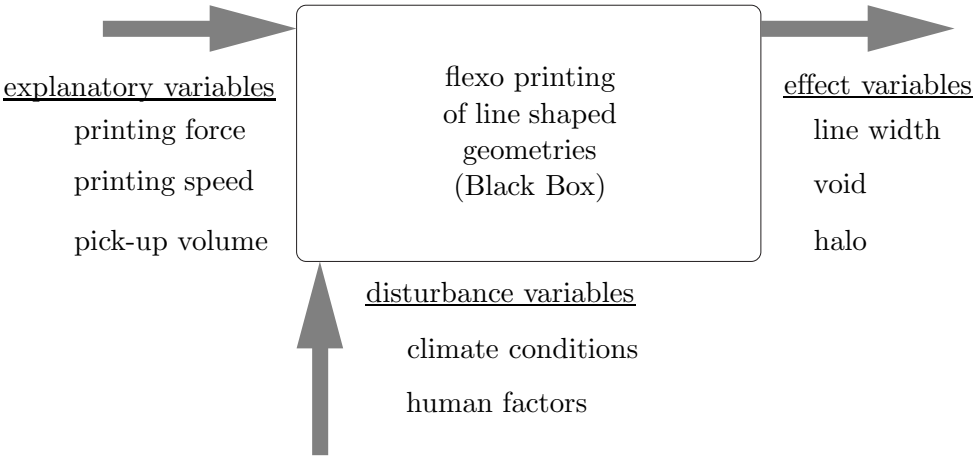

Figure 4.15.: Qualitative process model of printing line shaped geometries, adapted from [54, 134].

A similar approach was chosen by Yang. She investigated printing of line shaped geometries using DoE in [160][8]. The effect variables in her model were edge quality, void areas within the lines and increase of printed area.

[8] Yang conducted her Bachelor-Thesis under my supervision. I designed the printing plate layout she used and also used it in this study.

YANG used solvent based colored printing ink for flexography[9] on an IGT F1 printability tester with a PET-foil substrate as introduced above [160]. I used YANG's results as preliminary tests to identify possible difficulties during my trials.

Quotient space

As factors (i.e. input parameters) of DoE for printing line shaped geometries using an IGT F1 printability tester, I used printing force, speed and pick-up volume of the anilox roller as outlined in Table 4.5.

Table 4.5.: Factors of printing line shaped geometries using an IGT F1 printability tester.

factor	symbol	variation
printing force	F_{print}	$10 \ldots 450\,\mathrm{N}$
printing speed	v_{print}	$0.2 \ldots 1.5\,\mathrm{m/s}$
pick-up volume	$V_{pick-up}$	$4.5/8/24\,\mathrm{ml/m^2}$

The disturbance variables we are not able to eliminate are ambient conditions such as temperature, humidity and light / UV radiation plus random errors. As all printing trials were conducted in one day in a short amount of time, the ambient conditions varied only slightly and thus may be neglected as the printing results are compared relatively to each other. Nevertheless, I monitored the ambient conditions during the trials.

Table 4.6.: Effect variables of flexographic printed lines as illustrated in Figure 4.16.

effect variables	symbol	unit
line width	a	μm
halo, operating side	$\mathsf{H_{os}}$	μm
halo, drive side	$\mathsf{H_{ds}}$	μm
width of gap / void	e	μm

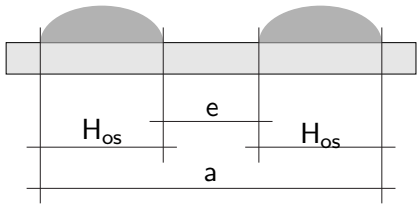

Figure 4.16.: Schematical cross section of printed lines with distinct halo effect to illustrate the effect variables in Table 4.6.

Table 4.6 lists the effect variables regarding DoE of flexographic printed lines, with Figure 4.16 illustrating the symbols. In a cross section of a printed line, the line width a represents

[9] Commercial colored flexographic ink: 36-2 Processblau 5600, Siegwerk Backnang GmbH

the length of the base line of the cross section. If the cross section features two peaks, i.e. two halos, H_{os} indicates the width of the halo on the operating side of the machine and H_{ds} the halo on the drive side of the machine. The width of the gap formed between H_{os} and H_{ds} is the void e.

Printing trials

In all experiments of this work I used PMMA (Poly(methyl methacrylate)) as an etch resist ($(C_5O_2H_8)n$; the structural formula is depicted in Figure 4.17). PMMA is a thermoplastic which is transparent in the visible light range (300 ... 700 nm) [93, Vol. 3, Methacrylic Ester Polymers]. It is also known under the trademark *Plexiglas*. In the semiconductor industry, PMMA is often used as an etch resist in electron beam lithography [116]; being opaque at wavelengths starting in the near infrared range (2800 nm) [93, Vol. 3, Methacrylic Ester Polymers].

Generally, PMMA is a positive resist [50, 58] (cf. Figure 3.13 on page 35). As I applied the PMMA already structured, there is no need for a patterning step using a mask. Therefore, its positive behavior is not significant here.

The PMMA printing fluid I used in this work is a custom made solution, containing 10 wt% PMMA with a molecular weight of 996,000 g/mol, 89.99 wt% of anisole[10] and 0.01 wt% of dye[11]. As PMMA itself, anisole and the substrate are transparent, I used the Lumogen as a dye for better optical measurability of the printed layers. I chose the composition of this solution on basis of the works of Stahl [140] and preliminary printing trials I conducted myself.

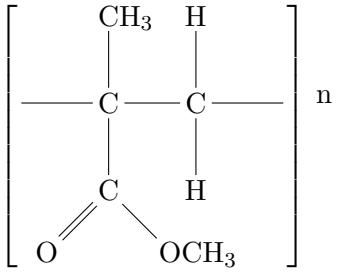

Figure 4.17.: Structural formula of Poly(methyl methacrylate) ($(C_5O_2H_8)_n$).

PMMA is fairly resistant against many etching solvents, as nitric acid or hydrochloric acid [19]. However, literature gives no etching rates of PMMA for wet etching. Etching rates for plasma (0.67 nm/s) and reactive ion etching (1.4 nm/s) are low [84].

The printing plate layout consists of several test structures for the investigation of small geometric shapes. Figure 4.18 depicts the line structures I focused on in this study. For the complete layout of the plate, I refer the reader to Appendix A.2. The layout includes different shapes and lines of different sizes and alignment relative to printing direction. For this study, I investigated lines with different line widths, aligned in printing direction. I neglected line shapes aligned not parallel to the printing direction, i.e. perpendicular or angled to printing

[10] Methyl phenyl ether, C_7H_8O, also known as Anisole, obtained from Sigma-Aldrich [137].

[11] Lumogen Red is a Perylene dye from BASF with a molecular weight of 963,956 g/mol and a good solubility in aromatic solvents [9].

direction. The influence of the angle respective to the printing direction may be obtained from Yang [160].

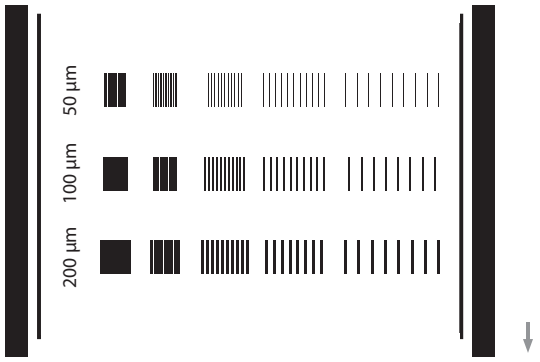

Figure 4.18.: Detail of printing plate layout: Line shaped elements. The grey arrow in the lower right corner indicates printing direction and is not part of the layout.

Most photopolymeric printing plates are not compatible with aromatic solvents as toluene [143] or anisole, the solvent used for the PMMA-ink here. Therefore, I used a proprietary fluorinated rubber[12] as plate material. This was incorporated into a blank sleeve, which then was engraved with the layout using a laser. To accomodate a sleeve plate in the IGT F1, I used a custom made sleeve cylinder.

To ensure the removal of residual organics in the silver layer that might be affected by the solvent of the PMMA-ink, I used photonic curing as pre-treatment. I set the bank voltage U_{bank} to 355 V and the pulse length to 1 ms resulting in a theoretical energy density of 2443 mJ/cm^2.

For printing of the PMMA resist structures onto the silver layers, I used the IGT F1 printability tester as introduced in Chapter 4.2.1 with the custom made substrate carrier intended for printing on glass slides. The specific printing parameters as obtained from DoE are listed in Appendix A.2. I printed three samples per parameter set. I cleaned all equipment in contact with the ink (printing plate, anilox roller, doctor blade) after each print run with toluene and the anilox roller with acetone after each parameter set. The printed layers were dried under ambient conditions.

4.3. Etching tests

The following section covers the implementation of the etching trials. Starting with the experimental setup, I then elaborate on how to determine the etching rate. The section concludes with a description of stripping, i.e. the removal of resist after etching.

4.3.1. Experimental setup

In Table 3.2 (Chapter 3.3.3), I introduced several etchants for silver with their respective etching rates. Although most show appropriate etching rates, I discarded some of them

[12] FKM from the company Felix Boettcher. For more details on the plate, I refer the reader to Appendix A.2.

because of their toxicitiy: thiourea-iron nitrate-ammonium fluoride solution and ammoniacal-methanole hydrogen peroxide solution [95, 138]. In [118], I published etching trials with phosphoric acid mixed with nitric acid diluted in a.p. achieving etching rates of 60 nm/s. I discarded the approach from [118] in this thesis as the etching rate is quite high with even higher etching rates expected for sintered silver layers.

Although KÖHLER states that nitric acid is unsuitable for etching small structures [84], FULEK[13] shows sufficient etching rates for layers similar to the ones used in this study [46]. Hence, I used diluted nitric acid as etchant for this study. I benefited from FULEK's results as preliminary tests on what etching rates to expect. As etchant for this study, I used nitric acid diluted with water in a ratio of 20% HNO_3 to 80% H_2O.

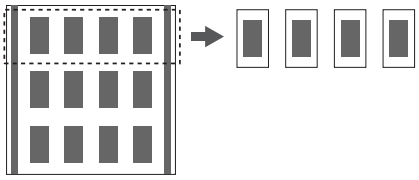

Figure 4.19.: Isolation of printed silver samples on glass slides as introduced in Figure 4.11 into individual rectangular samples for etching trials.

For the implementation of the etching trials it became necessary to isolate the printed arrays on the glass slides. Figure 4.19 illustrates this. Thus, I was able to etch each silver rectangle individually.

To "maintain a uniform [...] etching rate" [154] I used immersion etching with slight movement of the sample in the etchant [154]. I prepared a large volume of the etchant and extracted smaller volumes for the individual trials to avoid declining etching rates due to saturated etching bath. I used the same etching bath for the four consecutive silver samples of one print sample (cf. Figure 4.19).

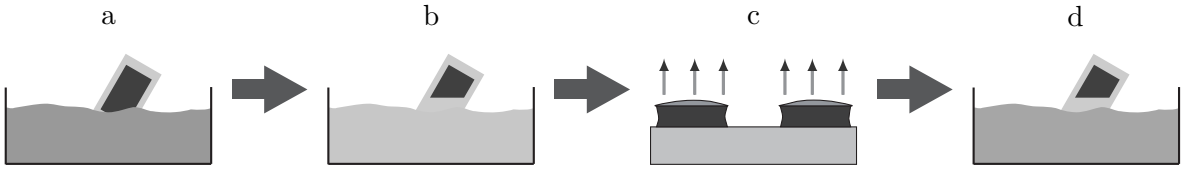

Figure 4.20.: Process steps of etching: a) etching, b) rinsing, c) drying and d) stripping. Adapted from [117].

I conducted all etching trials in a fume cupboard as I used open etching baths. Throughout the etching trials, I used clean glass ware which I additionally rinsed with the fluid intended for its use. The sequence of steps of the etching trials are as follows, cf. Figure 4.20 for illustration:

a) Dipping of sample in etchant for specified amount of time.
b) Immediately after etching, rinsing of sample with water to stop the etching reaction and remove residual etchant.
c) Drying of sample under ambient conditions.

[13] FULEK conducted her Bachelor-Thesis under my supervision. The silver layers she analyzed were printed on PET using the same parameters and ink as in this study.

d) Stripping of residual etch resist after completed measurements.

I etched all samples separately and timed the process to determine their individual etching rate.

4.3.2. Determining the etching rate

For determination of the etching rate, I use the method introduced in Chapter 4.1.3, calculating the mean etching rate r after the etching by dividing the etching time t_{etch} by the ablated layer thickness ($h_{etch} = h_{before} - h_{after}$), cf. Equation 4.9). Figure 4.21 illustrates the procedure: I measured the thickness of the respective layer before h_{before} and after h_{after} the etching tests to obtain the ablated layer thickness h_{etch}. To calculate the etching rate, I measured individual etching time t_{etch} and calculated the respective etching rate r for each sample. For comprehensive description on how I determined the layer thickness of each sample, I refer the reader to Appendix A.1.

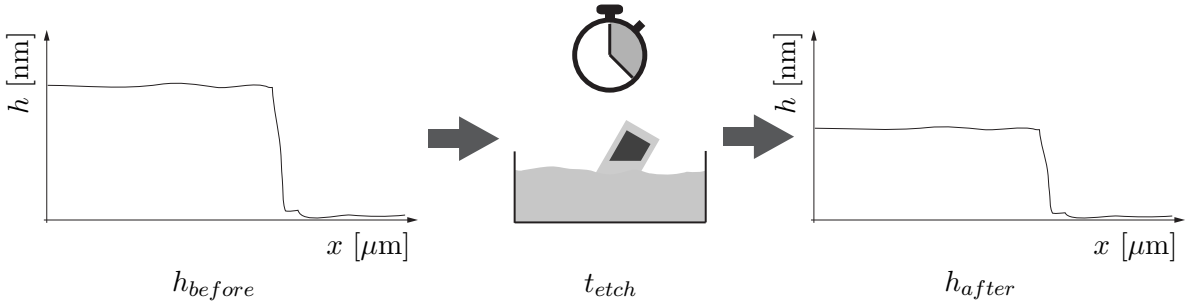

Figure 4.21.: Schematic of determining the etching rate of individual samples: Measuring the layer thickness before etching h_{before} (left), timing the etching process t_{etch} (middle), measuring the layer thickness after etching h_{after} (right).

For determining the etching rate using the approach explained above, we make the following assumptions:

1. The silver layers are quasi-homogeneous across the printed area, neglecting the halos surrounding them. Thus, certain layer properties may be generalized for their whole area. An example is the layer thickness.
2. As we assume the layer properties are homogeneous, thus the etching rate will be constant as well. We therefore can take the mean of all individual measurements.
3. As we determine the layer thickness from a top view, we are not able to determine underetching using this method. Therefore, we neglect underetching. We assume that, even if underetching will occur, it does not alter the profile as measured from above.

To substantiate the assumptions of constant layer thickness of the underlying spin-coated PMMA layer, I measured the thickness of the PMMA layer at several positions between the silver rectangles.

4.3.3. Removal of resist

In microfabrication, plasma etching is usually the method of choice for the removal of resist after an etching process [84]. I discarded this approach for this research as it takes a longer process time and brings higher effort and equipment to the process chain. PMMA is soluble

in esters, ketones, aromatics and glycol ethers [136]. Therefore, I used acetone to remove residual resist after etching. As explained above, I used open baths in a fume cupboard. This also applies for the stripping step.

As for the etchant, a high selectivity is also required for the stripping agent. Here, the selectivity is calculated reversely, cf. Equation 4.14. Note that the etching rate here refers to the ablation rate regarding the stripping agent.

$$S_{strip} = \frac{r_{res}}{r} \tag{4.14}$$

Ideally, the stripping agent should not affect the functional layer at all. As printed silver layers usually have residual organic compounds, those may be affected by the stripping agent. As a result, the layer properties may change. This phenomenon may be compared to incomplete sintering (cf. Chapter 5.1.3).

5. Results

In this chapter, I compile and interpret the measurement data obtained from the experiments explained above. The chapter includes three section according to the sequence of the experiments (printed silver layer, printed etch resist and structured silver layer) and a section recapitulating the results.

5.1. Printed silver layer

This section presents the results of the experiments regarding printed silver layers. Starting with the homogeneity, I then focus on the post-processing of said layers. The section concludes with considerations regarding the behavior of printed silver layers in a layer stack, conductivity depending on the location of the sample on the substrate and determination of layer isotropy using the correction factor in *van der Pauw* measurements.

5.1.1. Homogeneity

As introduced in Chapter 4.1.1, I use the layer roughness $\mathbf{R}_q$ as evaluation method for the homogeneity of printed layers. Still, we have to distinguish between waviness of the sample surface and its roughness.

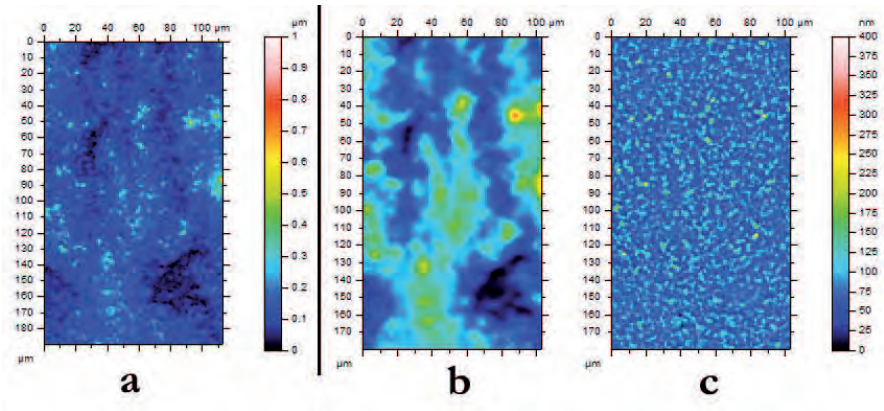

Figure 5.1.: Homogeneity of printed silver layers: a) confocal microscopic image of the sample surface, b) waviness at cut-off of 10 μm, c) roughness. Note the same scaling for waviness and roughness.

I therefore filtered the waviness of the surface. Figure 5.1 shows an example: a) is the sample surface, b) the waviness using a Gaussian filter at a wavelength of 10 μm and c) the roughness of the surface. Using this approach, I determined values of $\mathbf{R}_q$ of few ten nanometers for the filtered roughness, slightly higher values for the wavy surface and values between fifty and slightly more than hundred nanometers for the original sample surface.

5.1.2. Influences of post-processing parameters on the sheet resistance

The aim of post-processing a printed silver layer is foremost to increase its conductivity by decreasing its sheet resistance. Using photonic curing to alter the conductivity, there are several parameters, mainly regarding the shape of the light pulse, we can adjust to achieve this goal. This section first explains the effect of single pulses on the sheet resistance of printed silver layers. Then, I give a short introduction on how to interpret data obtained from DoE. The main part of this section covers the results of the DoE experiments and their interpretation.

Post-processing using photonic curing with single pulses

Using a single pulse in photonic curing, the variable influencing the result is the energy per area, also energy density w. The higher w is, the more the sample will be sintered. The energy density w can be adjusted by altering two variables: the length of the pulse t_{pulse} and the pulse height, i.e. the voltage driving the light bulb U_{bank}, also called bank voltage.

I increased the energy density w by increasing the bank voltage U_{bank} and keeping the pulse length t_{pulse} fixed at 1 ms. As expected, the sheet resistance decreases with increasing post-processing energy. Figure 5.2 illustrates these results. It depicts the sheet resistance before (left diagram) and after post-processing (right diagram) depending on the energy per area during post-processing. With increasing energy the sheet resistance after post-processing decreases. The trend of the sheet resistance before post-processing to also decrease with increasing energy is coincidental.

Note that the energy per area w is a theoretical value calculated by the control software of the PulseForge 1200. For measuring the actual energy per area reaching the sample surface, the manufacturer provides a bolometer[1]. Due to its installation space, I could not use it because of the short distance between light bulb and sample surface.

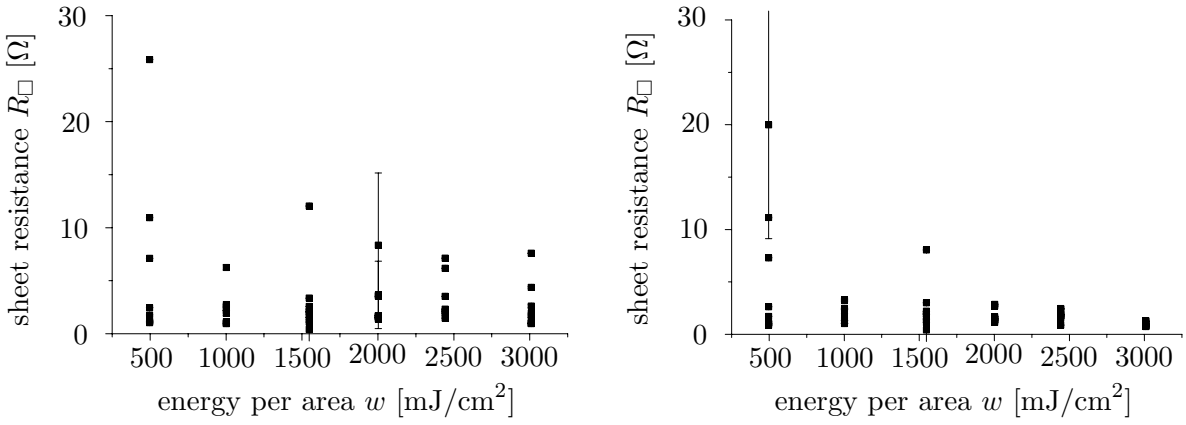

Figure 5.2.: Sheet resistance $R_\square$ of printed silver layers before (left diagram) and after (right diagram) photonic curing. With increasing energy during post-processing (abscissa) the sheet resistance decreases.

For this analysis, I randomly chose twelve printed samples with four silver rectangles each out of a sample pool consisting of samples with sheet resistances predominantly less than

[1] A bolometer is an instrument to detect and measure incident electromagnetic radiation.

$10\,\Omega/\square$. I measured the sheet resistance of the 48 individual silver rectangles before and after photonic curing, three times each. For each setting of w, I used two samples with 4 rectangles each. One bullet point in the diagrams represents the mean of the individual measurements of each silver rectangle.

To further illustrate the effect of post-processing, Figure 5.3 shows the shift of the sheet resistance, normalized to the sheet resistance $R_\square$ before post-processing. Note the decreasing ratio with increasing energy density w. The higher the energy during photonic curing, the lower is the sheet resistance after the post-processing step.

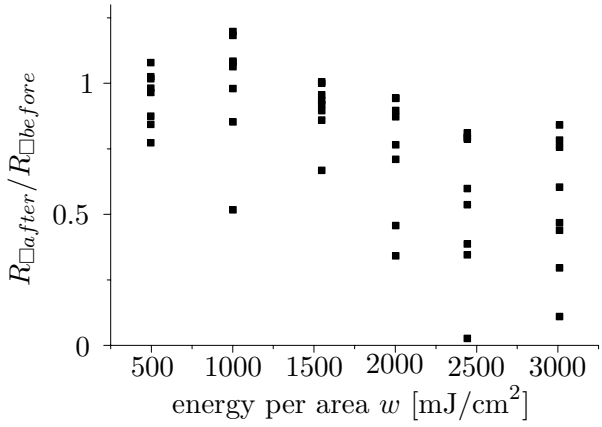

Figure 5.3.: Shift of sheet resistance $R_\square$ due to post-processing, normalized to $R_\square$ before photonic curing.

We can conclude that post-processing reduces the sheet resistance and thus increases the conductivity of a printed silver layer. How much the conductivity increases depends on the energy density during post-processing. At some point during photonic curing, the residual ink additives in the silver layer should be removed and the actual sintering, i.e. melting of the particles, begins. However, we are not able to deduct from the sheet resistance measurements, when the curing of the layer is finished and the sintering starts.

Interpreting results from DoE

As explained in Chapter 4.2.3, I used design of experiments for the analysis of the influence of several parameters in post-processing of a printed silver layer on the sheet resistance. I used the software Cornerstone for the planning of the experiments and also for the interpretation of the measurement data. I created all graphs and diagrams regarding the measurement data using said software. For the analysis of data obtained by DoE, several diagrams are feasible. In the following, I explain the graphs I used.

Pareto diagrams[2] illustrate the relative effect factors have on a variable. They provide a direct comparison of the factors and the weighting of their influence on the respective effect variable. This direct comparison is possible as their representation is orthogonally scaled, thus without unit. The factors in the are *Pareto* diagram are sorted by their value from left to right, starting with factors with strong influence, i.e. high values.

Interaction graphs illustrate how the combination of two factors affects a certain variable. They are relevant to understand the influence of certain factors whose implications are inter-

[2] *Pareto* diagram, named after Italian economist *Vilfredo Pareto*.

dependent. We read the graphs the following: Each row and each column represent a factor. At the intersection of a row and a column, a graph illustrates the effect of the interaction of both factors on the investigated variable.

The graphs used here depict the midpoint, minimum and maximum value of the respective factors. Their slope indicates the effect on the investigated variable. Steep slopes denote a large influence whereas horizontal graphs indicate a low influence. We can deduce interactions of different factors by means of their graphs. Parallel graphs indicate no interactions while crossing graphs indicate strong interactions.

Post-processing using photonic curing with shaped pulses

As introduced in Chapter 4.2.3, there are several options to shape the light pulses in photonic curing. In this study, I investigated the influence of the following factors on the sheet resistance of printed silver layers: bank voltage U_{bank}, envelope duration t_{env}, number of micropulses $n_{\mu pulse}$ and whether or not to use pre-drying P.

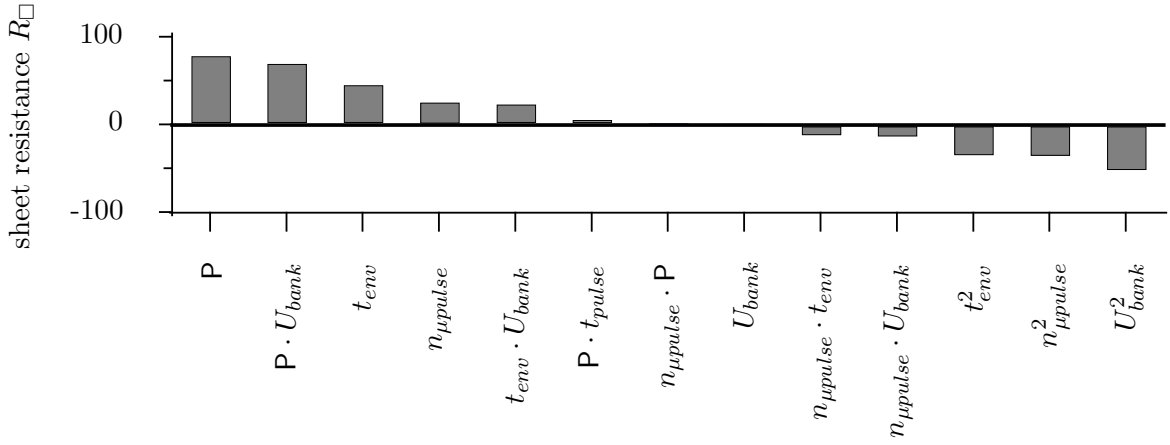

Figure 5.4.: *Pareto* diagram showing the influences of post-processing parameters and their combination on the sheet resistance $R_\square$, pre-drying P, bank voltage U_{bank}, envelope duration t_{env} and number of micropulses $n_{\mu pulse}$.

Figure 5.4 illustrates those parameters on the sheet resistance using a *Pareto* diagram. The main factor is pre-drying P, i.e. very short pulses with lengths of 100 μs at the beginning of the post-processing. Using pre-drying, we can significantly improve the conductivity of printed silver layers.

The second highest impact on $R_\square$ has a combination of the bank voltage U_{bank}, i.e. the energy density of the bulb, with pre-drying P. Less influence have, in descending order, the bank voltage U_{bank} squared, envelope duration t_{env} and the number of micropulses $n_{\mu pulse}$ squared and the envelope duration t_{env} squared. Low influence show the factors number of micropulses $n_{\mu pulse}$, the combination of envelope duration t_{env} and bank voltage U_{bank} as well as combinations of number of micropulses with bank voltage and number of micropulses with envelope duration. In this investigation, we can neglect the influence of pre-drying P with envelope duration t_{env}, pre-drying P with number of micropulses $n_{\mu pulse}$ and, surprisingly, the bank voltage U_{bank}.

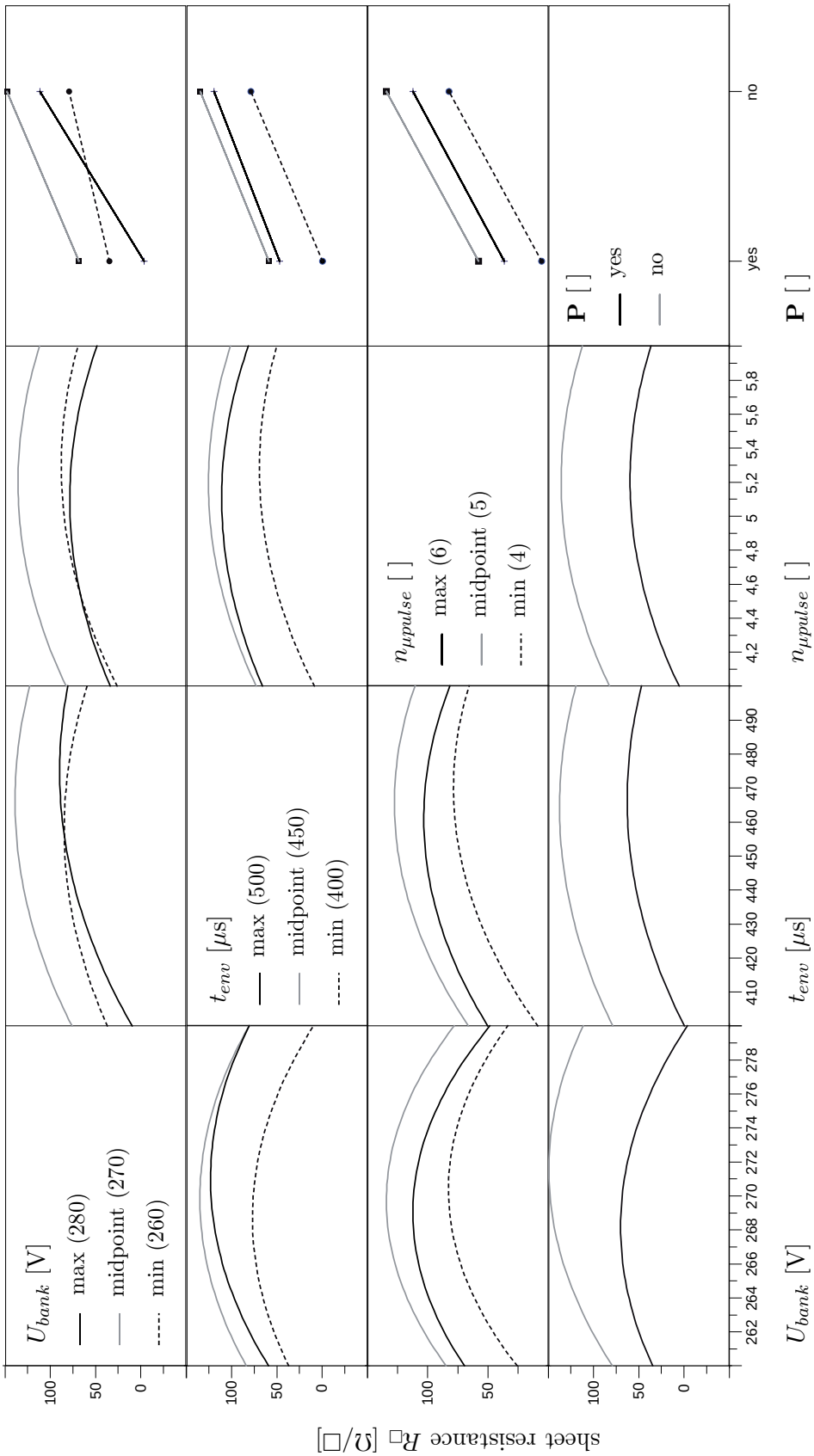

Figure 5.5.: Interaction graph for the sheet resistance $R_\square$. It illustrates the interdependence of the factors bank voltage U_{bank}, envelope duration t_{env}, number of micropulses $n_{\mu pulse}$ and pre-drying **P**.

Obviously, in post-processing with complex pulse shaping, the voltage driving the capacitor bank U_{bank} is less important than in single pulses. Using single pulses, bank voltage U_{bank} and envelope duration t_{env} are parameters directly contributing to the energy density applied to the sample surface. Thus, they ultimately influence the heating of the sample layer. When using pulse shaping, the influences on the temperature profile of the sample layer are considerably more complex. First, there are more parameters influencing the energy density. Second, the temperature profile of the sample layer has no longer only one peak but rather several [52], depending on the number of micropulses and whether we use pre-drying. Thus, the bank voltage driving the light bulb becomes less influential.

In studies with independent parameters, the influence of one parameter may depend on the level of another. One way to determine whether and how parameters influence each other is a so called interaction graph. From such graphs it is possible to determine if there are main effects or interactions influencing the result. A main effect means that the influence of one parameter on the result is not dependent on other parameters. An interaction means that a change in the result cannot be attributed solely to the change in one parameter but rather to a combination of several parameters. If there are no interactions between two parameters, the lines in the interaction graph are parallel. Crossing lines indicate an interdependence of both parameters regarding the result.

Figure 5.5 shows the interaction graph of the sheet resistance, depicting the investigated parameters and how they influence the sheet resistance.

The most noticable result we can obtain from this graph is the influence of pre-drying P (cf. Figure 5.5, last row and last column) on the sheet resistance: $R_{\square}$ will always be lower when using pre-drying. This effect occurs regardless of the values of the other parameters. There is no interaction between pre-drying and envelope duration t_{env} or number of micropulses $n_{\mu pulse}$, respectively. An interaction of bank voltage U_{bank} and pre-drying may be observed in Figure 5.5, last column topmost graph. A growing influence of pre-drying on the sheet resistance can be perceived with increasing value of the bank voltage.

Another noteworthy observation is the interaction of the bank voltage U_{bank} with all parameters (cf. Figure 5.5, first row and first column). In the first row, the starting values of the sheet resistance are in ascending order: maximum, minimum and midpoint of the bank voltage. But then the graphs of maximum and minimum intersect and the terminus of the interaction graphs are in the following order: ascending from minimum, maximum to midpoint. From this and the parabolic shape of the curves in the graphs we can deduce that an increase in bank voltage is not imperative for a reduction of the sheet resistance. We rather see an increase in sheet resistance when raising the bank voltage and after a maximum a decrease but not necessarily back to the starting value (cf. Figure 5.5, e.g. first row undermost graph). In the first row, we see crossing graphs of minimum and maximum bank voltage, with the envelope duration t_{env}, number of micropulses $n_{\mu pulse}$, and pre-drying P. This indicates an interaction between those parameters.

Looking at the envelope duration t_{env} in 5.5, second column, again we see a hyperbolic shape of the graphs although not very pronounced. With increasing envelope duration, the sheet resistance will also increase to a maximum at a little more than the medium envelope duration and then either decrease again or stay near at what appears to be a saturation level (cf. 5.5, second column, first row maximum bank voltage).

The graphs for the number of micropulses $n_{\mu pulse}$ show similar behavior as the envelope duration (cf. 5.5, third column). The lowest sheet resistance can be observed with the lowest

number of micropulses. Increasing this number, the sheet resistance will also increase. A maximum sheet resistance occurs slightly after the medium of the number of micropulses with a following decrease of $R_{\square}$. The slopes of the hyperbolic graphs of the number of micropulses are more pronounced than the ones of the envelope duration. From these results, we can deduce that it is reasonable to use either a low or a high number of micropulses to obtain low sheet resistance.

A remarkable result is that in each of the factors bank voltage U_{bank}, envelope duration t_{env} and number of micropulses $n_{\mu pulse}$ the midpoint results in the highest sheet resistance and the lowest settings of those factors result in the lowest sheet resistance.

We can conclude that using pre-drying improves the sheet resistance, as does a high bank voltage. Still, the highest settings of the parameters, i.e. the highest amount of energy introduced into the silver layer, do not automatically result in the lowest sheet resistance as would be expected. The settings need careful adjustment in order to obtain the optimum results. This especially applies to interacting parameters.

5.1.3. Multilayer behavior, placement dependency and isotropy

After interpreting the impact of post-processing on the sheet resistance of a printed silver layer, this section compiles three issues that are related to post-processing. The first is the behavior of printed silver layers in a multilayer stack. Then, I explain the influence of the placement of a sample on the substrate in relation to printing order. I conclude this section with a look on the correction factor in *van der Pauw* measurements.

Behavior of printed silver in a multilayer stack

The post-processing of printed silver layers using photonic curing does not only influence its conductive behavior but also its chemical properties. This is especially true for how the layer will behave when being overprinted with solvent based inks. The solvents used in those inks affect residual non-silver compounds in the layer and alter them. Figure 5.6 illustrates this phenomenon: The left image shows an imcompletely sintered silver layer overprinted with PMMA-ink. The solvent turns the affected areas of the silver layer dark. Although the conductivity of the sample was deemed sufficient, the post-processing of the layer is obviously not complete.

Contrary to this, the right image of Figure 5.6 shows a completely sintered silver layer overprinted using the same PMMA-ink. Clearly, here the solvent does not affect the layer underneath as we see no discoloration of the silver layer. The rainbow coloration results from interference structures in the PMMA layer.

The conclusion we can draw from those observations is the following: Although the conductivity of a layer may be sufficient for the desired application, the layer might still need post-treatment to prime it for further processing, depending on the individual application. If a silver layer is on top of a stack, the conductivity might be the most relevant property. As the layers underneath are already cured, their solvents should not compromise the silver layer. If the silver layer is at the bottom or in the middle of the stack, its chemical properties and how they are affected by solvents of subsequent layers play a vital role. The interactions of the respective inks with the silver layer should be considered beforehand. If necessary, tests with simple layer stacks should be conducted for evaluation.

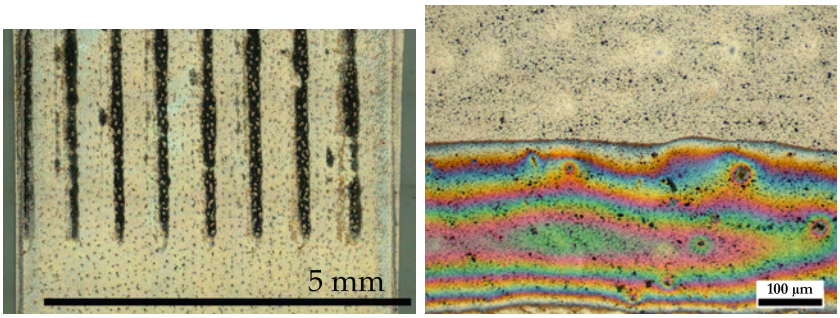

incomplete post-processing of silver layer

thorough post-processing of silver layer

Figure 5.6.: PMMA-ink can affect the silver layer underneath, turning it dark (left image) when the silver is not completely sintered. When the post-processing of the silver is sufficient, the PMMA-ink will not affect the silver layer (right image).

Placement on sample

While conducting the measurements regarding design of experiments of post-printing parameters, a trend became apparent tieing the sheet resistance to the placing of the measured area on the printed sample. Figure 5.7 illustrates this exemplarily. The ascending letters indicate the placing on the substrate with A being printed first and P last. Each row (A, B, C etc.) shows several measurements, one for each rectangle. There is not apparent correlation between the placement of the rectangle (further to the drive side or further to the operator side of the machine) and the repsective sheet resistance. For a layout of the printing plate, see Appendix A.2. Note the sudden drop of sheet resistance after the 5th row (E) on the substrate. This phenomenon occured reproducibly in every sample, i.e. impression.

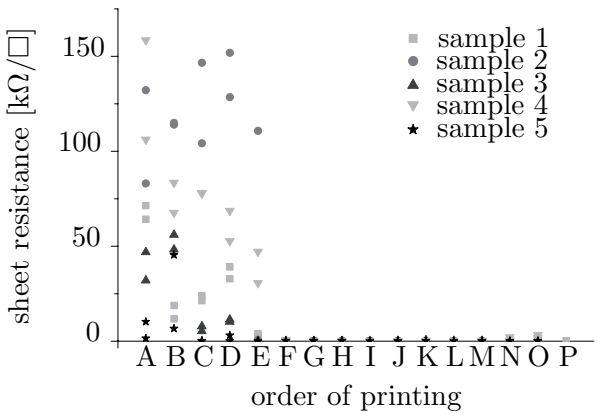

Figure 5.7.: Sheet resistance $R_{\square}$ in relation to the order of printing; ascending letters indicate the order of printing on one sample with A being printed first and P last. Different symbols denote subsequent samples, i.e. print runs. Note the drop of sheet resistance after the 5th printed row.

Currently, I am not able to attribute this phenomenon to a certain cause. A discussion of plausible reasons for this behavior of the sheet resistance may be obtain from Chapter 6.1.1.

However, as the cause of the deviation of the measurements is not obvious, I discarded the samples printed first, i.e. the ones showing a significantly higher sheet resistance than the rest, for interpretation.

Correction factor in van der Pauw measurements as indicator for layer isotropy

During the measurements of the sheet resistance $R_\square$, a certain trend appeared linking the correction factor f of the *van der Pauw* method (cf. Equation 4.8 on page 46) to the magnitude of the sheet resistance. The correction factor f is calculated as a function of the ratio of the potential difference in one direction of the sample to the one perpendicular thereto [150]. Figure 5.8 shows a diagram of the progression of f depending on the ratio of the potential differences.

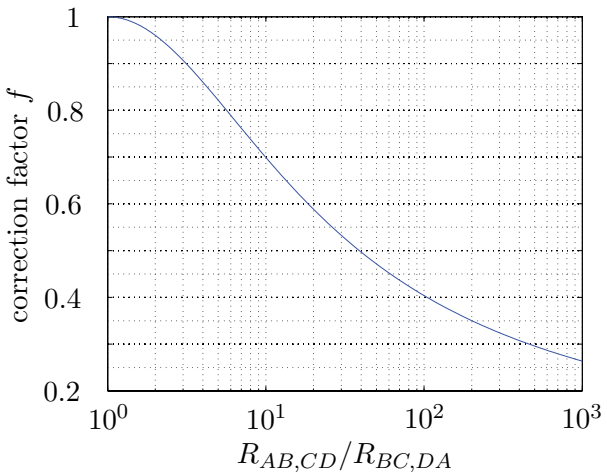

Figure 5.8.: Correction factor in *van der Pauw* method, calculated using VAN DER PAUW's approach in [150]. Matlab-code adapted from [79].

With increasing difference between $R_{AB,CD}$ and $R_{BC,DA}$, f will be lower. As a large difference between $R_{AB,CD}$ and $R_{BC,DA}$ also signals differences in the directionality of the electrical material properties, it indicates anisotropy. We therefore can use f as in indicator for the isotropy of a sample: The higher f is, the higher is the isotropy.

Figure 5.9 shows the correction factor f subject to the respective sheet resistance $R_\square$ of the measurements in this study. We notice several accumulations, indicated by dashed margins: The first one contains samples with a low sheet resistance of $R_\square \lesssim 10^3\,\Omega/\square$ and correction factors of $\gtrsim 0.4$. This indicates that samples with high conductivities also show a good isotropy.

The next accumulation contains samples in the range of $10^2\,\Omega/\square \lesssim R_\square \lesssim 10^6\,\Omega/\square$ and a correction factor of $\lesssim 0.5$. The correction factor of these samples indicates a high directionality of the electrical material properties (cf. Figure 5.8). Thus, they are anisotropic.

The third accumulation contains samples with sheet resistances of $R_\square \gtrsim 10^5\,\Omega/\square$ and correction factors of $\gtrsim 0.4$. Again, this indicates more isotropic samples.

These observations may seem inconsistent. But when we look more closely on the order of magnitude of the sheet resistance the results are conclusive. As stated above, the correction factor is calculated as a function of the ratio of potential differences. If the potential differences

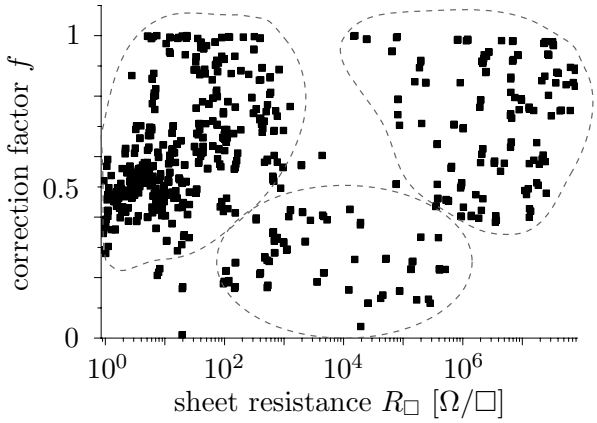

Figure 5.9.: Correction factor in *van der Pauw* measurements of printed silver layers in depency on the sheet resistance. High values of the correction factor indicate a high isotropy of the measured sample. The different accumulations are indicated by dashed lines.

themselves are low, the impact of their ratio is high. If the potential differences are high, smaller differences do not have the same impact as with lower potential differences.

Thus, we can deduce that the samples with low sheet resistances (first accumulation) are indeed more isotropic as their correction factor is high. The second accumulation with middle sheet resistances shows a distinct anisotropy. Although the third accumulation appears to indicate a certain isotropy of the layer properties, the inference should be considered carefully: As the values of $R_{AB,CD}$ and $R_{BC,DA}$ are very high in these samples, differences between both values have less impact on their ratio. Thus, those samples appear as isotropic as samples from the first accumulation, although they actually have a higher directionality.

The conclusion of the contemplations above is the following: For samples with a high conductivity, i.e. a low sheet resistance, the correction factor in *van der Pauw* measurements is a reasonable indicator for isotropic behavior of the electrical layer properties. The lower the conductivity, the less feasible is the correction factor.

5.2. Printed etch resist

This section focusses on the results of the trials regarding the etch resist using design of experiments for determining the printing parameters printing speed v_{print}, pick-up volume $V_{pick-up}$ and printing force F_{print}. First, I introduce lateral characteristics of printed lines based on microscopic images of printed etch resist. Then, I give an overview of the influence of single factors on the characteristics of the halo effect in printed lines. Concluding, I explain the interaction of different printing parameters and their impact on the line width.

5.2.1. Lateral characteristics of printed lines

I investigated the lateral characteristics of printed line shaped resist structures using an optical microscope. During the course of the analysis, several details became apparent that I exemplarily introduce in this section.

The most obvious result is the following: Every printed line is distinctivly wider than its nominal width. We can observe this phenomenon for every value of nominal line width, every length of spacing between the lines and for every parameter combination of the factors. This is common in flexographic printing. For further information, I refer the reader to the investigations of Bould [26] and Deganello [36]. The line width also increases with decreasing spacing between lines.

Regarding the edge quality, the following observation can be made: The quality increases with increasing pick-up volume of the anilox roller. Low pick-up volumina cause ragged lines and also bulging similar to inkjet printing [139]. With small pick-up volumina, phenomena as viscous fingering [128] are more pronounced than with a high pick-up volume. Amongst others, I attribute this to the fast evaporation of the solvent. When only little fluid volumina are transferred, the drying time is very short. Thus, the printed layer solidifies before the ink can level on the substrate. As a higher pick-up volume results in a higher fluid volume transferred, this will also increase drying time. Therefore, the levelling may be faster than the solidification of the printed layer (cf. the investigations of Bornemann for gravure printing [22]). As the investigations in this study are empiric and phenomenological, I refer the reader to literature regarding fluid dynamics.

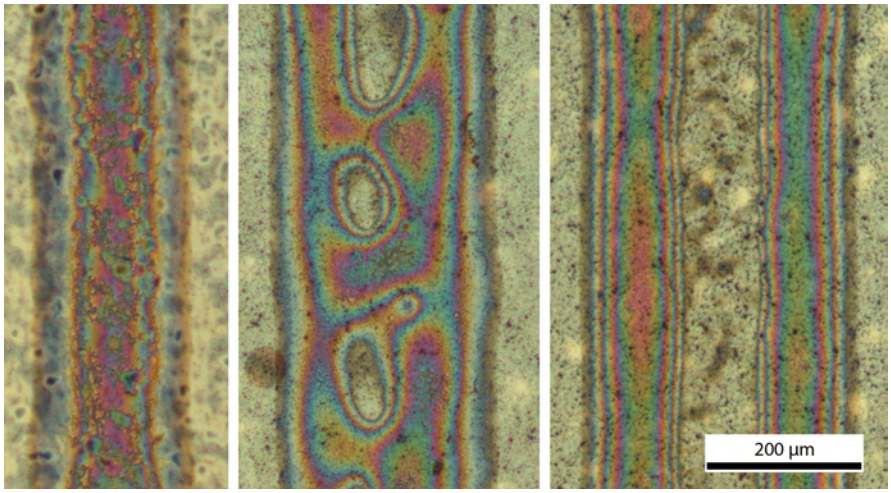

Figure 5.10.: Progressing halo effect in printed PMMA lines, values in parentheses indicate nominal line width. Left: line without halo effect (100 μm), middle: line with discontinuous void and incipient halo effect (200 μm), right: distinct halo without primary line (200 μm).

Figure 5.10 illustrates the progressing halo effect in printed line structures for high a pick-up volume ($V_{pick-up} = 24\,\mathrm{m}^3/\mathrm{m}^2$). The left image shows a single line (nominal line width 100 μm). The line depicted in the middle image (nominal line width 200 μm) exhibits an incipient halo effect, starting with small openings in the middle of the line. In the right image, the halo is very pronounced, splitting the primary line (nominal line width 200 μm) into two. The void between both lines is almost as wide as the nominal line width.

These observations do not support my hypothesis regarding the cross-sectional behavior of printed lines (cf. Chapter 4.2.4). There, I stated that with increasing printing force a printed line gradually changes its cross section from one peak (phase 1 & 2), forming a valley and two peaks (phase 3) to forming two separate lines with a void in-between (phase 4 & 5).

The parameter variation from the DoE experimental plan did not allow for varying only the printing force with all other parameters fixed to validate the hypothesis. Given the results presented, we can conclude that for the parameter variations used here, the hypothesis applies only partially: Phase 1 & 2 may be observed, although the exact juncture in the phases is not discernible. Phase 3 is not apparent, but we can observe phase 4. There was no distinct saturation regarding increasing line width. Thus, we can not reconstruct phase 5.

Regarding the presented results, phase 3 of the hypothesis should be altered. Instead of a gradually increasing valley we observe the formation of small openings, roughly in the middle of the line. The openings then grow into a discontinuous void before the formation of a distinct halo in phase 4.

We can conclude that the hypothesis regarding the gradual formation of the halo effect in printed lines due to increasing printing force is not fully applicable to the material system used in this study. I was able to validate parts of the hypothesis and I introduced a possible alteration regarding the part not applicable.

5.2.2. Influence of single factors

The following section introduces the *Pareto* diagrams (cf. Chapter 5.1.2, Section *Interpreting results from DoE*) of the characteristics of the halo effect in printed lines. The halo effect is represented by the line width a, the halo on both sides ($\mathsf{H_{os}}$, $\mathsf{H_{ds}}$) and the void in-between e. Figure 5.11 illustrates this with a microscopic image of a printed line (left) and a schematic cross section indicating said geometric features (right). Note that the printing direction is parallel to the length of the line. The factors used in this design of experiments are printing speed v_{print}, pick-up volume $V_{pick-up}$ and printing force F_{print}. As introduced in Chapter 4.2.1, the printablity tester IGT F1 was used for this trials.

The lines I analyzed have several nominal widths: 50 μm, 100 μm and 200 μm. For interpretation, I used the width of line properties (a, $\mathsf{H_{os}}$, $\mathsf{H_{ds}}$, e) in relation to the nominal line width as effect variables in the abovementioned design of experiments. Thus, the dimension of the effect variables is [%] for evaluation, although their actual dimension is [μm]. In the following, I introduce the *Pareto* diagrams of the geometric features line width a, width of halo on the operating side $\mathsf{H_{os}}$ and the drive side $\mathsf{H_{ds}}$ of the machine and the width of the void e.

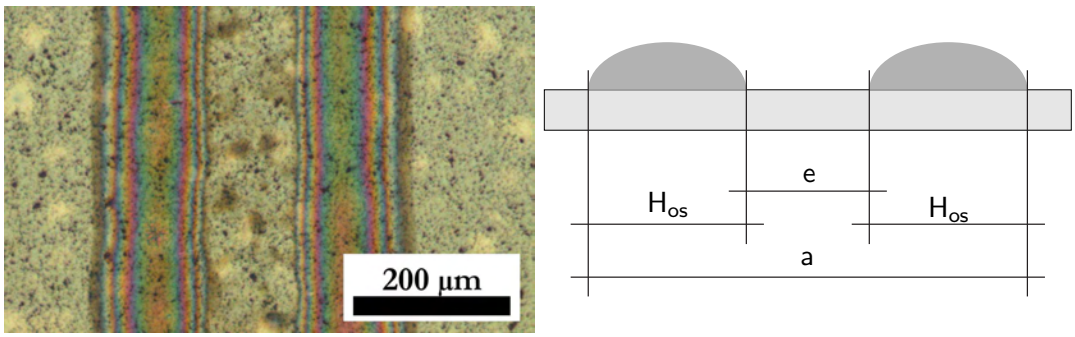

Figure 5.11.: Microscopic image (left) and schematical cross section (right) of printed lines with distinct halo effect: void e, halo on the operating side of the machine $\mathsf{H_{os}}$, halo on the drive side of the machine $\mathsf{H_{os}}$, line width a. Note the orthogonal printing direction to the cross section.

The *Pareto* diagram of the variation of the line width in Figure 5.12 identifies pick-up volume $V_{pick-up}$, printing force F_{print} and their product as the three main influencing factors on the line width. Less impact has the product of pick-up volume $V_{pick-up}$ and printing speed v_{print}. We can neglegt the influence of combined printing force F_{print} and speed v_{print} and the speed v_{print} squared. A negative influence show the printing force F_{print} squared and the printing speed v_{print}. Negative influence indicate a reversed proportionality, meaning with increasing printing speed, the line width will decrease.

We can conclude from those results to carefully adjust pick-up volume and printing force in order to achieve a certain the line width. The printing speed by itself is less important in this regard than the combined with the other parameters.

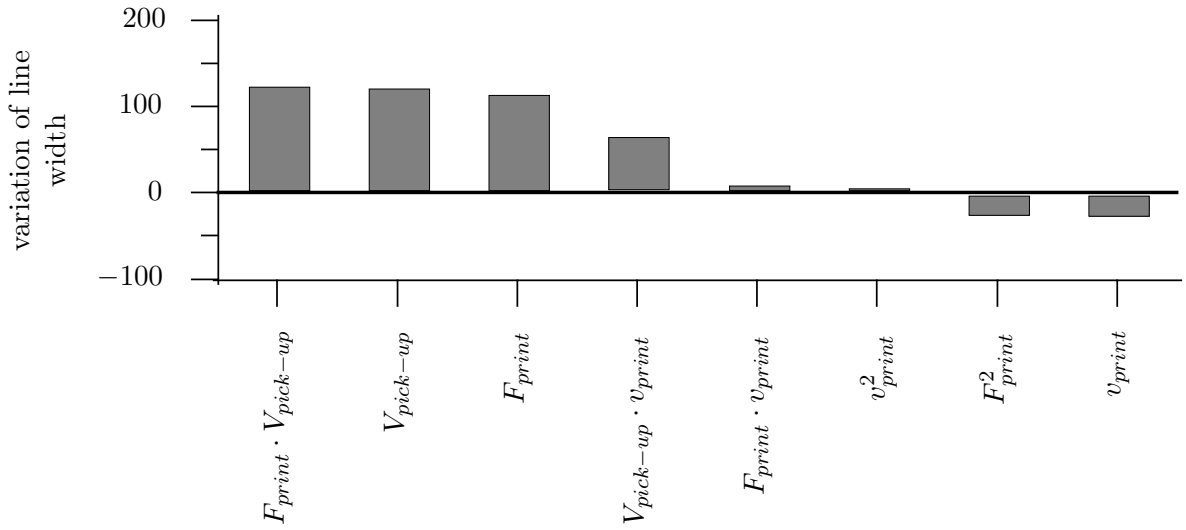

Figure 5.12.: *Pareto* diagram showing the influence of printing parameters (printing speed v_{print}, pick-up volume $V_{pick-up}$ and printing force F_{print}) and their combination on the overall line width as results of a design of experiments to determine their impact on the halo effect of printed lines.

Figure 5.13 depicts the *Pareto* diagram of the variation of the halo effect, i.e. the lines squeezed on both sides of a printed line in printing direction. Light grey bars represent the halo on the operating side of the machine, dark grey bars the halo on the drive side. Looking at the *Pareto* diagram, we see the pick-up volume $V_{pick-up}$, the printing force F_{print} and their product as the three main influencing factors (cf. Figure 5.13). Here, both pick-up volume $V_{pick-up}$ and printing speed v_{print} are more influential than regarding line width. The former is conclusive: more ink provided results in more pronounced halos. Note the differences between operating and drive side of the machine: The first three factors have a higher impact on the markedness of the halo on the drive side. $F_{print} \cdot v_{print}$, F_{print}^2, and v_{print}^2 even have a diametrical influence, whereas the effect of the printing force on the drive side halo is less pronounced.

The main factor influencing the void between two halos is the pick-up volume $V_{pick-up}$, as the *Pareto* diagram of the void in Figure 5.14 shows. The higher it is, the wider will also the

void be. A higher pick-up volume also means more ink is provided. That would explain a more pronounced halo effect, i.e. wider and higher lines at the edges. Along with this, the ink is drawn to the edges, leaving a wider void.

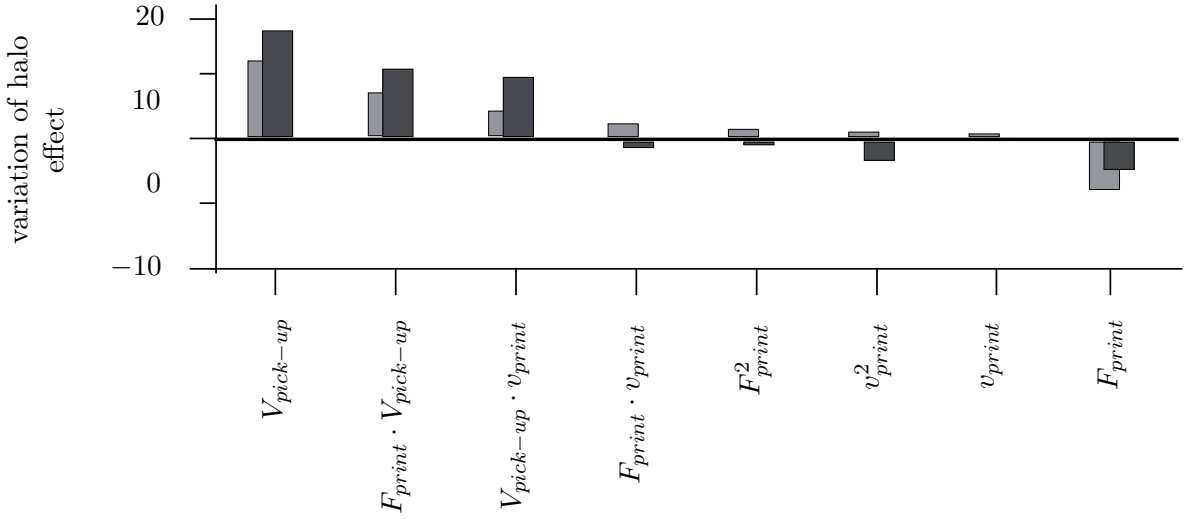

Figure 5.13.: *Pareto* diagram showing the influence of printing parameters and their combination on the halo effect of printed lines. Light grey bars represent the halo on the operating side of the printing press and dark grey bars the halo on the drive side.

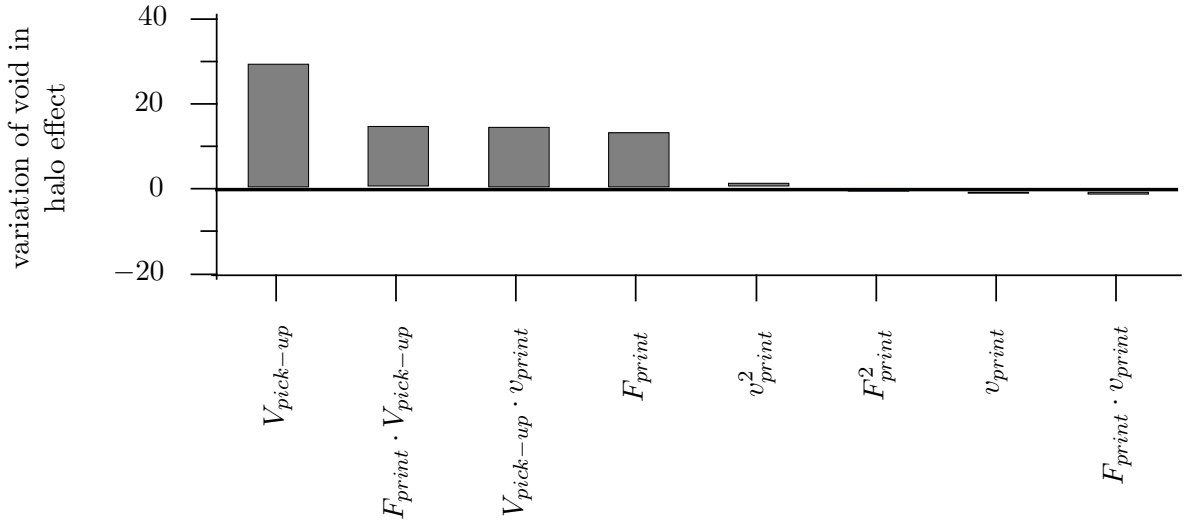

Figure 5.14.: *Pareto* diagram showing the influence of printing parameters and their combination on the void in printed lines caused by the halo effect.

5.2.3. Influence of factor combinations

Figure 5.15 depicts the interaction graph for the width of a printed line. As the majority of the graphs show non-linear behavior, it indicates a strong interdependence between the factors. Merely the implications of altering the pick-up volume $V_{pick-up}$ are hardly affected by other parameters, as the graphs in the last column show. Increasing the pick-up volume $V_{pick-up}$ will always lead to a broader line width. Although the printing force F_{print}, if set to minimum or maximum, compromises the linearity of the influence of the pick-up volume (cf. Figure 5.15, third column, second graph).

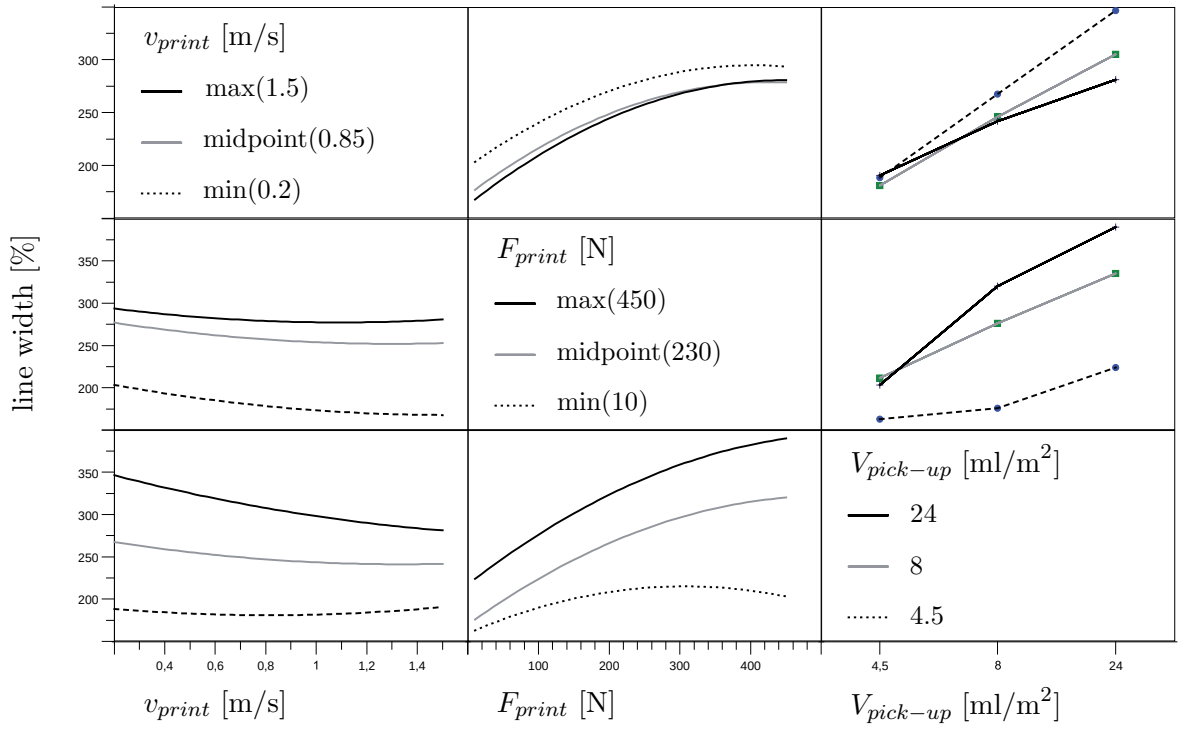

Figure 5.15.: Interaction graph for the width of a printed line relative to its nominal width. It illustrates the interdependence of the factors printing speed v_{print}, printing force F_{print} and pick-up volume $V_{pick-up}$.

Looking at the printing speed v_{print} (cf. Figure 5.15, first column), we see that the line width decreases with increasing speed. In combination with the pick-up volume $V_{pick-up}$ the graphs show almost linear behavior. The impact of the printing speed is more pronounced, the higher the pick-up volume is. At the minimal pick-up volume of 4.5 ml/m^2, a change in printing speed has almost no effect on the line width.

The interaction graph of printing speed and printing force indicate that at the lowest printing force, increasing printing speed leads to wider lines. At higher values of printing force the influence of varying printing speed is negligible.

The second column illustrates the influence of the printing force F_{print}. With increasing printing force, the lines will become wider. This effect becomes stronger with increasing pick-up volume: At a low pick-up volume, an increase in printing force leads to slightly wider lines. The higher the pick-up volume is, the more impact does an increase in printing force have on

the line width. The impact of the printing speed on the effect of altering the printing force is negligible.

We can conclude that altering the pick-up volume has the most impact on the effect of both printing speed and force. Printing force should also be considered as in influencing factor on the other parameters, whereas the impact of the printing speed on printing force and pick-up volume is negligible.

5.3. Etching process

5.3.1. Impact of sintering parameters

Figure 5.16 shows the influence of the energy density during the post-processing on the etching rate of a printed silver layer. To create this diagram, I used data from Fulek [46]. As the materials and printing parameters used are the same as in this study, I exploit these results as a preliminary test for the present study.

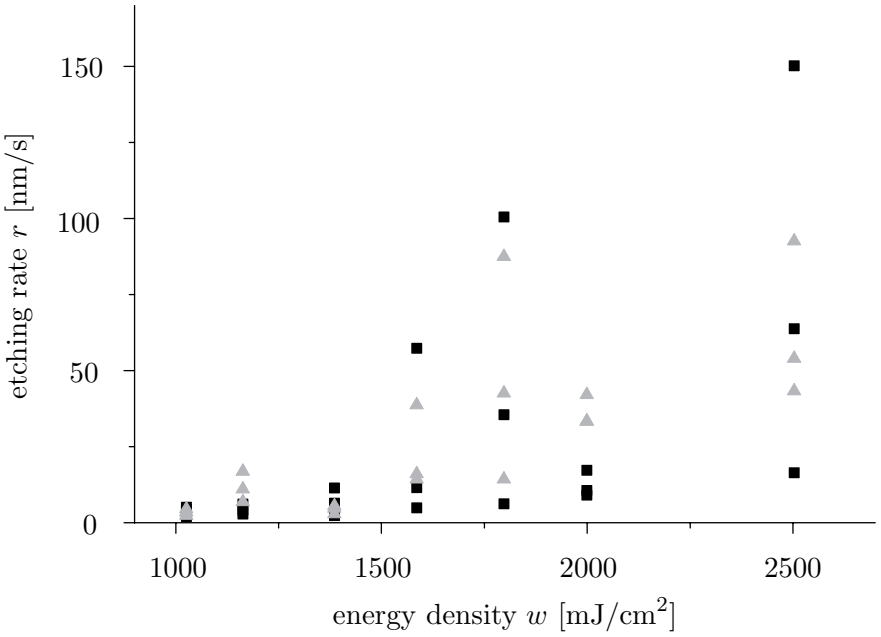

Figure 5.16.: Representation of the influence of the energy density w during post-processing on the etching rate r of a printed silver layer. Black squares indicate a proportion of nitric acid to water of 30:70; grey triangles a proportion of 26,7:73,3. With increasing energy density, the etching rate will increase and we also see a broadening of the range of values. Measurement data adopted from [46], own representation.

Note that the etching rate increases with increasing energy density and we also see a broadening of the range of values. I attribute this to residual organic compounds in the printed silver layer. With higher energy, less organics remain in the layer. This hypothesis only works if the etching rate of the organic compounds is higher than that of silver. The etching rate of samples sintered at low energy densities is a combination of the etching rates

of the residual organic compounds and the actual silver particles, respectively. The higher the applied energy during sintering, the lower will the proportion of the etching rate of the organics be. Figure 5.17 illustrates this schematically.

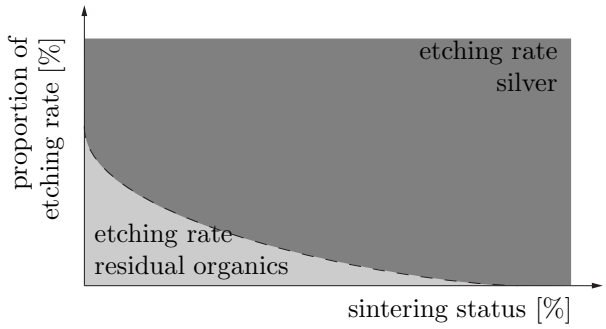

Figure 5.17.: Schematic of proportions of etching rates of silver and residual organic compounds in a printed and (partially) sintered layer. Note that the ratio may vary.

With the samples I printed, post-processed and etched for this study, I was not able to reproduce Fulek's results from [46]. Figure 5.18 shows the etching rate depending on the energy density w during post-processing measured for this study.

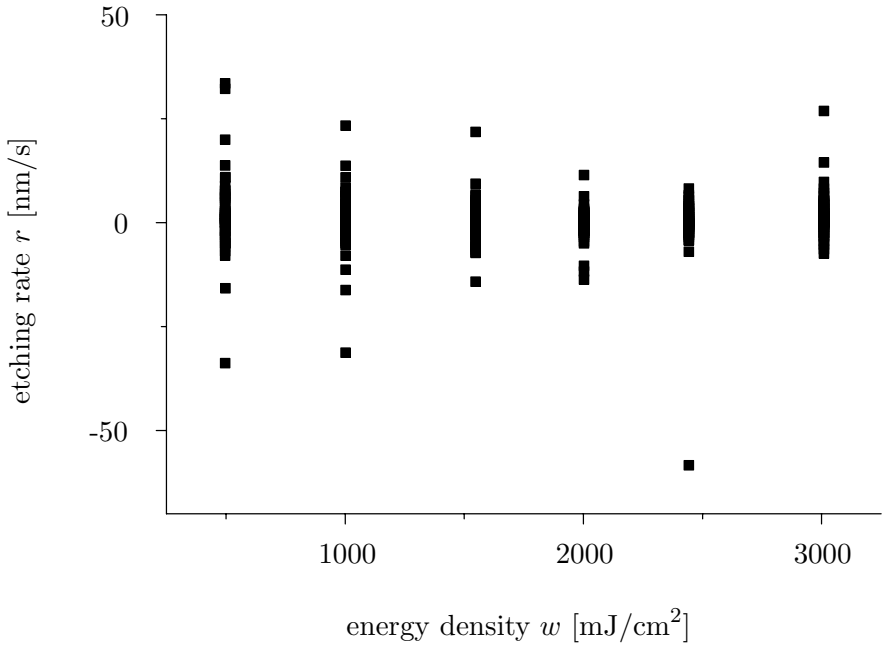

Figure 5.18.: Etching rate r of printed silver layers depending on the energy density w during sintering.

The trend shown by Fulek linking the etching rate to the energy density w (cf. Figure 5.16) during post-processing is not apparent for the samples in this study (cf. Figure 5.18). Here, there is no obvious trend on how the etching rate depends on the energy density w

during post-processing. We even see negative etching rates in the graph of Figure 5.18. As etching is an ablative process, negative etching rates indicate the raise of the layer thickness. An extensive discussion of this phenomenom can be found in Chapter 6.1.2.

5.3.2. Etching of the resist layer

During etching, the etchant not only ablates the functional, i.e. silver layer, but also affects the resist layer. Looking at the surface of a PMMA layer after the etching step, we notice the formation of small spheres with diameters of a few microns and heights in the range of few ten nanometers.

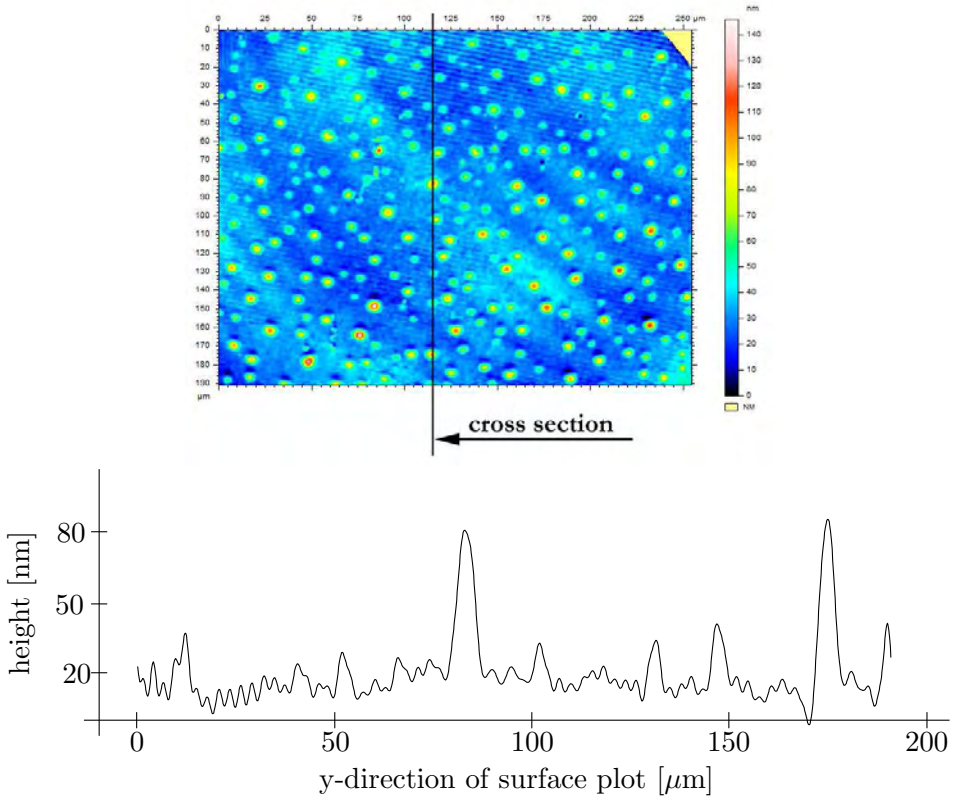

Figure 5.19.: Formation of droplets on the surface of a PMMA-layer after etching. Upper image: surface plot, lower image: cross section of surface at marked position. High, wide peaks indicate spheres whereas small, high frequent peaks are measurement artefacts.

Figure 5.19 illustrates this phenomenom with a map of the sample surface (upper image) and a cross section (lower image). The color of the surface plot indicates its height with blue/green being low values and yellow/red being high values.

The graph in the lower image illustrates the cross section at the marked position. High, wide peaks indicate spheres whereas lower peaks with a higher frequency are measurement artefacts. Note the different scaling of abscissis and ordinate.

The spheres appear predominantly on large PMMA areas, less on the surface of the silver layers. Images taken with an optical microscope show that the spheres are translucent, thus

most likely made of resist material. A plausible explanation of their origin is the following: During the etching process, a certain thickness of the resist layer absorps the etchant, partially dissolving and thus detaching from the solid part of the layer. After removal of the sample from the etching bath, rinsing contributes to this process. When the sample is left to dry, the partially dissolved portion of the layer forms shrinks due to evaporation, contracts and forms the spheres.

As I have no facility to investigate the chemical nature of the spheres or observe their formation in-situ, I cannot give a definite explanation of their origin.

5.3.3. Lateral characteristics of etched silver lines

As the determination of the etching rate using 20% nitric acid was inconclusive, I used a higher concentration (40% nitric acid; $r \approx 60\,\mathrm{nm/s}$) to transfer the resist structures into the silver layer. Figure 5.20 shows some exemplary images obtained by light microscopy. The black scaling bars in the upper two rows indicate $200\,\mu\mathrm{m}$ and the grey scaling bars in the lower row indicate $100\,\mu\mathrm{m}$.

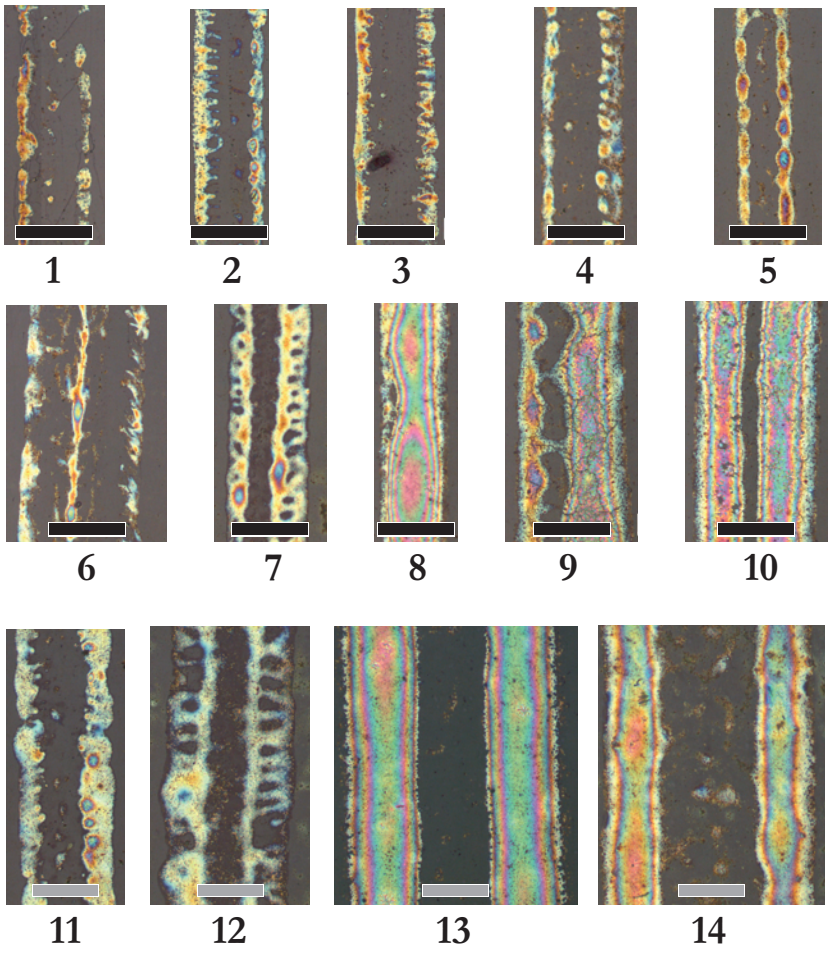

Figure 5.20.: Microscopic images of etched silver structures. Black scaling bars indicate $200\,\mu\mathrm{m}$ (1 - 10), grey scaling bars indicate $100\,\mu\mathrm{m}$ (11 - 14).

The nominal line width of the PMMA lines in the upper row (images 1 - 5) is 100 μm. Note that the halos are very small with a wide void in-between. The width of the halos is in a range lower than line widths possible by directly printing silver lines using flexographic printing. Nevertheless, the line quality is very poor: The edge sharpness of the halos in the direction of the void is very low (2 & 3). We can see bulging (1, 4 & 5) and also discontinuous lines. Those lines are not appropriate for printed electronics.

The second row depicts results from nominal line widths of 200 μm (6, 7, 9, 10) where the halo effect is very obvious, and 50 μm (8) where there is no halo effect. The etched lines applicable for printed electronics in this row would be 8 and 10. As the width of line 8 is slightly less than 100 μm, it could also be produced by directly printing silver ink. The same applies for image 10.

In the bottom row of Figure 5.20 the magnification of the lines is higher, note the different scaling bar of 100 μm. The nominal line width of the resist layer in image 11 was 50 μm, in images 12 - 14 200 μm. The results depicted in images 11 & 12 are not approbriate for printed electronics for the same reasons explained above. The line in image 13 is straight, has very sharp edges and no disruptions, whereas 14 is also continuous but is less straight. Both lines could be used for printed electronics, although regarding the line width of the halos, structured printing of silver ink, i.e. no etching step, may also result in similar lines.

5.4. Summary of the results

The printed silver layers were homogenous with a roughness of few ten nanometers. The main results regarding photonic curing of printed silver layers are the following: As expected, photonic curing does improve the conductivity. The extend of the increase depends on the energy density the sample is exposed to when using a single pulse. Using pulse shaping, the main impact has the so-called pre-drying where very short pulses prime the sample for the actual curing process. Envelope duration and number of micropulses also have a considerable influence on the conductivity.

When printing line shaped elements we need to consider the halo effect. Nearly all printed samples, regardless the printing parameters, show a more or less pronounced halo effect. Here, the most influential parameter is the pick-up volume. A high pick-up volume results in wide halos around a printed line with a distinct void in-between. The second largest impact has the printing force, whereas the influence of the printing speed is almost negligible.

I was not able to fully validate the hypothesis of the behavior of the cross-section of printed lines in dependency of the printing force. Nevertheless, I could relate parts of the hypothesis to the results of the experiments.

It was not possible to determine a relation between etching rate and degree of post-processing, i.e. energy density during photonic curing with the parameters used in the trials of this study. The measurements were inconclusive. Therefore, I used a different dilution of the etchant to transfer the layout of the printed resist structures into the silver layer. The width of the etched structures with high line quality, i.e. the ones that may be used for printed electronics are in the range of lines that are also printable using silver ink and flexography. The etched lines with widths significantly lower than what is possible to directly print have poor line quality.

6. Discussion

With the results presented above I showed that it is possible to structure printed silver layers using an etch resist structured by flexography. I was not able to link the etching rate to the parameters during post-processing of the silver layer. In this chapter, I will assess those results critically and discuss the procedure I applied.

The chapter starts with a discussion of details regarding the experiments and measurements. Then, I evaluate the presented method and compare it to other structuring techniques that may be incorporated into printed electronics production. The chapter concludes with remarks on upscaling of the process.

6.1. Discussion of the presented method

This section disputes on several details of the presented experiments and measurements. First, I describe topics regarding post-processing. Then, I analyze the etching process, especially regarding the inconclusive results of the determination of the etching rate.

6.1.1. Post-processing of printed silver layers

Quotient space of photonic curing

To better understand the mechanisms of photonic curing and the impact of individual parameters on printed silver layers, a more extensive approach may be used, expanding the quotient space by also vary the parameters I kept fixed in this study. In the following, I state them with a short explanation:

Distance between bulb and sample According to inverse-square law, the intensity of radiation decreases with the square of the distance (cf. Equation 6.1, [57]).

$$intensity \propto \frac{1}{distance^2} \tag{6.1}$$

Thus, the energy density w in photonic curing will also decrease with increasing distance between bulb and sample surface. The distance settings can be varied in millimeter-range. For low energy densities this effect may be neglected. It should be investigated whether the inverse-square law has an impact using low energy densities.

Inert gas Using the PulseForge 1200 for photonic during, it is possible to activate the flow of an inert gas in the processing chamber. Typically this would be Nitrogen, but other gases as Argon are also possible. The flow of the gas might cause a cooling effect on the sample surface. Also, possibly present reactive substances, e.g. from ambient air or gassing off the heated sample layer, are transported away from the sample surface.

UV filter It is possible to cover the bulb with a UV filter. This is originally intended for usage with delicate layers, e.g. organic semiconductors. The implications on the curing of printed silver layers should be investigated as less UV radiation might affect the removal of residual organics in the printed layer.

Ratio and distribution of pulse length and interval in envelope In this study, I used a uniform distribution of pulses and waiting time in an envelope. It is feasible to alter each pulse and the interval to the next pulse individually. Thus, the temperature profile of the sample layer may be customized very precisely.

Individual pulse height In this study, when altering the bank voltage, this applied for every pulse. The bank voltage may also be varied individually for each pulse. This also contributes to customizing the temperature profile of the sample layer.

The investigation of those parameters is predestined for design of experiments as they open a vast parameter space, especially regarding the impact of pulse distribution and height in an envelope.

Placement dependency of sheet resistance

As outlined in Chapter 5.1.3, we see a certain dependency of the placement of a sample on the substrate regarding the measured sheet resistance. In the following, I discuss plausible causes for this extrem deviation of measurement values:

Chemical influences Residual solvent from cleaning of the printing plate before each print run is not a plausible cause of the deviations of the sheet resistance. I used IPA for this purpose. As IPA evaporates quickly it should not have been transferred into the printed layer. However, if it did, it would have been evaporated during oven drying. Though the area of the printed sample where the silver layer shows the highest sheet resistance is the one which came in contact with the plate first, the time between cleaning and printing is significantly longer than the whole print run itself. Thus, the sheet resistance should change more gradually and over a longer time frame.

Influences related to the printing process The printing process itself has a mechanical impact on the printed layer. For the sheet resistance to vary so strongly, its mechanically influenced properties have to drift strongly as well. Such parameters could be the layer thickness or its homogeneity. As I used the same printing parameters for each print run and they should not change during the run, the layer parameters should not change as well. As the rollers in the IGT F1 have a one-sided bearing, eccentricity might occur, resulting in a variation of the rotational speed.

Machine related causes When starting a printing run, the first rotation of the anilox roller inks it. Then, the ink is transferred onto the printing plate and directly onto the substrate. Possibly, the ink of the first rotation, transferred onto the substrate causes the deviations in the sheet resistance.

The deviation of the sheet resistance of the samples printed first on a substrate cannot be definitely attributed to one of the possible causes introduced above. To understand the reasons for the deviation, further investigations are necessary.

Sheet resistance

To rule out a possible shift of the sheet resistance during measurement, I measured the same sample over a period of time. Figure 6.1 depicts the results, normalized to the starting value ($R_{\square} = 30.24\,\Omega/\square$). The dashed lines indicate a permutation of the probe needles due to suddenly inconsistent measured values in MΩ-range.

Noticable is the low deviation from a starting value within a measurement series with roughly the same probe placement. Low deviations occur when permuting the probes. Also,

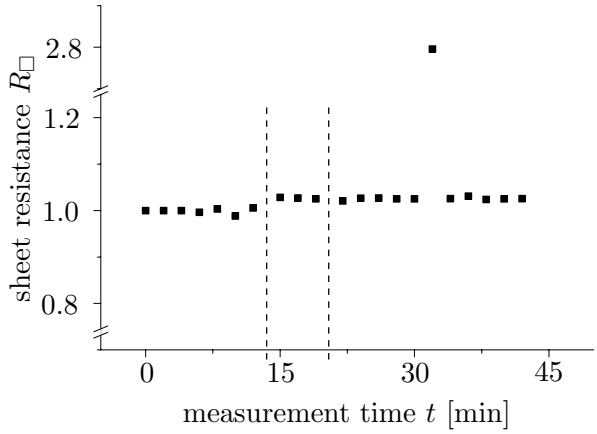

Figure 6.1.: Shift of sheet resistance of printed silver layers during measurement over a period of time. Dashed lines indicate permutation of the probe needles. Note the discontinuity of the ordinate.

permutation of the probe needles results in only a slight shift of the data. The value at 32 min clearly is a freak value as all other data show little deviation from the starting value.

We can conclude that the measurements of the sheet resistance as introduced in Chapter 4.1.2 are valid.

Blom states in [17] that the expected resistivity of the ink used in this study (InkTec TEC-PR030) is about $5,5\times$ the resistivity of bulk silver at 600 nm layer thickness. Equation 6.2 calculates the expected sheet resistance $R_{\square exp}$ based on Equation 4.6 (cf. page 45) and Blom with ρ_{Ag} as the resistivity of bulk silver [101] and h_{Blom} as Blom's layer thickness.

$$R_{\square exp} = \frac{\rho}{h} = \frac{5.5 \cdot \rho_{Ag}}{h_{Blom}} = \frac{5.5 \cdot 1.59 \cdot 10^{-8}\,\Omega\mathrm{m}}{6 \cdot 10^{-7}\,\mathrm{m}} = 0.14575\,\Omega/\square \tag{6.2}$$

In this study, the layer thickness of the silver layer is significantly lower than Blom's, about half as thick. The measured sheet resistances in this study are one to two orders of magnitude higher than Blom's. I attribute this to a) different post-processing methods, b) different layer quality and c) variations in the quality of the ink batch as introduced in Chapter 3.2.1.

6.1.2. Etching trials

The results of the determination of the etching rate in relation to the energy density during post-processing are inconclusive. We cannot see a trend and we also see negative etching rates. I calculated the etching rate subtracting the layer thickness after the etching process from the one measured before ($h_{etch} = h_{before} - h_{after}$) and dividing the result by the etching time t_{etch} (cf. Equation 4.9 on page 47). As etching is a subtractive process, negative etching rates imply an increase of layer thickness during the etching process. The following section will discuss why the results of these experiments are inconclusive and where the errors might be. Therefore, we analyze each part of the process in the following.

For this, we first dissect the complete process from a bare glass substrate to the calculation of the etching rate, illustrated by Figure 6.2.

1. The glass slide was prepared for spin-coating of the PMMA bonding layer by using ultrasonic baths with acetone and IPA. After spin-coating of the PMMA-ink, it was dried on a hot plate. Except for the PMMA-ink itself, there are no possible errors in this process step.
2. The silver layer was printed onto the PMMA bonding layer. Afterwards, the silver layer was dried in a ventilated oven to remove the solvent. Although the drying temperature was below the temperature of glass-transistion of the PMMA (105 °C), it might have affected the polymer.
3. The next step was to measure the sheet resistance of the silver layer. There are no possible errors in this process step.
4. Photonic curing of the silver layer might also affect PMMA. To this date, there are no investigations known related to the influence of photonic curing, i.e. exposure to very intensive broad band light pulses, on PMMA. This process step might affect the polymer.
5. The next step was to measure the sheet resistance of the silver layer again. There are no possible errors in this process step.
6. To determine the layer thickness, I marked edges into the layer stack using a scalpel. This manipulation affects the layer stack mechanically, cutting into it, possibly even compressing it.
7. Measurement of the edges and thus the layer thickness was done by confocal microscopy. Exact details may be obtained from Appendix A.1. Possible errors of this process step might be systematical errors of the microscope or software, assigning a wrong reference plane during levelling of the surface data, faulty mean profile or step height.
8. The next step was the actual etching step. Possible errors here might be the dilution of the etchant or the determination of the etching duration. I measured all components of the etchant carefully, using clean glass ware in a fume cupboard. Even if there was an error in preparing the etchant, it would be a systematical one and should only shift a possible trend of the etching rate regarding energy density during photonic curing. For determination of the etching duration, I timed each etching step manuall using a digital stop watch. Here, a systematic error of the stop watch may occur and a random error, resulting from my reaction time. As this most likely only prolongs the etching time, it cannot lead to negative etching rates.
9. The last step was again measuring of the layer edges to determine the thickness. The errors possible here are the same as in step 7. An additional error may occur in not measuring the exact same spot again. We can neglect this as I matched the spots before and after the etching process.

Between processing steps, the samples were stored in a climatized room with 50% rel. humidity and 23.5 °C. After contemplating possible errors during the process, we now consider the materials involved.

Substrate

The substrate is one of the main parameters distinguishing the experiments in this study from the ones of Fulek [46]. She used PET-foil as a substrate in contrast to glass and a PMMA bonding layer here. As glass is inert to nitric acid, it should not be affected by the etching step. The implications of a PMMA bonding layer are explored below.

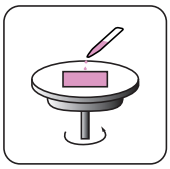

1) Cleaning of the glass slide, spin-coating of PMMA onto glass slide, drying on a hot plate.

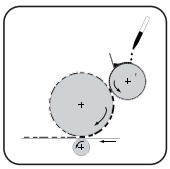

2) Printing of silver layer, drying in ventilated oven.

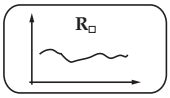

3) Measurement of the sheet resistance.

4) Photonic curing of silver layers.

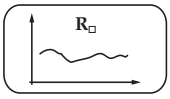

5) Measurement of the sheet resistance.

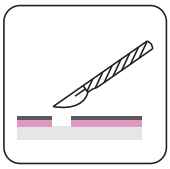

6) Marking of edges in the layer stack.

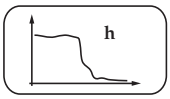

7) Measurement of the height of the layer stack.

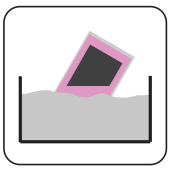

8) Etching of samples.

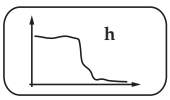

9) Measurement of the height of the layer stack.

Figure 6.2.: Process of determining the etching rate.

Silver layer and etchant

We calculate negative etching rates when the layer after the etching step has a higher thickness than before. Several mechanisms lead to an increase in layer thickness. The only one applicable here is swelling, i.e. layer growth due to influence of a liquid phase. The etchant used in this study, diluted nitric acid, is a known etchant for silver in microfabrication [84]. Ranfeld [117] and Fulek [46] showed that it is possible to etch printed silver layers of the same ink used here. Therefore, we can neglect swelling of the silver layer due to the etchant as cause for negative etching rates.

I chose the dilution of nitric acid in water (20% nitric acid, 80% water) based on own experiments [117], the results of Fulek [46] and literature. Köhler stated in [84] that the etching rate of silver in nitric acid is too high for small structures. Thus, I chose an etchant with a high dilution of nitric acid. I was expecting etching rates of few ten nanometers per second.

As the etching results were inconclusive (cf. Chapter 5.3.1), I suspected that the etching rate is very low, i.e. that the ablated layer height is within the measurement error. Thus, I immersed one sample in the etchant for several hours. The hypothesis was confirmed as the only visible effect was a partial ablation of the PMMA bonding layer from the glass substrate.

Therefore, I used a higher dilution (40% nitric acid, 60% water) for the structuring etching trials, i.e. transferring the layout of the resist into the functional layer. The etching rate obtained here was roughly 60 nm/s.

PMMA as a bonding layer

I introduced an auxiliary layer of PMMA to improve bonding between the silver layer and the glass substrate. As silver layers printed directly on PET foil show reasonable etching rates [46, 117], the PMMA layer is a likely explanation for the increase in layer thickness during the etching process. The PMMA layer might absorb parts of the etchant and start swelling. An indicator for the absorption is also the formation of small spheres as introduced in Chapter 5.3.2. As PMMA is mainly used as a resist in dry etching, little is known about its swelling behavior in wet etchants.

To determine whether the silver layer on top of the PMMA layer or storage time after the actual etching step had an impact on the etching behavior of the PMMA, I conducted etching trials with samples consisting only of a PMMA on a glass slide. For this, I measured the layer thickness directly before and after the etching. Figure 6.3 illustrates the results with the calculated etching rate related to the layer thickness before the etching step (left) and for different samples with roughly the same etching times (sample A: $t_{etch} = 20.2\,\mathrm{s}$, sample B: $t_{etch} = 20.38\,\mathrm{s}$, sample C: $t_{etch} = 20.44\,\mathrm{s}$). The diagram shows no apparent trend linking the etching rate to initial layer height, also all three samples show different etching rates.

For better comparison, I also plotted those graphs for the original measurement data (cf. Figure 6.4). The left diagram shows a slight trend linking the etching rate to the height of the layer before the etching step: The lower the layer height is, the lower is also the etching rate. The right diagram does not indicate any trend.

6.1.3. Recapitulation

In the sections above, I analyzed possible explainations for the negative etching rates obtained in Chapter 5.3.1. Two main causes emerged. The first is the etchant in its employed dilution.

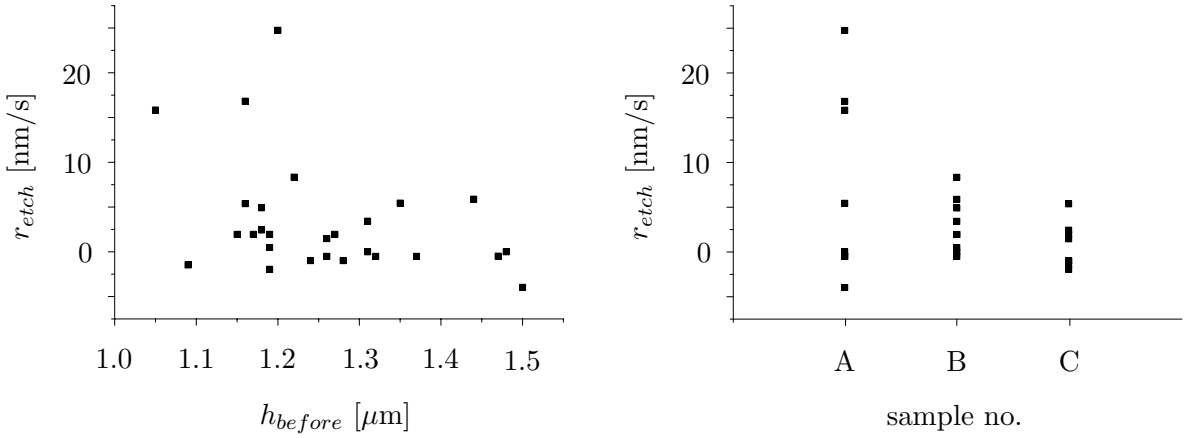

Figure 6.3.: Etching rate r_{etch} of PMMA in diluted nitric acid (20% nitric acid, 80% water) in dependency on the primary layer height h (left) and different samples (A, B, C) with roughly the same etching times.

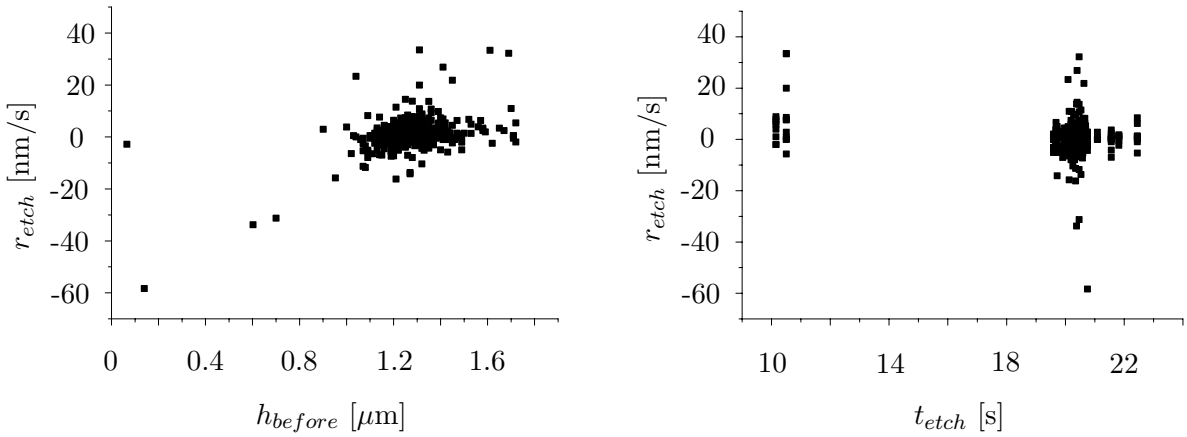

Figure 6.4.: Etching rate r_{etch} of layer stack (glass, PMMA, silver) in dependency on the primary layer height h (left) and immersion time in etchant t_{etch} (right).

The proportion of nitric acid was too low thus resulting in not enough removal of the functional layer. For printed silver layers as introduced in this study, other dilutions or even etchants with other components should be chosen. The second cause is the PMMA bonding layer. Its behavior in nitric acid is not fully investigated. Swelling of the layer due to absorption of etchant may occur.

6.2. Comparing the presented method to other structuring processes

When introducing a process as complex as the one presented here, usually the question occurs whether the same goal could be achieved using an easier approach. This section compares the presented method to two other methods, one structuring of a solid layer using as laser ablation and the other combining application and structuring in one step, i.e. printing.

6.2.1. Laser ablation

As stated in Chapter 1.2.1, this study started within the research project Kosadis. The main goal of Kosadis was to produce CMOS-like[1] integrated circuits for display applications. One of the sub-projects was to investigate a combination of additive and subtractive patterning methods to increase the resolution and thus reduce the feature size of solution processed organic field effect transistors. Here, especially flexographic printing as an additive method and laser ablation as a subtractive method were used to produce source/drain electrodes for OFETs.

During the course of the Kosadis project, knowledge was accumulated regarding laser ablation of printed nanoparticle silver layers as used in this study. This section compares wet etching to some of the results of Kosadis regarding laser ablation. Table 6.1 summarizes the considerations at the end of the section.

The main differences between wet etching and laser ablation are the processing time and the possible precision of the respective techniques. Wet etching is significantly faster with processing times of few seconds independent of the size of the area to be ablated, meaning the same time is needed for small as for large areas. The limiting factor here is the layer thickness and the etching rate depending on the chosen etchant. Laser ablation, though, highly depends on the area to be processed: The larger the area, the longer will the processing time be [10]. This is mostly due to the working principle of laser ablation where the laser beam edits the surface of the sample line by line whereas wet etching affects the whole surface at once.

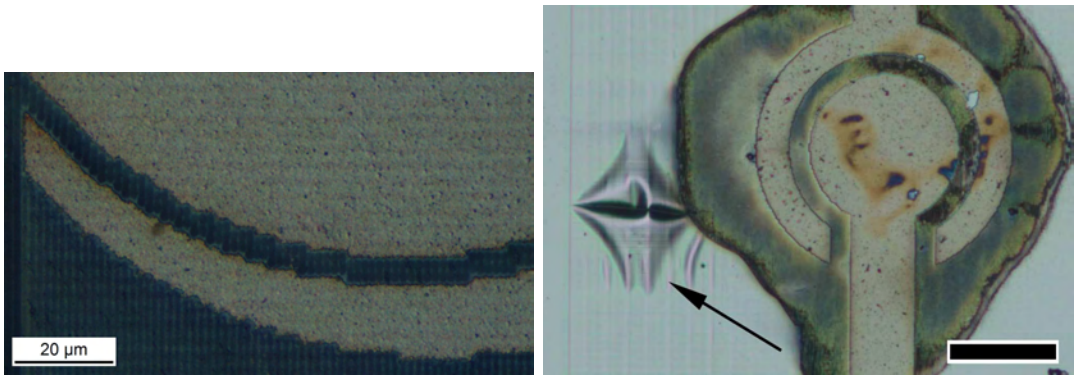

Figure 6.5.: Microscopic images of a silver layer structured by laser ablation. Left: stepped edges due to the laser feed (scaling bar: 20 μm), right: tearing of layers underneath the silver due to laser energy (cf. black arrow; scaling bar: 100 μm).

The precision of feature sizes feasible in laser ablation highly depends on the diameter of the laser's focal area and the precision of the drive moving either the optical system of the laser or the sample. A drawback of laser ablation is the stepped feed. As Figure 6.5 (left) illustrates, the edges not parallel to the feeding direction of the laser are stepped. Thus, although the edge quality on a very small scale, i.e. the length of one laser dot, is very high, the edges on a large scale are rather jagged. For some applications, e.g. OFETs, this is an exclusion criterion for laser ablation for the production of source and drain electrodes. As the current

[1] CMOS, complementary metal-oxide-semiconductor, is a technique of producting integrated circuits with field effect transistors made of both n- and p-type metal-oxide semiconductors. In printed and organic electronics, the name CMOS is used for field effect transistors with both n- and p-type organic semiconductors.

in a field effect transistor generally takes the shortest path, voltage peaks would form at the edges thus hindering a homogeneous voltage distribution throughout the OFET-channel. The feature sizes in wet etching are determined by the resist structure. This, again, depends on the method of structuring. The lower the desired feature sizes, the higher will the cost of the structuring be.

When ablating printed silver layers that are not sintered properly (cf. Chapter 5.1.3), the residual organic compounds of the ink seem to generate unwanted offgassing during laser ablation [119]. This results in unwanted alterations of the non-ablated areas of the functional layer. Using laser ablation on a silver top layer of a stack, layers underneath may also be affected (cf. Figure 6.5, right). In case of OFETs, this may lead to short circuits, rendering the devices faulty [120].

Table 6.1.: Comparison of wet etching and laser ablation

properties	wet etching	laser ablation
processing time	depending on etchant and etching rate	depending on ablation area
precision of feature size	depending on method for structuring the resist layer	depending on focal area of laser and precision of drive system
work place requirements	wet processing environment	vibration-free

Regarding complexity of work space, both methods have significantly different requirements. Laser ablation requires vibration-free equipment, whereas for wet etching, a work space with wet processing areas, fume cupboards and possibly waste treatment is needed.

Nevertheless, laser ablation offers a crucial benefit by being a digital technique: Every layer may be structured differently. In wet etching processes, an adhesive mask is needed which, in this study, is structured by a flexographic printing plate resulting in the same layout in every print run.

6.2.2. Structured printing of silver layers

With the rise of printed electronics, a growing number of researchers investigate flexographic printing of conductive traces using silver nanoparticle inks. As introduced in Chapter 1.2.3, one of the main applications is the production of conductive networks to supporting or surrogating transparent electrodes.

Several investigations regarding the track width in such conductive grids are known from literature: Two examples are given here: Deganello used flexography for printing conductive networks with the same ink as used in this study, investigating the impact of pick-up volume and nominal line width on the printing plate on the printed line widths [36]. Yu compared inkjet printing, screen printing and flexography regarding their minimum achievable resolution [161].

Deganello measured minimum line widths of roughly 75 μm [36] with the actual line width significantly higher than the nominal one on the printing plate [36, 35]. Yu defines the

minimum achievable resolution of line width printed by flexography as 32 μm with a width of 100 μm as reproducibly achievable [161].

The reproducibly achievable line widths in this study are of the same dimension as DEGANELLO's and YU's. At this time, line widths significantly smaller than those are producible. Nevertheless, their parameters are hard to control and they show poor line quality (cf. Chapter 5.3.3).

Therefore, it is not feasible at the moment to add more complexity to the process of producing conductive lines with line widths of order of 100 μm. The method introduced in this study is generally capable to achieve lines smaller than directly printed but not with the introduced parameters.

6.2.3. Industrial-scale wet etching

For the production of printed circuit boards (PCB) or flexible printed circuits (FPC), industrial-scale wet etching installations for copper are available. Usually, those installations offer a continuous process of structuring the conductive pattern by combining development of the resist, etching of the copper and stripping of the resist. For PCB, machinery is equipped with conveyors to transport the rigid boards. For FPC, also roll-to-roll processing is available. Processing times are usually a few meters per minute. The processing parameters are optimized to structure copper layers between 17 μm and 70 μm in hydrochloric acid[2].

6.2.4. Classification of the presented method

As explained above, the method introduced in this study is not competitive regarding flexographic printing of silver lines. However, it is applicable for structuring other functional layers. In FOLAE, some layers are applied solid, i.e. unstructured. Pre-coated substrates are also common, e.g. ITO (indium tin oxide, a transparent, inorganic conductive material) or gold layers vacuum processed on polymer foils.

It is feasible to apply the method of structuring a resist layer using flexography on such layers. Thus, the structuring step may be integrated into a continuous production process. Necessary parameters for adapting the method would be the etching rate and thus the etchant. Both should be matched to the functional material.

To compare the introduced method to other structuring techniques, Figure 6.6 illustrates the magnitude of several direct writing and structuring methods.

As obvious from Figure 6.6, the introduced method is, in comparison to the other depicted techniques, not competitive regarding feature size. Nevertheless, apart from inkjet printing and laser machining[3], it is the only one feasible for a continuous process of printed electronics production.

Also, regarding the processing speed of the method presented in this study, it is much faster than the processes introduced in Figure 6.6. FIB direct writing and LACVD require a vacuum chamber, thus limitting the substrate size to the capacity of the chamber and adding additional time for evacuating the chamber. FIB direct writing, LACVD and LIGA are are not compatible with continuous production but require batch processing. As laser machining

[2] These information were obtained by visiting the Erkelenz plant of Mektec Europe GmbH, a German manufacturer of FPC.

[3] Laser ablation, as introduced in Chapter 6.2.1, may also be called laser machining, the term used in the studies of VAEZI.

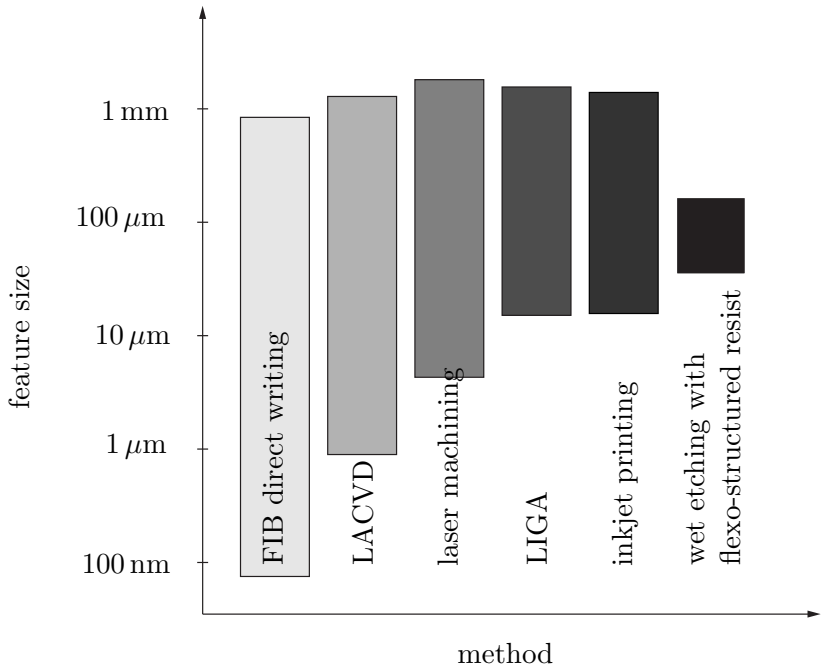

Figure 6.6.: Classification of magnitudes of direct writing and structuring methods with FIB direct writing, LACVD, laser machining, LIGA and wet etching with flexo-structured resist as introduced in this study. Following [149], wet etching added.

and inkjet printing create structures dot by dot, they also are usuall slower than flexographic printing with a subsequent etching step with a high etching rate.

6.3. Upscaling

6.3.1. Transferring the presented method onto industrial production equipment

The processing times shown in Chapters 4 and 5 indicate a possible transferability of the presented method to an industrial process. Figure 6.7 illustrates a notional roll-to-roll process including two printing units (functional layer, resist layer), several drying units and an etching and stripping unit.

Nevertheless, especially the printing process of the resist structures needs adjustment when using it on an industrial scale printing unit. The printablity tester used in this study differs significantly from industrial printing presses. Table 6.2 highlights some process parameters where the proofer and an industrial press[4] differ profoundly.

For implementing the method introduced in this study into a production process, the following section roughly estimates the required speeds and etching baths.

[4]I used a Gallus RCS330HD as an example which is available at the Institute of Printing Science and Technology. This press is intended for printing labels, although at IDD, mostly research printing trials are implemented.

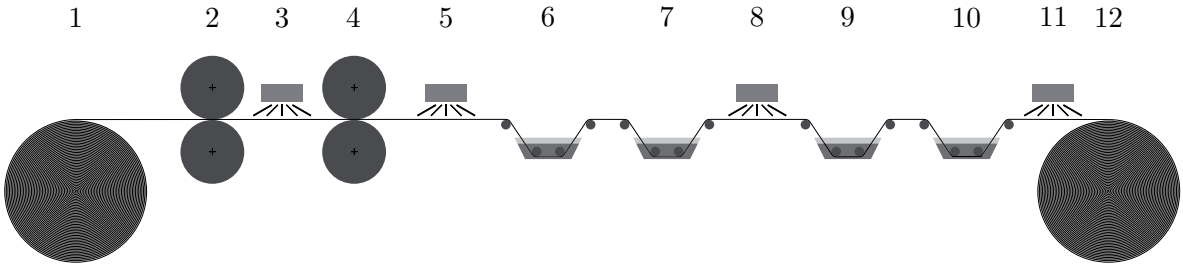

Figure 6.7.: R2R-processing of FOLAE using the method introduced in this study with 1) unwinding, 2) printing: functional layer, 3) drying / sintering, 4) printing: resist layer, 5) drying, 6) etching, 7) rinsing, 8) drying, 9) stripping, 10) rinsing, 11) drying and 12) winding. Following [118].

Table 6.2.: Comparing process parameters of IGT F1 [72] and an industrial printing press (Gallus RCS330HD at IDD) [74].

Parameter	IGT F1	Industrial printing press
printing speed	12 . . . 90 m/min	1 . . . 160 m/min
printing force	10 . . . 500 N	n/a
substrate handling	sheet material (manual feed)	roll material (automatic feed)
inking unit	manually (pipette)	chambered doctor blade (continuous flow)
drying / curing	not available	UV, IR, hot air
controlled by	force	engagement

We assume an etching rate[5] of 150 nm/s and a layer thickness of the silver layer of 300 nm. The overall etching time should be slightly longer than the layer thickness divided by etching rate to compensate variations in the layer thickness and local variations of the etching rate [84]. Thus, we need an etching time of $t_{etch} > 2\,\mathrm{s}$ (cf. Equation 4.9 on page 47). At a printing speed of 160 m/min the etching bath would have a length of $l_{etchingbath} \approx 1\,\mathrm{m}$ (cf. Equation 6.3). Additional rinsing and stripping units would also be needed.

$$l_{etchingbath} = v_{print} \cdot t_{etch} \tag{6.3}$$

To reduce the length of the etching bath, a higher etching rate or lower printing speed would be needed.

The processing times for drying and sintering of the silver layer may be neglected as literature states its feasibility [65].

6.3.2. Pointers for industrial implementation

As shown above, it is feasible to implement the structuring method introduced in this study into industrial fabrication processes for printable electronics and FOLAE. However, some

[5] Chapter 5.3.3 shows the etching of silver layers with an etching rate of roughly 60 nm/s using 40% nitric acid. With a higher concentration, higher etching rates are expected.

aspects will differ significantly from the results presented here. This section will point out what to heed when upscaling this method from stage 1 to stage 2 or even 3.[6]

First of all, in industrial fabrication processes, especially using reel-to-reel equipment, the substrate of choice would probably be PET, PEN or PC. Thus, the bottommost layer of PMMA I used as bonding agent between substrate and functional layer would likely not be needed. Either, substrates with a pre-coated functional layer would be used or the functional layer would be printed directly onto the substrate.

The compatibility of functional layer, resist and etchant is important, as they individually influence the processing time. Their pairing will ultimately define the machine speed.

Another important process step when considering upscaling is stripping. Just like the etchant, the stripping agent needs to show a certain selectivity between resist and functional layer.

Table 6.3 lists some process parameters that may be a source of deviation from the intended structure sizes after etching. Upscaling the process, the impact of those parameters increases.

Table 6.3.: Possible sources of deviations from intended etched structure sizes. Adapted from [84].

parameter	source of deviation
functional layer	material / pureness
	thickness variations
	ink composition
resist layer	printing plate (structure sizes)
	ink composition
	printing parameters (layer parameters)
etching	concentration of etchant
	temperature of etchant
	anisotropy of removal
	control of etching time

Most important in the functional layer are the material itself, variations of its layer thickness and the composition of the ink. Those parameters influence which etchant to choose and the etching rate. The ink composition, if applicable, also influences the post-processing of the functional layer as explained in Chapter 5.1.2.

Regarding the resist layer, the printing plate may cause size deviations for two reasons: First, it may swell due to incompatibility with the solvent of the ink (cf. [143]) and second, the material and production method influence the obtainable feature size on the plate (cf. [55]). The ink composition influences the layer formation of the resist layer and also its drying behavior. The influence of printing parameters has been extensively discussed in this study. Anisotropy is less important for printed layers as they usually show an isotropic behavior. The etching time should be monitored closely.

[6] The Institute of Printing Science and Technology implemented a three-stage laboratory concept with stage 1 in the scale of few microliters of ink and few square centimeters of substrate. Stage 2 implies substrates of order of DIN A4 and few deziliters of ink whereas stage 3 is industrial production size equipment.

Of course, before implementing wet etching using an etch resist structured by flexography in a larger scale, the individual parameters have to be attuned in small scale preliminary trials.

7. Conclusion and further work

In the presented study, I investigated the wet etching of printed silver layers using an etch resist structured by flexographic printing. I also evaluated the post-processing of said silver layers using photonic curing. In Chapter 2.2 *Objectives and approach*, I introduced four guiding questions that were driving my research. In the following, I answer those questions based on my results.

Question 1 Is it possible to obtain smaller line widths of a functional layer by combining the halo effect in flexographic printing for the application of the etch resist and a wet etching process than by flexographic printing alone?

Yes, it is possible as the microscopic images of etched silver structures in Chapter 5.3.3 show. However, at this time it is not possible to control the exact width of the silver lines using the material set introduced in this study. Using the halo effect in flexographic printing for structuring the resist layer, we can obtain line widths smaller than those attainable by directly using flexographic printing. To achieve this, anilox rollers with low pick-up volume are needed. Nevertheless, those lines are hardly reproducible. Their line quality needs further improvement regarding edge sharpness, bulging and interruptions.

Wider lines obtained from higher pick-up volumes are easier to control and reproduce. I attribute this to the relation of line width to available ink volume. To transfer this effect to lower pick-up volumes, a possible solution might be the use of smaller lines on the printing plate, i.e. downscaling, and thus imitating the relation of wider lines to larger pick-up volume.

Question 2 Can wet etching using a printed etch resist be integrated into continuous production lines (e.g. roll-to-roll printing) for structuring pre-coated solid area layers?

Yes. Contemplations regarding the processing time show that it is theoretically possible to integrate wet etching into continuous printed electronics production. Assuming processing speeds of 160 m/min, a processing segment for the etching bath of 1 m would be required, for etching rates of 150 nm/s. The process parameters need careful adjustment, especially regarding material selection. It is complex to add units for etching, rinsing and stripping into printing and production lines as most parts need to be acid-proof for etching or solvent resistant for stripping.

Question 3 Do printed silver layers behave significantly different in a wet etching process than layers obtained in vacuum processes (i.e. bulk layers)?

With regards to the results of this study it is not possbile to give a final answer to this question. The results regarding the etching rate of printed silver layers were inconclusive. With the employed material set, there was no obvious relation between the parameters in post-processing of the silver layers and their etching rates. However, other investigations show that the etching rate of printed silver layers depend on energy density during post-processing [46]. Thus, we can derive that printed silver layers behave differently than bulk silver as the etching rate of the latter only depends on the etchant.

Question 4 Do we need new specifications to describe printed lines in flexography, especially regarding the halo effect?

Yes, we do. Line description in literature mostly focusses on basic features as line width, length and height as well as edge quality. Recent approaches also consider the cross-sectional area [35]. However, features as halos, width of void, asymmetry or the behavior of line ends are not specified. With the hypothesis regarding the geometrical parameters of the cross sections of printed lines with increasing printing force I moved forward in this regard, introducing several parameters to describe the cross section of a printed line.

In this study, I presented a method for wet etching printed silver layers using an etch resist structured by flexography, taking into consideration the behavior of said layers regarding post-processing. I obtained structured silver layers with line widths less than 100 μm. With decreasing line width, the quality as well as the reproducibility of the silver structures decreased. I was not able to link the etching rate of the silver layers to the parameters of their post-processing. I found a method to evaluate the isotropy of the electrical properties of printed silver layers using the correction factor in *van der Pauw* measurements.

Regarding those investigations, a logical continuation would be the investigation of several etchants providing predictable results. Their etching rate should be customizable to the functional layer and the processing time used. Ideal would be an etchant with a linear behavior regarding its concentration. A further evaluation of post-processing methods for printed conductive layers is vital, especially regarding extensive investigations of parameters in photonic curing. Pointers may be obtained from Chapter 6.1.1.

I introduced a hypothesis on the behavior of cross-sectional parameters of printed lines relative to the printing force. With the printing trials I conducted, I could partially validate this hypothesis. As a result of the printing trials of line shaped geometries, we now have a better understanding of the impact of pick-up volume of the anilox roller, printing force and printing speed on the halo effect in printed lines.

As the investigations regarding the halo effect in this study are only valid for printed line shaped elements, other geometries should be considered.

A logical step is porting the method presented in this study to larger machines and substrate sizes. Some pointers for industrial implementation may be obtained from Chapter 6.3.2. There, also different functional layers may be structured, e.g. ITO.

A transfer of the results to microcontact printing is feasible, as the flexible stamp in microcontact printing imitates flexography on a smaller scale. For this, the mechanisms of the halo effect have to be fully understood and adequate control of the process parameters is mandatory.

References

[1] ISO / IEC 13660:2001 (E). Information technology – Office equipment – Measurement of image quality attributes for hardcopy output – Binary monochrome text and graphic images, 2001.

[2] Acheson Industries. Electrodag pm-460a. Product Data Sheet, without year.

[3] Thomas M. Adams. *Introductory MEMS: fabrication and applications*. Springer, New York, 2010.

[4] Vahid Akhavan, Kurt Schroder, Dave Pope, Ian Rawson, Andrew Edd, and Stan Farnsworth. Reacting Thick-Film Copper Conductive Inks with Photonic Curing. In *Proceedings of the 13th International Symposium on Electronics Packaging (ICEP2013)*. The Japan Institute of Electronics Packaging (JIEP), 2013.

[5] Joseph C. Anderson. *Materials science for engineers*. Nelson Thornes, Cheltenham, England, 2003.

[6] Apex. Plate to anilox screen calculator. http://http://www.apex-groupofcompanies.com/en/system/files/Apex_calculator_PlatetoAnilox_linch_0.pdf, without year. Last accessed: 01.03.2015.

[7] Peter W. Atkins. *Einführung in die Physikalische Chemie*. Wiley-VCH, Weinheim New York Basel Cambridge, 1st edition, 1993.

[8] Gerhard Bandow and Hartmut H. Holzmüller, editors. *"'Das ist gar kein Modell!"': unterschiedliche Modelle und Modellierungen in Betriebswirtschaftslehre und Ingenieurwissenschaften*. Gabler Research. Gabler Research | GWV Fachverlage GmbH, Wiesbaden, 1st edition, 2010.

[9] BASF Aktiengesellschaft. Lumogen F. Collector dyes. Technical Information, November 1997.

[10] Dieter Bäuerle. *Laser Processing and Chemistry*. Springer, Heidelberg Dordrecht London New York, 4th edition, 2011.

[11] Torsten Becker. *Prozesse in Produktion und Supply Chain optimieren*. Springer, Berlin, 2005.

[12] Helmut Behler. *Die Randstruktur von Druckpunkten - eine experimentelle Untersuchung der Farbspaltungsströme*. Dissertation, Technische Hochschule Darmstadt, Darmstadt, 1993.

[13] Tyrone E. Benson, Leonard I. Kamlet, Pete Klimecky, and Fred L. Terry jr. In-situ spectroscopic reflectometry for polycrystalline silicon thin film etch rate determination during reactive ion etching. *Journal of Electronic Materials*, 25(6):955–964, 1996.

[14] Juri Bery. Mechanisms governing gravure printing. In *Proceedings*, pages 149–159, Atlanta, GA, 1985. Tappi Press.

[15] Bharat Bhushan. *Springer Handbook of Nanotechnology*. Springer, Berlin Heidelberg, 2010.

[16] Anne Blayo and Bernard Pineaux. Printing processes and their potential for RFID printing. In *Proceedings of the 2005 joint conference on Smart objects and ambient intelligence innovative context-aware services: usages and technologies - sOc-EUSAI '05*, pages 27–30, Grenoble, France, 2005.

[17] Paul Blom. Technical presentation. http://www.ribuilt.eu/LinkClick.aspx?fileticket=ox5qwBGuwII%3D&tabid=70, without year. Last accessed: 19.11.2013.

[18] Joachim Böhringer, Peter Bühler, and Patrick Schlaich. *Kompendium der Mediengestaltung*. Springer, Berlin Heidelberg, 2nd edition, 2006.

[19] Martin Bonnet. *Kunststoffe in der Ingenieuranwendung verstehen und zuverlässig auswählen*. Vieweg Teubner, Wiesbaden, 1st edition, 2009.

[20] Nils Bornemann. From Graphical to Functional Gravure Printing: A Discussion of Several Issues. In *Forschungsvorträge zur gedruckten und organischen Elektronik am iL*, Heidelberg, October 2012.

[21] Nils Bornemann. *Characterization and Investigation of Large Area, Ultra-Thin Gravure Printed Layers*. Dissertation, Technische Universität Darmstadt, Darmstadt, 2013.

[22] Nils Bornemann, Hans Martin Sauer, and Edgar Dörsam. Thin film behaviour after ink transfer in printing process. In *Proceedings of Large-Area, Organic and Polymer Electronics Convention 2010 (LOPE-C 10)*, Frankfurt, 2010. Organic Electronics Association (OE-A).

[23] Nils Bornemann, Hans Martin Sauer, and Edgar Dörsam. Gravure Printed Ultrathin Layers of Small-Molecule Semiconductors on Glass. *Journal of Imaging Science and Technology*, 55(4):040201, 2011.

[24] Nils Bornemann, Hans Martin Sauer, and Edgar Dörsam. Experimental Investigation of the Filling and Emptying of Gravure Cells. In *Materials Science Engineering (MSE 2012)*, Darmstadt, September 2012.

[25] David C. Bould. *An Investigation into Quality Improvements in Flexographic Printing*. PhD Thesis, University of Wales Swansea, Swansea, April 2001.

[26] David C. Bould, Tim C. Claypole, and David T. Gethin. Improving the resolution of the flexographic printing process for r2r electronics. In *Proceedings of Large-Area, Organic and Polymer Electronics Convention 2010 (LOPE-C 10)*, pages 186–190, Frankfurt, 2010. Organic Electronics Association (OE-A).

[27] David C. Bould, Simon M. Hamblyn, David T. Gethin, and Tim C. Claypole. Effect of impression pressure and anilox specification on solid and halftone density. *Proceedings of the Institution of Mechanical Engineers, Part B: Journal of Engineering Manufacture*, 225(5):699–709, May 2011.

[28] Dag Brune, Ragnar Hellborg, Harry J. Whitlow, and Ola Hunderi, editors. *Surface Characterization: A User's Sourcebook*. Wiley-VCH, Weinheim Berlin New York, 1997.

[29] Martyn Cherrington, Tim C. Claypole, Davide Deganello, Ian Mabbett, Trystan Watson, and David Worsley. Ultrafast near-infrared sintering of a slot-die coated nano-silver conducting ink. *Journal of Materials Chemistry*, 21(21):7562, 2011.

[30] Chwan K. Chiang, C. R. Fincher, Yung W. Park, Alan J. Heeger, Hideki Shirakawa, Edwin J. Louis, Shek C. Gau, and Alan G. MacDiarmid. Electrical conductivity in doped polyacetylene. *Phys. Rev. Lett.*, 39:1098–1101, Oct 1977.

[31] Tim C. Claypole, Simon Hamblyn, and David Gethin. The effective of engagement and image carrier profile on the printing of conductive lines by flexography. In Mladen Lovrecek, editor, *Advances in Printing and Media Technology. Digitalization of Print - Exchanging Ideas Across Generations. Proceedings of the iarigai Conference 2013*, volume XL. iarigai, 2013.

[32] Leica Microsystems CMS. Leica dm4000-6000. Brochure, 2013.

[33] Gregory P. Crawford. *Flexible flat panel displays*. John Wiley & Sons, Chichester, England, 2005.

[34] Alejandro de la Fuente Vornbrock. *Roll Printed Electronics: Development and Scaling of Gravure Printing Techniques*. PhD thesis, University of California Berkeley, Berkeley, CA, 2009.

[35] Davide Deganello, J.A. Cherry, David T. Gethin, and Tim C. Claypole. Impact of metered ink volume on reel-to-reel flexographic printed conductive networks for enhanced thin film conductivity. *Thin Solid Films*, 520(6):2233–2237, January 2012.

[36] Davide Deganello, J.A. Cherry, D.T. Gethin, and T.C. Claypole. Patterning of microscale conductive networks using reel-to-reel flexographic printing. *Thin Solid Films*, 518(21):6113–6116, August 2010.

[37] Edgar Dörsam, Nils Bornemann, Larisa Salun, Constanze Ranfeld, and Dieter Spiehl. Printing Technology for Electronics. Lecture notes at Technische Universität Darmstadt, 2011.

[38] Heinrich Dubbel and Karl-Heinrich Grote. *Taschenbuch für den Maschinenbau*. Springer, Berlin Heidelberg, 21st edition, 2005.

[39] Paul C. Duineveld. The stability of ink-jet printed lines of liquid with zero receding contact angle on a homogeneous substrate. *Journal of Fluid Mechanics*, 477, March 2003.

[40] Rita Faddoul, Nadège Reverdy-Bruas, Anne Blayo, Thomas Haas, and Christian Zeilmann. Optimisation of silver paste for flexography printing on LTCC substrate. *Microelectronics Reliability*, 52(7):1483–1491, July 2012.

[41] Daniela Fell. *Dynamic wetting of complex liquids*. Dissertation, Johannes Gutenberg-Universität, Mainz, 2013.

[42] Flexographic Technical Association, editor. *Flexography: Principles & Practices*. Foundation of Flexographic Technical Association, Inc., Ronkonkoma, 5th edition, 1999.

[43] FlintGroup Flexographic Products. nyloflex FAH. nyloflex FAH Digital. Product Data Sheet, April 2013.

[44] Michael Frey, Florian Clement, Stefan Dilfer, Denis Erath, and Daniel Biro. Front-side metalization by means of flexographic printing. *Energy Procedia*, 8:581–586, January 2011.

[45] Joachim Frühauf. *Werkstoffe der Mikrotechnik: Lehrbuch für Ingenieure*. Fachbuchverlag Leipzig im Carl-Hanser-Verlag, München Wien, 2005.

[46] Anke Fulek. Untersuchung der Ätzrate gedruckter Silber- und PMMA-Schichten. Bachelor-Thesis, Technische Universität Darmstadt, Darmstadt, September 2013. Supervisor: Dipl.-Ing. Constanze Ranfeld.

[47] David Galton, David C. Bould, and Tim C. Claypole. The effect of surface properties on the printability of flexographic printing plates. In Nils Enlund and Mladen Lovrecek, editors, *Advances in Printing and Media Technology. Proceedings of the iarigai Conference 2010*, volume XXXVII, Darmstadt, 2010. International Association of Research Organizations for the Information Media and Graphic Arts Industries (iarigai).

[48] Hans-Jürgen Gevatter. *Handbuch der Mess- und Automatisierungstechnik in der Produktion*. Springer, Berlin New York, 2006.

[49] Sabine Globisch. *Lehrbuch Mikrotechnologie für Ausbildung, Studium und Weiterbildung*. Fachbuchverlag Leipzig im Carl-Hanser-Verlag, München Wien, 2011.

[50] James S. Greeneich. Developer characteristics of Poly-(Methyl methacrylate) electron resist. *Journal of The Electrochemical Society*, 122:970–976, 1975.

[51] Stefan Griesheimer. *Experimentelle Untersuchung zur Farbspaltung und Farbübertragung im Flexodruck*. Dissertation, Technische Universität Darmstadt, Darmstadt, 2013.

[52] Martin J. Guillot, Steve C. McCool, and Kurt A. Schroder. Simulating the thermal response of thin films during photonic curing. In *Proceedings of the 12th International Conference on Nuclear Engineering IMECE12*, Houston, November 2012. ASME.

[53] Maria Haas, Hans Martin Sauer, and Edgar Dörsam. Optical surface characterization method of silicone layers used for manufacturing of dielectric elastomer actuators. In Mladen Lovrecek, editor, *Advances in Printing and Media Technology. Digitalization of Print - Exchanging Ideas Across Generations. Proceedings of the iarigai Conference 2013*, volume XL. iarigai, 2013.

[54] Martin Haas. *Untersuchungen zum Verdrucken von Interferenzeffektfarben im Flexodruckverfahren*. Dissertation, Technische Universität Darmstadt, Darmstadt, 2012. http://tuprints.ulb.tu-darmstadt.de/id/eprint/3011.

[55] Simon M. Hamblyn, Glyn R. Davies, David T. Gethin, and Tim C. Claypole. The effect plate exposure on halftone ink transfer in flexographic printing. In Mladen Lovrecek,

editor, *Advances in Printing and Media Technology. Digitalization of Print - Exchanging Ideas Across Generations. Proceedings of the iarigai Conference 2013*, volume XL. iarigai, 2013.

[56] Kathrin Happel. *LED-Based Light Scattering Measurements of Papers for Printing Applications*. Dissertation, Technische Universität Darmstadt, Darmstadt, 2011. http://tuprints.ulb.tu-darmstadt.de/id/eprint/2850.

[57] Ulrich Harten. *Physik. Einführung für Ingenieure und Naturwissenschaftler*. Springer, Berlin Heidelberg New York, 2nd edition, 2005.

[58] Michael Hatzakis. Electron resists for microcircuit and mask production. *Journal of The Electrochemical Society*, 116(7):1033, 1969.

[59] Ekbert Hering. *Photonik: Grundlagen, Technologie und Anwendung: mit 50 Tabellen*. Springer, Berlin, New York, 2006.

[60] Gerardo Hernandez-Sosa, Nils Bornemann, Ingo Ringle, Michaela Agari, Edgar Dörsam, Norman Mechau, and Uli Lemmer. Rheological and drying considerations for uniformly gravure-printed layers: Towards large-area flexible organic light-emitting diodes. *Advanced Functional Materials*, 23(25):3164–3171, July 2013.

[61] Ulrich Hilleringmann. *Mikrosystemtechnik: Prozessschritte, Technologien, Anwendungen*. Teubner, Wiesbaden, 2006.

[62] Michael Hirner. Überblick über die Terminologie der Nanotechnologie (Dt.-Engl.). Diplomarbeit, Universität Wien, Wien, 2005.

[63] Erik Hallberg Hofstrand. *Flexographic Post-printing of Corrugated Board: Contact Mechanics and Print Quality*. PhD thesis, Department of Chemical Engineering, Karlstads Universitet, 2006.

[64] Herbert Holik. *Handbook of paper and board*. Wiley-VCH, Weinheim, 2013.

[65] Markus Hösel and Frederik C. Krebs. Large-scale roll-to-roll photonic sintering of flexo printed silver nanoparticle electrodes. *Journal of Materials Chemistry*, 22(31):15683, 2012.

[66] Arved C. Hübler, Maxi Bellmann, Georg C. Schmidt, Stefan Zimmermann, Andre Gerlach, and Christian Haentjes. Fully mass printed loudspeakers on paper. *Organic Electronics*, 13(11):2290–2295, November 2012.

[67] Arved C. Hübler, F. Doetz, Heiko Kempa, Howard E. Katz, Matthias Bartzsch, Nicole Brandt, I. Henning, Uta Fügmann, Suresh Vaidyanathan, Jimmy Granstrom, S. Liu, A. Sydorenko, Tino Zillger, Georg Schmidt, Karin Preißler, Elsa Reichmanis, Peter Eckerle, F. Richter, Thomas Fischer, and Ulrich Hahn. Ring oscillator fabricated completely by means of mass-printing technologies. *Organic Electronics*, 8(5):480 – 486, 2007.

[68] Arved C. Hübler, Ulrich Hahn, Nicole Brandt, Thomas Fischer, Uta Fügmann, Z. Shalabutov, and Dirk Zielke. Production of electronic devices using offset printing. In *Proceedings of the TAGA MicroTech*. TAGA, 2003.

[69] Gunter Hübner. *Ein Beitrag zum Problem der Flüssigkeitsspaltung in der Drucktechnik*. Dissertation, Technische Hochschule Darmstadt, Dissertation, 1991.

[70] Christopher F. Huebner, Joseph B. Carroll, David D. Evanoff, Yurong Ying, Brian J. Stevenson, Justin R. Lawrence, J. Michael Houchins, Alexandra L. Foguth, Jay Sperry, and Stephen H. Foulger. Electroluminescent colloidal inks for flexographic roll-to-roll printing. *Journal of Materials Chemistry*, 18(41):4942–4948, 2008.

[71] IGT Testing Systems. Rasterwalzen für F1. http://www.igt.nl/DE/product_details.asp?product=93. Last accessed: 30.08.2013.

[72] IGT Testing Systems. IGT F1 printability tester for flexo and gravure inks, 2002.

[73] InkTec Co., Ltd. Inktec leads new paradigm in printed electronics materials. Product brochure. http://www.inktec.com/english/pdf/upload_pdf/%28E%29Electronic_Ink_3.3_72dpi.pdf. Last accessed: 03.09.2013.

[74] Institute of Printing Science and Technology. Technische Universität Darmstadt. Equipment - printing lab. http://www.idd.tu-darmstadt.de/re_search/equipm/printing_lab/index.en.jsp. Last accessed: 05.01.14.

[75] Ellen Ivers-Tiffee and Waldemar von Münch. *Werkstoffe der Elektrotechnik*. B. G. Teubner Verlag | GWV Fachverlage, Wiesbaden, 10th edition, 2007.

[76] Mark J. Jackson. *Micro and nanomanufacturing*. Springer, New York, 2007.

[77] Danliang Jin and Ed S. Ramakrishnan. Manufacturing of high resolution conductive patterns using organometallic ink and banded anilox rolls, 2013. Patent WO2013165567 A1.

[78] Johanna Johnson. *Aspects of flexographic print quality and relationship to some printing parameters*. PhD thesis, Karlstads Universitet. Faculty of Technology and Science Chemical Engineering, Karlstad, 2008.

[79] Bala K. Juluri. van der Pauw correction factor. http://juluribk.com/2012/01/08/van-der-pauw-correction-factor/, January 2012. Last accessed: 23.02.2014.

[80] Heiko Kempa, Arved C. Hübler, Ulrich Hahn, Uta Fügmann, Matthias Bartzsch, Thomas Fischer, Georg C. Schmidt, Kay Reuter, Karin Preißler, and Barbara Meier. Massendruck von organischen funktionsmaterialien. In *EFDS-Workshop Verfahren für die Grossflächenbeshcichtung mit Halbleitermaterialien.*, Wörlitz, October 2006. EFDS.

[81] Helmut Kipphan. *Handbook of Print Media: Technologies and Production Methods*. Springer Science & Business Media, Berlin Heidelberg, 2001.

[82] Wilhelm Kleppmann. *Versuchsplanung. Produkte und Prozesse optimieren*. Carl Hanser Verlag, München, 2010.

[83] Reinhard Kluger. Der Fortschritt kam gedruckt aus Europa. *Elektronikpraxis*, 14:72–73, July 2006.

[84] Michael Köhler. *Ätzverfahren für die Mikrotechnik*. Wiley -VCH, Weinheim, 1998.

[85] Michael Köhler and Wolfgang Fritzsche. *Nanotechnology: An Introduction to Nanostructuring Techniques*. Wiley-VCH, Weinheim, 2007.

[86] Eric Langner. Untersuchung des Verhaltens von Druckfarbe und Klischee im Flexodruck mittels optischer Erfassung im Druckspalt. Bachelor-Thesis, Technische Universität Darmstadt, Darmstadt, January 2014. Supervisor: Dipl.-Ing. Constanze Ranfeld and Felipe Fernandes, M.Sc.

[87] Laurent G. Leloup. *Measurement and prediction procedures for printability in flexography: (MP3 Flexo)*. PhD thesis, Tekniska högskolen, Stockholm, 2002.

[88] Yi Li, Daniel Lu, and C. P. Wong. *Electrical conductive adhesives with nanotechnologies*. Springer, New York, 2009.

[89] J. S. Lloyd, C. M. Fung, Davide Deganello, R. J. Wang, Thierry G. Maffeis, Shu-Ping Lau, and Kar S. Teng. Flexographic printing-assisted fabrication of ZnO nanowire devices. *Nanotechnology*, 24(19):195602, May 2013.

[90] Andreas Lorenz, Andre Kalio, Gunter T. Hofmeister, Sebastian Nold, Lorenz Friedrich, Achim Kraft, Jonas Bartsch, Dietmar Wolf, Martin Dreher, Florian Clement, and Daniel Biro. Flexographic printing - high throughput technology for fine line seed layer printing on silicon solar cells. In A. Mine, editor, *Proceedings of the 28th European PV Solar Energy Conference and Exhibition (EU PVSEC)*, pages 1017–1023, Paris, 2013.

[91] John M. Malouff, Ashley J. Emmerton, and Nicola S. Schutte. The risk of a halo bias as a reason to keep students anonymous during grading. *Teaching of Psychology*, 40:233–237, July 2013.

[92] manroland AG. Terminologie. Internal Document, July 2008.

[93] Herman F. Mark. *Encyclopedia of polymer science and engineering*. Wiley, New York Chichester, 2004.

[94] Helmut Mathes. Flexo troubleshooting. Most common flexo printing issues, part 4. *Flexo & Gravure Global*, 1:10f, 2012.

[95] Merck KGaA. Ammoniumfluorid. Sicherheitsdatenblatt, November 2011.

[96] Merriam-Webster.com. "Halo". http://www.merriam-webster.com/dictionary/halo, 2013. Last accessed: 02.08.13.

[97] Merriam-Webster.com. "Process". http://www.merriam-webster.com/dictionary/process, 2013. Last accessed: 13.09.2013.

[98] Ulrich Mescheder. *Mikrosystemtechnik: Konzepte und Anwendungen*. Teubner, Stuttgart Leipzig Wiesbaden, 2004.

[99] Karl-Heinz Meyer. *Technik des Flexodrucks*. Rek & Thomas, St. Gallen, 5th edition, 2006.

[100] Mitsubishi Polyester Film GmbH. Technical Datasheet Hostaphan, May 2012.

[101] Shyam P. Murarka. *Metallization: theory and practice for VLSI and ULSI*. Butterworth-Heinemann, Stoneham, MA, 1993.

[102] Georg Niggemeier. Streifzug um die Rasterwalze. Company information, Zecher GmbH, February 2002.

[103] Michael Nitsche. *Polygraph Wörterbuch für die Druckindustrie und Kommunikationstechnik: Deutsch-Englisch, Englisch-Deutsch*. Polygraph Verlag, Bielefeld, 2001.

[104] NovaCentrix. Metalon HPS-021LV. Datasheet, April 2012.

[105] NovaCentrix. PulseForge 1200. Photonic Curing Tool for Printed Electronics. Datasheet, 2012.

[106] NovaCentrix. PulseForge 1200 Operations, Safety and Maintenance Manual. Company Information, 2013.

[107] D. K. Owens and R. C. Wendt. Estimation of the surface free energy of polymers. *Journal of Applied Polymer Science*, 13(8):1741–1747, August 1969. 03595.

[108] PChem Associates. PFI-722 Conductive Flexo Ink. Product Data Sheet, November 2010.

[109] PChem Associates. How it works. particle size. http://nanopchem.com/technology/how-it-works, 2012. Last accessed: 12.02.2014.

[110] Jolke Perelaer, Mark Klokkenburg, Chris E. Hendriks, and Ulrich S. Schubert. Microwave flash sintering of inkjet-printed silver tracks on polymer substrates. *Advanced Materials*, 21(47):4830–4834, December 2009.

[111] Jolke Perelaer, Patrick J. Smith, Dario Mager, Daniel Soltman, Steven K. Volkman, Vivek Subramanian, Jan G. Korvink, and Ulrich S. Schubert. Printed electronics: the challenges involved in printing devices, interconnects, and contacts based on inorganic materials. *Journal of Materials Chemistry*, 20(39):8446, 2010.

[112] Christopher O. Phillips, Sridhar Govindarajan, Simon M. Hamblyn, R. Steven Conlan, David T. Gethin, and Tim C. Claypole. Patterning of antibodies using flexographic printing. *Langmuir*, 28(25):9878–9884, June 2012.

[113] Jenna Pollock. The halo effect: The influence of attractiveness on perceived promiscuity. *sentience. The University of Minnesota Undergraduate Journal of Psychology*, 7:34–37, Fall 2012.

[114] preussner grafik design. Flexodruck. http://www.preussner-grafik-design.de/typo_lexikon/f/flexodruck.html, July 2013. Last accessed: 22.07.2013.

[115] Puetz Folien. http://www.puetz-folien.com/wb/pages/deutsch/produktFCbersicht/polyester.php. Last accessed: 30.08.2013.

[116] P. Rai-Choudhury, editor. *Handbook of microlithography, micromachining, and microfabrication*. Number 12A-12B in IEE materials and devices series. SPIE Optical Engineering Press, Institution of Electrical Engineers, Bellingham, WA London, 1997.

[117] Constanze Ranfeld, Edgar Dörsam, and Hans Martin Sauer. Flexography as a structured application method for etching resist. In Mladen Lovrecek, editor, *Advances in Printing and Media Technology. Digitalization of Print - Exchanging Ideas Across Generations. Proceedings of the iarigai Conference 2013*, volume XL. iarigai, 2013.

[118] Constanze Ranfeld and Edgar Dörsam. Structured wet etching of printed silver layers using a printed etch resist. In *Winter School of Organic Electronics*, Heidelberg, March 2012.

[119] Constanze Ranfeld, Hans Martin Sauer, and Edgar Dörsam. Zwischenbericht 2011 zum Teilvorhaben Drucktechnik für gedruckte flexible Displays im Verbundprojekt Kosadis. Unpublished, February 2012.

[120] Constanze Ranfeld, Hans Martin Sauer, and Edgar Dörsam. Abschlussbericht zum Teilvorhaben Drucktechnik für gedruckte flexible Displays im Verbundprojekt Kosadis. February 2013.

[121] Constanze Ranfeld, Hans Martin Sauer, and Edgar Dörsam. Using the halo effect in flexographic printing for the manufacturing of Source/Drain-Structures for thin film transistors. In *Proceedings of Large-Area, Organic and Polymer Electronics Convention 2011 (LOPE-C 11)*, Frankfurt, 2011. Organic Electronics Association (OE-A).

[122] Constanze Ranfeld, Alexandra Theopold, and Edgar Dörsam. Flexographic printing for the production of inorganic electroluminescent devices. In Reinhard R. Baumann, editor, *Proceedings of the 4th International Scientific Conference Printing Future Days 2011*, pages 151–157, Berlin, 2011. VWB - Verlag für Wissenschaft und Bildung.

[123] Ingo Reinhold, Chris E. Hendriks, Rebecca Eckardt, Johannes M. Kranenburg, Jolke Perelaer, Reinhard R. Baumann, and Ulrich S. Schubert. Argon plasma sintering of inkjet printed silver tracks on polymer substrates. *Journal of Materials Chemistry*, 19(21):3384, 2009.

[124] Maria Rentzhog. *Characterisation of water-based flexographic inks and their interactions with polymer-coated board*. PhD thesis, Ytkemiska institutet, Institutionen för kemi, Kungliga Tekniska högskolan, Stockholm, 2004.

[125] Andreas Risse. *Fertigungsverfahren der Mechatronik, Feinwerk- und Präzisionsgerätetechnik*. Vieweg+Teubner, Wiesbaden, 2012.

[126] Philip M. Rosenzweig. *The halo effect - and the eight other business delusions that deceive managers*. Free Press, New York, 2007.

[127] Jason H. Rouse and Dave Klein. High conductive water-based silver ink, 2011.

[128] Hans Martin Sauer, Nils Bornemann, and Edgar Dörsam. Viscous fingering in functional flexo printing: an inevitable bug? In *Proceedings of Large-Area, Organic and Polymer Electronics Convention 2011 (LOPE-C 11)*, Frankfurt, 2011. Organic Electronics Association (OE-A).

[129] Susanne Scheinert, Theodor Doll, Axel Scherer, Gernot Paasch, and Ingo Hörselmann. Organic field-effect transistors with nonlithographically defined submicrometer channel length. *Applied Physics Letters*, 84(22):4427, 2004.

[130] Georg C. Schmidt, Maxi Bellmann, Barbara Meier, Mike Hambsch, Kay Reuter, Heiko Kempa, and Arved C. Hübler. Modified mass printing technique for the realization of source/drain electrodes with high resolution. *Organic Electronics*, 11(10):1683–1687, October 2010.

[131] Kurt A. Schroder. Mechanisms of photonic curing: Processing high temperature films on low temperature substrates. In *Proceedings of the NSTI Nanotechnology Conference*, volume 2, pages 220–223, Boston, USA, 2011. Nano Science & Technology Institute, Taylor & Francis.

[132] Kurt A. Schroder, Steve C. McCool, and Wayne F. Furlan. Broadcast photonic curing of metallic nanoparticle films. In *Proceedings of the NSTI Nanotechnology Conference*, volume 3, pages 198–201, Boston, USA, 2006. Nano Science & Technology Institute, Taylor & Francis.

[133] Sensofar. Sensofar PLu neox 3D Optical Profiler. Brochure, without year.

[134] Karl Siebertz, David van Bebber, and Thomas Hochkirchen. *Statistische Versuchsplanung: Design of Experiments (DoE)*. Springer, Heidelberg Dordrecht London New York, 2010.

[135] Siegwerk Druckfarben AG & Co. KGaA. Ink, heart & soul. flexodruck ratgeber. Brochure, March 2013.

[136] Sigma-Aldrich. Poly(methyl methacrylate). http://www.sigmaaldrich.com/catalog/product/aldrich/445746?lang=de&region=DE&cm_sp=abstract-_-23470253-_-445746. Last accessed: 30.01.2014.

[137] Sigma-Aldrich. Anisol. Sicherheitsdatenblatt, June 2009.

[138] Sigma-Aldrich. Methanol. Sicherheitsdatenblatt, February 2013.

[139] Dan Soltman and Vivek Subramanian. Inkjet-printed line morphologies and temperature control of the coffee ring effect. *Langmuir*, 24(5):2224–2231, March 2008.

[140] Simon Stahl. *Einfluss der Druckform und der Fluidviskositaet auf die Schichtdicke von im Tiefdruck hergestellten Funktionsschichten und deren Charakterisierung*. Dissertation, Technische Universität Darmstadt, Darmstadt, 2013. http://tuprints.ulb.tu-darmstadt.de/id/eprint/3529.

[141] Michael Strecker. University of Stuttgart. Personal Conversation, September 2011.

[142] Helmut Teschner. *Druck & Medien Technik: Informationen gestalten, produzieren, verarbeiten*. Fachschriften-Verlag, Fellbach, 11th edition, 2003.

[143] Alexandra Theopold. *Charakterisierung von Flexodruckformen hinsichtlich der Eignung für die gedruckte Elektronik*. Dissertation, Technische Universität Darmstadt, Darmstadt, 2014.

[144] Alexandra Theopold and Edgar Dörsam. Characterization of flexographic printing plates with regard to the field of printed electronics. In *Proceedings of Large-Area, Organic and Polymer Electronics Convention 2011 (LOPE-C 11)*, pages 330–334, Frankfurt, 2011. Organic Electronics Association (OE-A).

[145] Sebastien Thibert, Johann Jourdan, Bernard Bechevet, Simon Mialon, Davide Beneventi, Didier Chaussy, and N. Reverdy-Bruas. Flexographic process for front side metallization of silicon solar cells. In A. Mine, editor, *Proceedings of the 28th European PV Solar Energy Conference and Exhibition (EU PVSEC)*, pages 1013 –1016, Paris, 2013.

[146] Robert Thieme, Dieter Spiehl, Simon Stahl, Constanze Ranfeld, Alexandra Theopold, and Jürgen Willmann. Lastenheft Druckverfahrenstechnik. Internal Document, December 2012.

[147] Bob Thompson. *Printing materials: Science and technology.* Pira International, Leatherhead, 2nd edition, 2004.

[148] Edward L. Thorndike. A constant error in psychological ratings. *Journal of Applied Psychology*, 4(1):25–29, 1920.

[149] Mohammad Vaezi, Hermann Seitz, and Shoufeng Yang. A review on 3D micro-additive manufacturing technologies. *The International Journal of Advanced Manufacturing Technology*, 67(5-8):1721–1754, nov 2012.

[150] Leo J. van der Pauw. A method of measuring specific resistivity and hall effect of discs of arbitrary shape. *Philips Research Reports*, 13(1):1–9, 1958.

[151] VEGRA GmbH. Hinweise für die Verwendung von VEGRA Iriodinlacken. http://www.vegra.com/Info.php?InfoId=7, November 2005. Last accessed: 05.11.2013.

[152] Friedemann Völklein and Thomas Zetterer. *Praxiswissen Mikrosystemtechnik*. Programm Elektrotechnik. Friedr. Vieweg & Sohn Verlag | GWV Fachverlage GmbH, Wiesbaden, 2. edition, 2006.

[153] Christian Voss. *Analytische Modellierung, experimentelle Untersuchungen und dreidimensionale Gitter-Boltzmann Simulation der quasistatischen und instabilen Farbspaltung*. Dissertation, Bergische Universität Gesamthochschule Wuppertal, Wuppertal, 2002.

[154] John L. Vossen and Werner Kern, editors. *Thin film processes*. Academic Press, New York, 1978.

[155] John G. Webster. *The measurement, instrumentation, and sensors handbook*. CRC Press published in cooperation with IEEE Press, Boca Raton, Fla., 1999.

[156] Ronald Weidel. Flexographic printing. Part 4: Print quality. *PrintPromotion Newsletter*, (94):15–16, December 2013.

[157] Frederic Lyman Wells. A statistical study of literary merit. *Archives of Psychology*, 7:1–30, 1907.

[158] Jeff West, Michael Carter, and James Sears. *Sintering - Methods and Products*, chapter Photonik Sintering of Silver Nanoparticles: Comparison of Experiment and Theory, pages 173–188. InTech, 2012.

[159] Jürgen Willmann. *Innovationen in der druckbaren Elektronik: Von der Idee zur Produktion. Eine technische und wirtschaftliche Analyse.* Dissertation, Technische Universität Darmstadt, Darmstadt, 2012. http://tuprints.ulb.tu-darmstadt.de/id/eprint/3644.

[160] Lina Yang. Theoretische und experimentelle Beschreibung gedruckter Linien im Flexodruck - Eine Parameterstudie. Bachelor-Thesis, Technische Universität Darmstadt, Darmstadt, September 2013. Supervisor: Dipl.-Ing. Constanze Ranfeld.

[161] Jong-Su Yu, Inyoung Kim, Jung-Su Kim, Jeongdai Jo, Thue T. Larsen-Olsen, Roar R. Södergaard, Markus Hösel, Dechan Angmo, Mikkel Jörgensen, and Frederik C. Krebs. Silver front electrode grids for ITO-free all printed polymer solar cells with embedded and raised topographies, prepared by thermal imprint, flexographic and inkjet roll-to-roll processes. *Nanoscale*, 4(19):6032, 2012.

[162] Winco K. Yung, X. Gu, C.P. Lee, and H.S. Choy. Ink-jet printing and camera flash sintering of silver tracks on different substrates. *Journal of Materials Processing Technology*, 210(15):2268–2272, November 2010.

[163] Mohd S. Yusof, Tim C. Claypole, David T. Gethin, and Ahmad M. Zaidi. Application of finite elements on non-linear deformation of flexographic photopolymer printing plate. In S. I World Congress on Engineering, Ao and International Association of Engineers, editors, *Proceedings of the World Congress on Engineering: WCE 2008, Imperial College London, London, U.K.*, volume II, pages 1197–1201, Hong Kong, July 2008. International Association of Engineers, Newswood Ltd.

Own publications

Hans Martin Sauer, Constanze Ranfeld, Edgar Dörsam. An investigation of the screen printing process for electroluminscent panels and the influence of printing parametes on the performance of the panels. In *Proceedings of Large-Area, Organic and Polymer Electronics Convention 2010 (LOPE-C 10)*, Frankfurt, 2010. Organic Electronics Association (OE-A).

Constanze Ranfeld, Alexandra Theopold, Edgar Dörsam. Flexographic printing for the production of inorganic electroluminescent displays. In Baumann, Reinhard R. editor, *Proceedings of the 4th International Scientific Conference "Printing Future Days 2011" Chemnitz*, pages 151-157, Berlin, 2011. VWB - Verlag für Wissenschaft und Bildung.

Constanze Ranfeld, Hans Martin Sauer, Edgar Dörsam. Using the halo effect in flexographic printing for the manufacturing of source/drain-structures for thin film transistors. In *Proceedings of Large-Area, Organic and Polymer Electronics Convention 2011 (LOPE-C 11)*, Frankfurt, 2011. Organic Electronics Association (OE-A).

Constanze Ranfeld, Hans Martin Sauer, Edgar Dörsam. Using the Halo Effect in Flexographic Printing for the Manufacturing of Source/Drain-Structures for Thin Film Transistors. In *Clusterconference Forum Organic Electronics*, Heidelberg, 2011.

Constanze Ranfeld, Edgar Dörsam. Structured wet etching of printed silver layers using a printed etch resist. In *2nd Winter School of Organic Electronics*, Heidelberg, March 2012.

Kathrin Happel, Constanze Ranfeld, Thorsten Euler, Edgar Dörsam, Thomas Walther. The influence of defects in flexographic post-printing of corrugated board on register control. In Mladen Lovrecek, editor *Advances in Printing and Media Technology. Digitalization of Print - Exchanging Ideas Across Generations*, volume XL. iarigai, Chemnitz, 2013.

Constanze Ranfeld, Edgar Dörsam, Hans Martin Sauer. Flexography as a structured application method for etching resist. In Mladen Lovrecek, editor, *Advances in Printing and Media Technology. Digitalization of Print - Exchanging Ideas Across Generations*, volume XL. iarigai, Chemnitz, 2013.

Supervised student papers

Bachelor theses

Anke Fulek: Untersuchung der Ätzrate gedruckter Silber- und PMMA-Schichten. *Engl. Investigation of the etching rate of printed silver and PMMA-layers.* September 2013. Supervisor: Constanze Ranfeld.

Eric Langner: Untersuchung des Verhaltens von Druckfarbe und Klischee im Flexodruck mittels optischer Erfassung im Druckspalt. *Engl. Investigation of ink and plate behavior in the nip of a flexographic printing process using optical inspection.* February 2014. Supervisor: Constanze Ranfeld and Felipe Fernandes.

Marcus May: Erarbeitung eines Moduls zum Thema 3D-Drucken für das Tutorium Drucktechnologie. *Engl. Conception of a module of the tutorial "printing technology" regarding 3D-printing.* February 2013. Supervisor: Constanze Ranfeld.

Thorsten Schäfer: Untersuchung von Defektbildern im Wellpappe-Direktdruck. *Engl. Investigation of defects in post-printing of corrugated board.* September 2013. Supervisor: Constanze Ranfeld.

Lina Yang: Theoretische und experimentelle Beschreibung gedruckter Linien im Flexodruck - Eine Parameterstudie. *Engl. Describing a flexographic printed line. A parameter study.* September 2013. Supervisor: Constanze Ranfeld.

Seminar papers

Semik Kumar Bhelsat: Untersuchungen zum Einfluss verschiedener Druckparameter auf das Druckergebnis hinsichtlich des Halo-Effektes im Flexodruck. *Engl. Influences of different printing parameters on the characteristics of the halo effect in flexographic printing.* April 2012. Supervisor: Constanze Ranfeld.

Research seminars

Felipe Fernandes: Strukturiertes Beschichten von 3-dimensionalen Oberflächen. Verfahrensübersicht, Eignung für verschiedene funktionale Fluide. *Engl. Structured coating of 3-dimensional surfaces. Process overview, suitability for several functional inks.* February 2012. Supervisor: Constanze Ranfeld.

Yanlong Gao: Herstellung von 3D-Mikrostrukturen aus Kunststoff durch additive Verfahren. *Engl. Additive processes for the manufacturing of 3D microstructures.* February 2013. Supervisor: Constanze Ranfeld

Sebastian Groß: Elektronische Bauelemente und deren Herstellung im Flexodruck. *Engl. Electronic devices and their manufacturing using flexography.* August 2012. Supervisor: Constanze Ranfeld.

Volker Hübner: Strukturierungsverfahren in der Mikrofertigungstechnik. *Structuring methods in micro production technologies.* February 2013. Supervisor: Constanze Ranfeld

Daniel Maßfelder: Möglichkeiten und Grenzen des Flexodrucks für das Funktionale Drucken. *Engl. Chances and limits of flexography regarding functional printing.* August 2012. Supervisor: Constanze Ranfeld.

Bilel Salem: Möglichkeiten und Grenzen des Flexodrucks für das Funktionale Drucken. *Engl. Chances and limits of flexography regarding functional printing.* February 2012. Supervisor: Constanze Ranfeld.

Advanced design projects

Jens Focke, Anton Iarovyi, Christian Passow, Jan Schmitt: Aufbau und Evaluation eines kommerziellen Low-Budget 3D-Druckers. *Engl. Setup and evaluation of a commercial low-budget 3D-printer.* June 2011. Supervisor: Dieter Spiehl and Constanze Ranfeld.

A. Details regarding measurement and experimental procedures

A.1. Procedure of determining layer thicknesses

This section details the procedure of obtaining the layer thickness of printed samples on the example of determining the layer thickness before and after etching as introduced in Chapter 4.3.2. I will explain the interpretation of the x/y/z-measurement data obtained by confocal microscopy using the software SensoMap[1]. The software is a tool to display, interpret and manipulate two- and three-dimensional data.

A common problem in printed electronics is the lack of methods to determine layer thicknesses over a large area. Stahl and Bornemann introduced measurement methods for large areas in the range of DIN A5 sheets. Unfortunately, both require transparent layers as they are based on absorption (Stahl [140]) and interference (Bornemann [21]). To this day, I have no knowledge of methods that are able to determine the layer thickness of opaque samples non-destructively over a large area. For this study, non-destructive measurement techniques are required as we need to measure the same position on the sample before and after the etching process.

In the following, I explain the procedure I followed to obtain the layer thickness of the investigated samples. Figure A.1 illustrates the remarks below with corresponding numeration.

1. As we need an edge of the layer to determine its thicknesss, I first make a marking ($< 1\,\mathrm{cm}^2$) using a scalpel. The glass substrate is very robust, thus the scalpel does not affect ist surface[2].
2. To obtain the surface data of the marked edge, I use confocal microscopy as introduced in Chapter 4.1.1.
3. The thusly obtained date, I then import into the surface analysis software SensoMap.
4. Due the to non-ideal surface of the measurement table, the measurement data needs to be leveled. As reference plain, we use the surface of the glass slide which has been uncovered with the scalpel. I used the method implemented in the software where a reference plain is calculated using three spots marked by the operator.
5. I then obtained a cross-sectional profile series over the surface, also calculating a mean profile.
6. Using the mean profile, I determined the layer thickness using the implemented method *step height*. The lower step is the glass surface, the upper step the surface of the printed layer. Note that the calculation of the step height is a mean over a selected section of the profile. Thus, the less rough the profile is, the more accurate is the height determination.

[1] SensoMap is a brand name of the software MountainsMap from the company DigitalSurf. The software is intended for analysis of 2D and 3D surface measurements. I used version 3.1.2.16.

[2] As scratches generated by high force are clearly visible and also detectable with confocal microscopy, I assume that scribing the layers with low force will not leave noticable tracks. The measurements support this thesis.

A. Details regarding measurement and experimental procedures

I thusly measured the layer height of each sample three times on each marked spot with three spots on each silver rectangle, before and after etching. I also measured the height of the PMMA bonding layer on five spots on each glass slides, three times each.

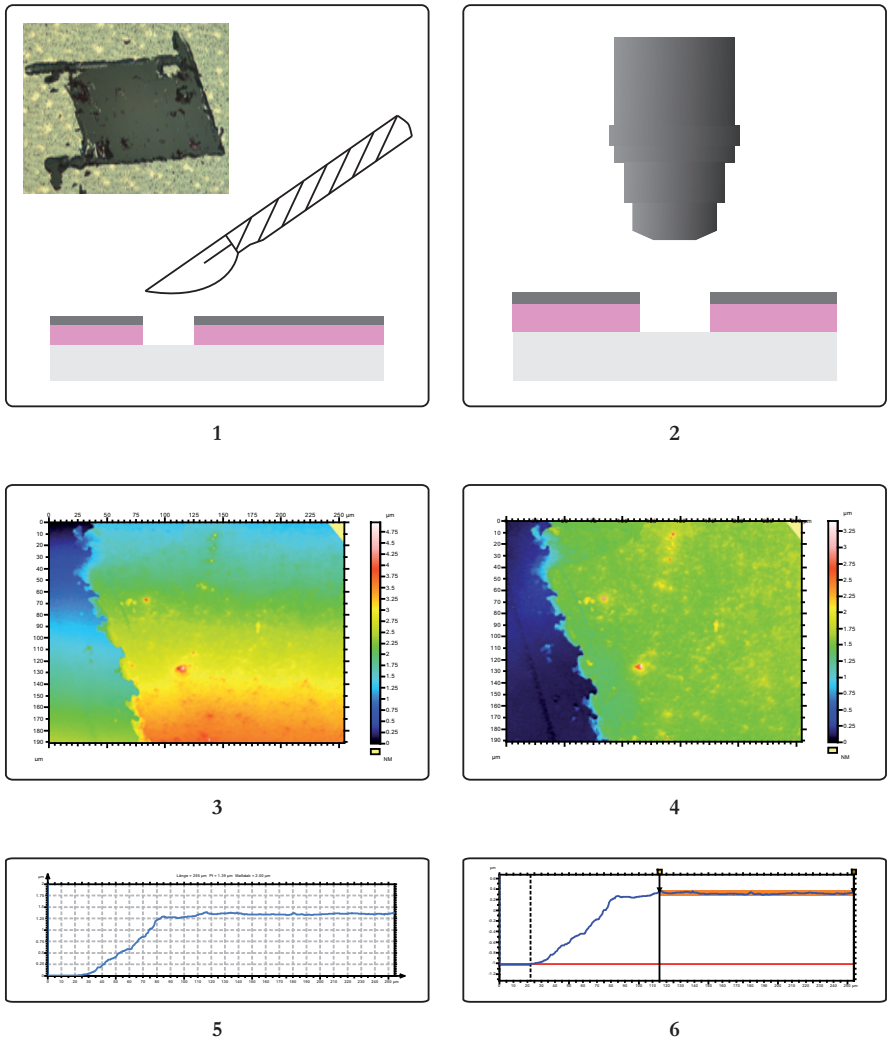

Figure A.1.: Procedure of determining the layer thickness of a printed layer: 1) marking of the sample to create edges (inlet: optical microscopic image of marked spot), 2) confocal microscopy of the marked spot, 3) importing surface data into SensoMap, 4) leveling of surface, 5) mean profile of sample cross section, 6) determining the step height.

A.2. Details regarding printing trials

The anilox rollers I used for the printing trials of the resist layer were the following:

- INOMETA 030.003420N001254: screen ruling 300 L/cm, pick-up volume 4.5 cm^3/m^2, screen angle 60°. This anilox roller has the same specifications as IGT 402-422.
- IGT 402-402: screen ruling 180 L/cm, pick-up volume 8 ml/m^2, screen angle 60°
- IGT 402-416: screen ruling 80 L/cm, pick-up volume 24 ml/m^2, screen angle 60°

The individual parameter combinations for the printing trials of the resist layer may be obtained from Table A.1.

Table A.1.: Experimental for printing etch resist: factors, i.e. printing parameters of the IGT F1.

ser. no.	printing speed [m/s]	printing force [N]	pick-up volume [ml/m^2]
1	1.5	10	4.5
2	0.2	10	4.5
3	1.5	500	4.5
4	0.2	500	4.5
5	0.2	10	8
6	0.9	10	8
7	0.9	500	8
8	1.5	500	8
9	0.2	500	8
10	1.5	260	8
11	1.5	10	8
12	0.2	260	8
13	0.2	10	24
14	1.5	500	24
15	0.2	500	24
16	0.9	260	24
17	1.5	10	24

Properties of printing plate for silver layer [43]:

- material group: photopolymer
- mounting technique: double sided tape
- manufacturer: FlintGroup Flexograhpic Products
- product name: nyloflex FAH
- thickness: 1.70 mm
- relief depth: 0.7 . . . 0.9 mm

Properties of printing plate for resist layer:

- material group: flourinated rubber (Viton, internal notation: FKM 751)
- mounting technique: sleeve
- manufacturer: Felix Boettcher GmbH & Co. KG
- thickness: 1.68 mm
- benefit: thermal stability, chemical resistance [93, Vol. 2 Fluorocarbon Elastomers]

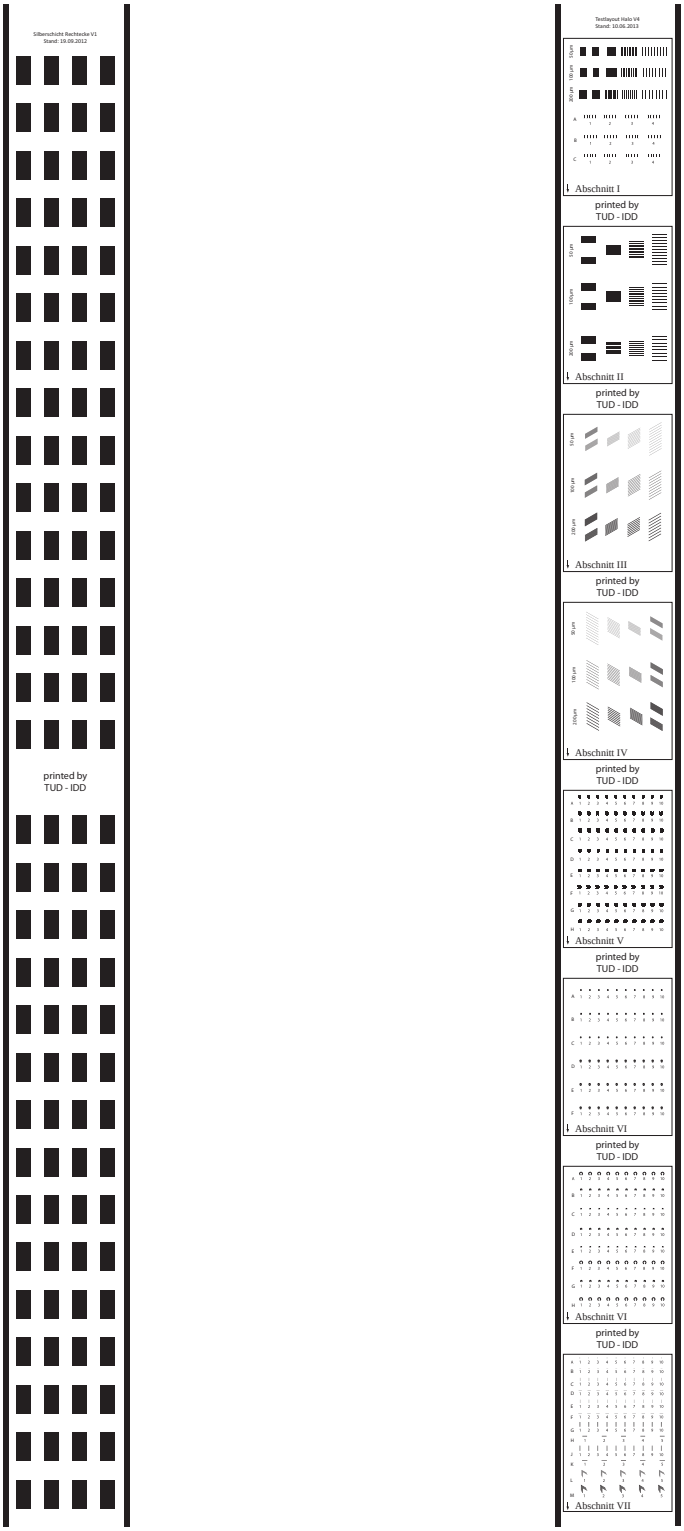

Figure A.2.: Layouts of printing plates used in this study. Left: silver layer, right: resist layer.

A.3. Details regarding post-processing

Table A.2.: Experimental plan for post-processing trials: factors, i.e. machine parameters of the PulseForge1200.

ser. no.	bank voltage U_{bank} [V]	envelope duration t_{env} [μs]	number of micropulses $n_{\mu pulse}$ [ ]	pre-drying P
1	270	400	4	yes
2	260	450	4	yes
3	280	500	4	yes
4	260	400	5	yes
5	280	400	5	yes
6	270	500	5	yes
7	260	400	6	yes
8	270	400	6	yes
9	280	450	6	yes
10	260	500	6	yes
11	260	400	4	no
12	280	400	4	no
13	280	450	4	no
14	260	500	4	no
15	270	450	5	no
16	280	400	6	no
17	260	450	6	no
18	260	500	6	no
19	280	500	6	no
20	260	400	4	yes

A.4. Specifications of measurement equipment

PLu neox SENSOFAR®

SPECIFICATIONS

Confocal objectives						
	5X	10X	20X	50X	100X	150X
Working Distance (mm)	23.5	17.5	4.5	1.0	1.0	0.3
NA	0.15	0.30	0.45	0.80	0.90	0.95
FOV (µm) [1]	2546 x 1509	1270 x 950	636.61 x 477.25	254.64 x 190.90	127.32 x 95.45	84.83 x 63.60
Spatial sampling (µm) [2]	3.32	1.66	0.83	0.33	0.17	0.11
Optical Resolution (L&S) (µm) [3]	0.93	0.47	0.31	0.17	0.15	0.14
Maximum Slope [4]	8º	14º	21º	42º	51º	71º
Vertical Resolution (nm) [5]	<100	<50	<20	<3	<2	<1
Confocal Frame rate (frame/s)	12.5 fps					
Scanning speed (µm/s)	20 - 320	10 - 160	5 - 80	1 - 16	1 - 16	0.5 - 8
Typical measurement time (s) [6]	5					

Interferometric objectives						
	2.5X	5X	10X	20X	50X	100X
Working Distance (mm)	10.3	9.3	7.4	4.7	3.4	2.0
NA	0.055	0.15	0.30	0.45	0.55	0.7
FOV (µm) [1]	5093 x 3818	2546 x 1909	1270 x 950	637 x 477	254 x 190	127 x 95
Spatial sampling (µm) [2]	6.64	3.32	1.62	0.83	0.33	0.17
Optical Resolution blue (L&S) (µm) [3]	2.55	0.93	0.46	0.31	0.25	0.20
Optical Resolution white (L&S) (µm) [3]	3.04	1.11	0.56	0.37	0.30	0.24
Maximum Slope [4]	3.15º	8.6º	14º	21º	25º	42º
Vertical Resolution (nm) PSI [7] Vertical Resolution (nm) ePSI [7]	<0.1 nm (down to 0.01 nm with PZT)					
Vertical Resolution (nm) VSI [8]	1 nm					
Vertical Range PSI (µm)	5 µm					
Vertical Range ePSI (µm)	100 µm					
Vertical Range VSI (mm)	10 mm					
Scanning speed (µm/s)	PSI: 3-15 µm/s VSI/ePSI: 4-18 µm/s					
Typical measurement time (s) [9]	PSI: 3 s VSI: 10s ePSI: 30s					

1) Maximum field of view with ½" camera and 0.5X optics.
2) Pixel size on the surface
3) Half of the diffraction limit according to the Rayleigh criterion. L&S: Line and Space. Blue wavelength 460 nm, and White central wavelength 550 nm.
4) On smooth surfaces
5) System noise measured as the difference between two consecutive measures with 2 confocal image averages on a calibration mirror placed perpendicular to the optical axis.
6) For 21 scanning planes.
7) System noise measured as the difference between two consecutive measures with 10 phase averages on a calibration mirror placed perpendicular to the optical axis. Vibration isolation activated. The 0.01 nm are achieved with Piezo stage scanner and temperature controlled room.
8) System noise measured as the difference between two consecutive measures on a calibration mirror placed to the perpendicular axis. Vibration isolation activated.
9) For 10 µm scan range

Other Specifications

Measurement Array: 576 x 768
Bright Field Frame Rate: 50 fps
Other Objectives Are Available.
Confocal: Water immersion, Super Long Working Distance, Extra Long Working Distance, Collar Ring depth focusing correction
Interferometry:Variable reflectance, Michelson, Mirau and Linnik
Sample Height: from 40 mm to 500 mm. Larger under request
Sample Reflectivity: from 0.1% to 100%
Display Resolution: 0.01 nm
Maximum Vertical Scanning Range: 40 mm with Linear Stage. Up to 200 µm with Piezo stage
Linearity: better than 0.05%. <0.5 µm/mm with Linear Stage, and <50 nm/100 µm with PZT

Step Height Repeatability: 0.1%
Roughness Repeatability: <0.2%
Step Height Accuracy: 0.5%

Environment

Temperature: 5ºC to 40ºC
Humidity: <80% RH
Altitude: <2000 m

Power Requirements

Input Voltage: 110/220Vac, single phase 50/60Hz

Figure A.3.: Specifications of the optical profiler Sensfoar PLu neox [133].

Specifications

			DM4000 B LED	DM5000 B	DM5500 B	DM6000 B	DM4000 M LED	DM6000 M
Stand	Power supply	– integrated in stand	x				x	
		– in electronics box		CTR5000	CTR5500	CTR6000		CTR6000
	Display	– display	x				x	
		– Leica SmartTouch		x	x	x		x
	Ports	– USB 2.0 + I²C	x	x	x	x	x	x
Operation	Focus	– mechanical	x	x			x	
		– 2-ratio gearbox						
		– motorized			x	x		x
		– 5 electronic ratios						
		– incl. parfocal function						
		– switch between coarse and fine mode						
		– memory location for 2 z-positions						
	Obj. nosepiece	– absolute coded	x	x	x	x	x	x
		– motorized				x		x
		– incl. dry and immersion mode						
		– 6x M25 thread	x					
		– 7x M25 thread	x	x	x	x		
		– 6x M32 thread					x	x
	Stage	– motorized			x	x		x
		– stepper motor						
		– switch between fast and precision mode						
		– incl. memory location for 6 stage positions						
		– mechanical	x	x	x	(x)	x	(x)
		– ceramic-coated						
		– y-drive with cable						
		– telescopic stage drive						
		– adjustable torque						
		– 110° rotation						
		– optional left-handed version						
	Controls	– 6 programmable function buttons	x	x	x	x	x	x
		SmartMove			x	x		x
		– controls for z (focus) movement						
		and x,y (stage) movement						
		– 4 programmable function buttons						
		Leica STP6000			x	x		x
		– controls for z (coarse and fine focus)						
		and x,y (stage) movement						
		– 11 programmable function buttons						
		– touch panel with information and control panels						
TL-axis	Illumination	– LED	x				x	
		– 12 V 100 W halogen lamp		x	x	x		x
	Automation	– light manager (brightness, field and aperture stop)	x	x	x	x	x	x
		– contrast manager	x	x	x	x	x	x
		– constant color intensity control	x	x	x	x	x	x
	Contrast method	– BF	x	x	x	x	x	x
		– PH, DF, POL	x	x	x	x	(x)	(x)
		– DIC (semi automated)					(x)	
		– DIC (automated)		x	x	x		(x)
Fluo axis	Mot. filter disk	– 5x	x	x	x	x		
		– 8x		x	x	x		
	Illumination	– 100 W Hg lamp, EL6000, SFL100/4000/7000*	x	x	x	x		
	Automation	– fluorescence intensity manager (FIM)	x	x	x	x		
		– contrast manager	x	x	x	x		
		– round and square illuminated field diaphragms for						
		ocular and camera observation	x	x	x	x		
RL axis	Mot. filter disk	– 4x					x	x
		– 2 fixed positions						
		– 2 adjustable positions						
	Illumination	– 12 V 100 W halogen lamp or LED (only Leica DM4000 M LED)					x	x
		– 100 W Hg lamp					x	x
		– 50 W Hg lamp					x	x
	Automation	– light manager (brightness, field and aperture stop)					x	x
		– contrast manager					x	x
		– round and square illuminated field diaphragms for						
		ocular and camera observation					x	x
	Contrast method	– BF, DF, POL					x	x
		– DIC (semi automated)					(x)	
		– DIC (automated)						(x)
Condenser	Automation	– condenser head, mot.	x	x	x	x	x	x
		– 7x condenser disk, mot. (optional)	x	x	x	x	(x)	(x)
		– polarizer, mot. (optional)	x	x	x	x	(x)	(x)

*SFL7000 (for DM5000-6000 B)

Figure A.4.: Specifications of the optical microscope Leica DM4000 [32].